December 2020

Power Scaling of Single-Mode Ytterbium and Erbium High-Power Fiber Lasers

Tuerhong Maitiniyazi
Clemson University, turghunmatniyaz@gmail.com

POWER SCALING OF SINGLE-MODE YTTERBIUM AND ERBIUM HIGH-POWER FIBER LASERS

A Dissertation
Presented to
the Graduate School of
Clemson University

In Partial Fulfillment
of the Requirements for the Degree
Doctor of Philosophy
Photonic Science and Technology

---

by
Turghun Matniyaz (Tuerhong Maitiniyazi)
December 2020

Accepted by:
Prof. Liang Dong, Committee Chair
Prof. John Ballato
Prof. Eric Johnson
Prof. Lin Zhu

ABSTRACT

Power scaling of rare-earth-doped fiber lasers is vital to many emerging applications. Average output power scaling with Yb doped fiber lasers operating near 1.1 μm was very successful in the 10 years between 2000 and 2010. The discovery and rediscovery of many limiting factors such as nonlinear effects, thermal lensing, optical damage, and so forth showed various bottlenecks in further power scaling of output power from a single fiber. On the other hand, single-mode average output power scaling of fiber lasers operating at ~980 nm and ~1560 nm has lagged much behind their pioneering counterparts at ~1.1 μm. Single-mode high-power fiber lasers at these scarce wavelengths are in great demand for many applications such as pumping ultrafast lasers, nonlinear frequency conversion, lidar, free-space optical communication, etc. However, currently, commercial single-mode laser didoes at ~980 nm have very limited output power of near 1 W. Many different types of Yb-doped fibers for ~980 nm lasers were reported previously but the record output power has only reached to ~15 W from a monolithic single-mode Yb fiber laser. One of the major limiting factors is the amplified spontaneous emission (ASE) at ~1030 nm which has a net positive gain at very low inversion (>5%) while Yb laser operation at ~980 nm needs very high inversion (>50%).

In the first part of this dissertation, we propose the utilization of a Yb-doped multiple cladding resonance (MCR) based all-solid photonic bandgap fiber (AS-PBF) for power scaling of single-mode laser operating at ~980 nm. This novel type of AS-PBF provides three major advantages, including large core to cladding ratio, superior HOM

suppression, and built-in wavelength filtering to suppress ASE at ~1030 nm. We have experimentally explored the power scaling of ~980 nm Yb fiber laser pumped at 915 nm. An optimized Yb PBF with 24 μm core and 130 μm cladding was fabricated after several fine-tuning processes of fiber dimensions (thus bandgap positions) by carefully characterizing the Yb AS-PBF and analyzing the output diagnostics of the laser oscillator. Eventually, we were able to obtain a near-diffraction-limited laser output with ~150 W from an all-fiber Yb fiber laser operating at ~980 nm, which represents a factor of 15 improvement over the previously reported record. This monolithic fiber laser demonstrates the potential of building a compact and robust commercial high-power single-mode fiber laser operating at ~980 nm. Additionally, it shows the potential of MCR AS-PBF to be incorporated in many other fibers for power scaling of fiber lasers at other wavelengths.

In the second part of this dissertation, we explore the power scaling of single-mode fiber lasers operating at ~1.5-1.6 μm using Er/Yb co-doped LMA fibers. Due to its good atmospheric transmission and "eye-safe" nature of single-mode fiber lasers operating at this wavelength range, there is a growing demand for applications in many areas such as pumping Tm fiber lasers, CW coherent lidar, free-space optical communication, remote sensing, etc. Yb-free Er-doped fibers are another option to generate lasers at this wavelength, but further power scaling is limited due to low pump absorption cross section of Er fiber at ~980 nm. On the other hand, co-doping with Yb enables a factor 100 increase in pump absorption (10× from higher absorption cross section and 10× from higher maximum doping level) thus shortens effective fiber length. There are two major limiting factors for power scaling with Er/Yb co-doped fiber laser, including Yb→Er energy

transfer bottleneck and excessive heat load due to large quantum defect. The former leads to strong Yb ASE (or parasitic lasing) at ~1.06 μm at certain threshold pump powers and will eventually clamp output power at ~1.6μm when the pumping rate exceeds the energy transfer rate. However, the working principle regarding the ASE threshold and output power clamping was not well understood as conventional models assume that all Yb-ions are equally responsible for Yb→Er energy transfer. The new model proposed in this dissertation is based on two types Yb ions, including coupled Yb ions and isolated Yb ions. The numerical simulations results show perfect agreement with experimental results, and it can predict and explain all the observed behaviors very well.

We have also carried out a detailed experimental study on a master oscillator power amplifier (MOPA) using a commercial Er/Yb fiber (LMA-EYDF-25P/300-HE), which was counter pumped by kW-level multi-mode pump diode at 915nm. The achieved record single-mode output power of 302W was not limited by ASE (i.e. energy transfer bottleneck) but by fiber fuse in our case. Further analysis of MOPA output diagnostics and Er/Yb fiber parameters shows that lower Yb to Er ions ratio and pumping at a shorter wavelength (915 nm or 940 nm) played a major role in better ASE suppression, i.e high Yb ASE threshold power. Finally, we conclude that the energy transfer bottleneck will eventually come in with any Er/Yb fiber albeit at a much higher threshold pump power depending on how well the Er/Yb fiber is optimized.

In the third part which is also the last part of this dissertation, we report our preliminary experimental results for power scaling of 1064 nm high-power single-frequency Yb fiber laser system based on a 976 nm counter-pumped MOPA configuration.

There are two main limiting factors in this case, including SBS and TMI. Utilizing an LMA fiber could mitigate SBS by lowering laser intensity in the core, but the large core also leads to a low TMI threshold due to the excitation of HOMs. We propose to incorporate the previously studied MCR AS-PBF design into a new Yb AS-PBF with ~56 μm core and ~401 μm cladding, which expected to have a high SBS threshold above 1 kW. The preliminary experimental results show that single-frequency output power reaches ~500W before the onset of TMI. Also, the MOPA output does not show any signs of SBS indicated by careful characterizations such as backward power, spectrum, and linewidth measurement.

DEDICATION

To my late mother Hörnisakhan Meshuk and father Matniyaz Amet, and the millions of Uyghur people who have been suffering under the most pervasive and brutal ethnic persecution since 2017.

ACKNOWLEDGMENTS

First and foremost, I would like to express my sincere appreciation and gratitude to my advisor and mentor, Prof. Liang Dong, for guiding and supporting me throughout my Ph.D. studies at Clemson University. I've always admired his profound knowledge in our research field and many other fields one of them being history. I've learned so much from him not only about fibers and lasers, but also about work ethics, critical thinking, and so many other things. Without his constant guidance, my Ph.D. dissertation work would not have reached this far.

I also would like to thank my Ph.D. committee members, Prof. John Ballato, Prof. Eric Johnson, and Prof. Lin Zhu. I appreciate all of your valuable advice and thought-provoking questions on my research and dissertation.

Pursuing a Ph.D. is an extremely challenging work, to put it mildly. For me, it was not only about learning the technical aspect of it in the lab and from the books and papers, but also about learning how to work with people as a team. The completion of all the research projects in this dissertation work was indeed the result of hard work and team collaborations. For this, I would like to thank every past and current members of our research team. One way or another, all of you either taught me something valuable or I learned from you on my own. It was a great privilege to work with y'all.

I would like to especially thank my amazing wife and the love of my life, Halide Imir. This wonderful yet at times challenging and frustrating journey of pursuing Ph.D. would not have been possible without the support and love from you. This grand achievement belongs to you as much as it does to me. I cannot imagine going through the

ups and downs along this journey without you. You have been an amazing mom to our two wonderful kids, Otkur and Berna. You made a huge sacrifice for our little family by giving up your job and staying at home to take care of our kids. For this, I would also like to thank my parents-in-law for giving their blessings to us.

Last but never the least, I would like to thank my late mother Hörnisakhan Meshuk and father Matniyaz Amet. It was you two who originally inspired me to do well in school and eventually pursue higher education, although none of you had received a formal education beyond the middle school level. I was indeed very devastated when my mother passed away in November of 2016 and I was only able to reach home after the funeral. Yet, I continued my Ph.D. study and have come this far mainly because I knew my wonderful mom would have told me to do so. I also would like to thank my siblings Aysakhan Matniyaz (deceased), Tunsakiz Matniyaz, Tursunjan Matniyaz, Gulkiz Matniyaz, and Alimjan Matniyaz. I thank you all for having my back when I was studying far away from home since 2003. I don't know whether I will be able to see any of you again anytime soon, but I do hope that day will come sooner.

"Truth will ultimately prevail where pains is taken to bring it to light."- George Washington, 1794.

TABLE OF CONTENTS

Page

LIST OF TABLES

LIST OF FIGURES

List of Figures (Continued)

Figure Page

List of Figures (Continued)

Figure Page

List of Figures (Continued)

Figure Page

List of Figures (Continued)

Figure Page

List of Figures (Continued)

Figure Page

LIST OF ACRONYMS

ASE — Amplified Spontaneous Emission

AS — All-Solid

PBF — Photonic Bandgap Fiber

MCR — Multiple Cladding Resonance

MFD — Mode Field Diameter

PCF — Photonic Crystal Fiber

CW — Continuous Wave

HOM — Higher Order Mode

FM — Fundamental Mode

PM — Polarization Maintaining

OSA — Optical Spectrum Analyzer

LMA — Large Mode Area

FBG — Fiber Bragg Grating

MOPA — Master Oscillator Power Amplifier

TMI — Transverse Mode Instability

SBS — Stimulated Brillouin Scattering

SRS — Stimulated Raman Scattering

CHAPTER ONE

INTRODUCTION

This chapter presents a brief background of continuous wave (CW) high-power fiber lasers, challenges and limits of power scaling. Section 1.1 presents a brief review of high-power Yb, Er and Er/Yb co-doped fiber lasers. Section 1.2 presents the major challenges and limits of power scaling in high-power fiber lasers. Lastly, Section 1.3 concludes this chapter with an outline of the dissertation.

1.1 Background of high-power fiber lasers

The fiber laser is essentially just another type of solid-state lasers, with the gain medium being an optical fiber rather than a rod, a slab, or a disk. Fiber lasers have many advantages over conventional solid-state lasers due to their unique geometry and optical properties. Compared to its two other main industrial competitors, thin-disk laser and CO2 laser, a fiber laser does not require internal optics alignment and cleaning. This is a crucial cost-saving factor for industrial applications. Besides, a fiber laser also operates at much higher efficiency and running cost is, consequently, much less [1]. Other key advantages of fiber lasers include good (i.e. near-diffraction-limited) beam quality, high efficiency, high brightness, high reliability, good heat dissipation, broad wavelength range, turnkey operation, and compact size.

The development of fiber lasers goes all the way back to the good old days of 1960s when lasers were still called masers and consequently fiber lasers were initially called glass masers. The first glass laser was demonstrated by E. Snitzer using a Nd^{3+} doped glass in

1961 [2,3]. Shortly after, E. Snitzer and C. Koester reported a high gain Nd^{3+} doped fiber laser pumped by flash lamps [4]. But much of the further development and increased research interest on fiber lasers and amplifiers came in the 1980s, due to the demand for optical telecommunication which in turn led to the improvement of optical fibers and semiconductor diode lasers [5]. In 1986, Payne et al demonstrated the first single-mode fiber laser with an output power of ~1 mW which was realized using a single-mode Nd^{3+} doped fiber [6]. Power scaling of fiber lasers above watt-level really took off after the invention of double-cladding fibers and cladding-pumping technique [Fig. 1.1] using multi-mode diode lasers in 1988 by E. Snitzer et al [7]. Nonetheless, the record for single-mode (diffraction-limited) high-power fiber lasers was only 10 W by 1996. The next wave of research attention was directed to high-power fiber laser development after the burst of the telecom bubble around 2001[5]. A 1.36 kW single-mode Yb-doped fiber laser was

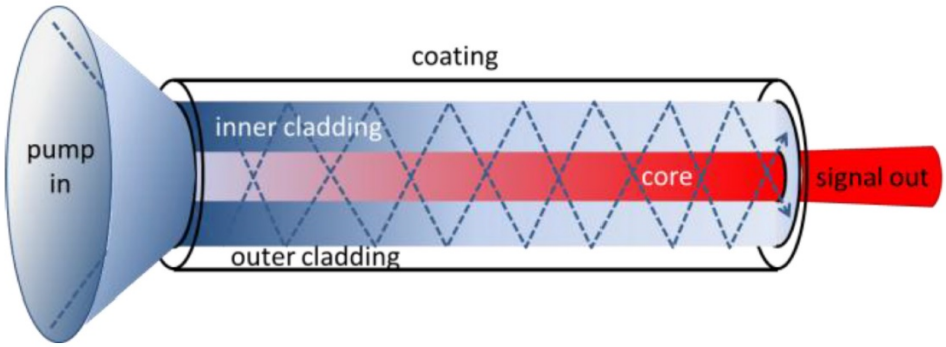

Fig. 1.1 Schematic of cladding pumping using a double-clad fiber end-pumped by a multi-mode diode laser, which results in a high brightness fiber laser output compared to the low brightness diode pump [8].

reported by researchers at the University of Southampton in 2004 [9]. The next big step was the use of master oscillator power amplifier (MOPA) architecture and tandem pumping

(i.e. using fiber lasers as pump sources) for high-power fiber lasers. As the need for further scaling of average power and pulse energy in fiber lasers increase, conventional large mode area (LMA) fibers faced difficulty in scaling core diameter above 30 μm without sacrificing beam quality. In the last decade or so, a great deal of research has been focused on developing specialty fibers with novel fiber designs, such as photonic crystal fibers (PCF), leakage channel fibers (LCF), photonic bandgap fibers(PBF), etc. [10]. In summary, besides the funding and market need, the development of continuous wave (CW) high-power fiber lasers is driven by the development of novel optical fibers, high-power diode lasers, fiber splice, fiber Bragg grating (FBG), cladding-pumping, and tandem pumping. There are many good review papers available on this topic for more detailed review of high-power fiber lasers and amplifiers[8,11–17]. There are several commonly used rare earth doped fibers, but the focus of this dissertation will be on Yb^{3+}, Er^{3+}, and $Er^{3+/}Yb^{3+}$ doped fiber lasers.

Silica glass based Yb-doped fiber lasers have become the workhorse of high-power fiber lasers in industry and defense. As briefly described earlier, the early days of fiber laser development was dominated by Nd^{3+} doped fiber lasers using flash lamp pumping [2,4]. However, Yb-doped fiber lasers reached a much better performance with the invention of cladding-pumping and the availability of higher and higher powers from commercial multi-mode diode lasers operating at 9xx nm.

The Nd^{3+} operates as a standard four-level system [Fig. 2.2] which can be pumped at 8xx nm with the early pumping schemes with flash lamps. However, Yb^{3+} has simple

two-level system which behaves like a three-level system at shorter wavelengths and four level (or quasi three-level) at longer wavelengths [18,19]. So, it is understandable that the

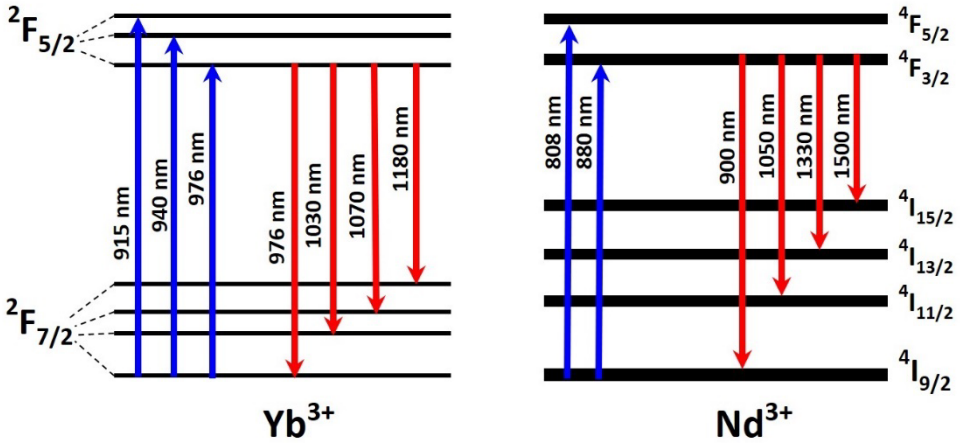

Fig. 1.2 Typical energy level diagram of $Yb^{3+}$and Nd^{3+} ions in silica glasses where the blue line arrows are the common pumping wavelengths and the red line arrows are the emission wavelength.

readily available high-power diode lasers at 9xx nm which matured in the late 1990s accelerated the power scaling of Yb-doped fiber lasers because of the much higher power density available compared to flash lamp pumps and early version of diode pumps. In addition, the development of high-power didoes also made the threshold level less important for Yb-doped high-power fiber lasers [20]. Other key advantages of Yb^{3+} fibers over its Nd^{3+} counterparts include small quantum defect, high active dopant concentration, strong pump absorption, and negligible excited state absorption (ESA). Thanks to the above developments, Yb-doped fiber lasers first reached the 110 W output power level in 1999 [21]. This marked the beginning of rapid development in power scaling of CW high-power fiber lasers. In 2004, the first 1 kW Yb fiber laser operating at ~1100 nm was demonstrated using a 43/600 μm core/cladding diameter double clad Yb-doped fiber

cladding-pumped by a high power diode stack at 975 nm [22]. By 2009, a 10-kW tandem-pumped single-mode Yb-doped high-power fiber laser operating at 1070 nm was reported by IPG Photonics [23].

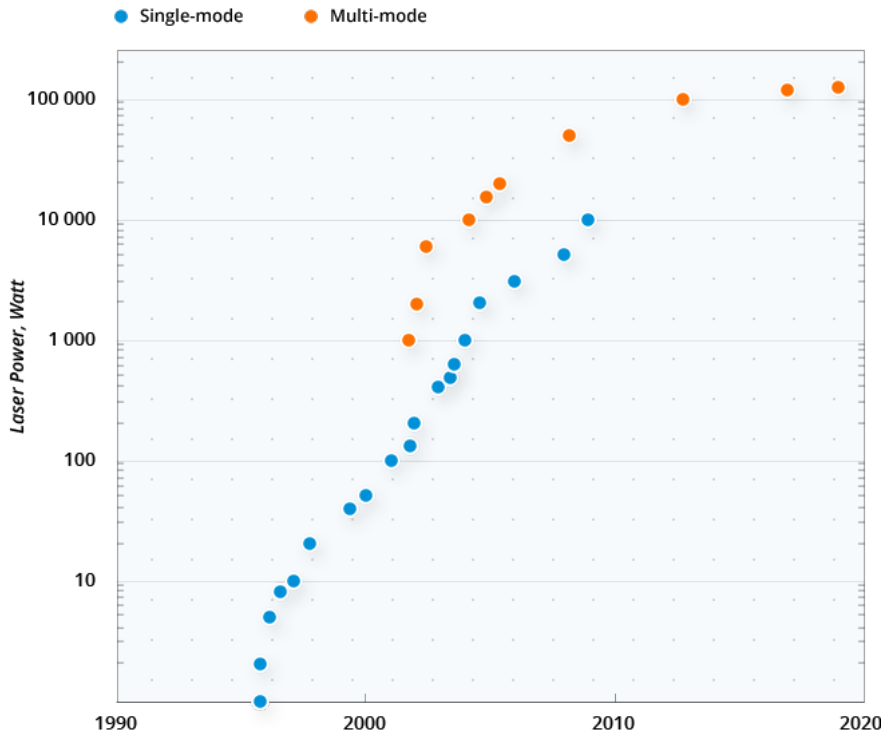

Fig. 1.3 The evolution of CW output power of single-mode and multi-mode commercial high-power Yb fiber lasers/amplifiers over the past 20 years or so [24].

So far, the highest CW output power from Yb-doped high-power fiber laser systems (including direct diode pumped oscillators and tandem pumped amplifiers) has been achieved at operating wavelength range 1060-1090 nm. In contrast, a Yb fiber laser operating at ~980 nm and ~1180 nm has not shown performance (output power and efficiency) anywhere near the multi-kW level power Yb fiber lasers at ~1.1 μm. In fact, the highest average output power from Yb fiber lasers operating at ~980 nm was only 94 W

by 2008 [25,26] and has only recently reached 151 W [27] in 2019 with the experimental result of our work to be detailed in Chapter 2 and 3. The current state-of-the-art results from Yb-doped fiber lasers operating at ~1180 nm was reported to be only ~40 W for a 976 nm direct diode pumped Yb fiber laser operating at 1178 nm and ~200 W for 1120 nm fiber laser pumped Yb fiber laser in random laser configuration operating at 1173 nm [17]. The difference between the performances of Yb-doped fiber lasers at various wavelengths

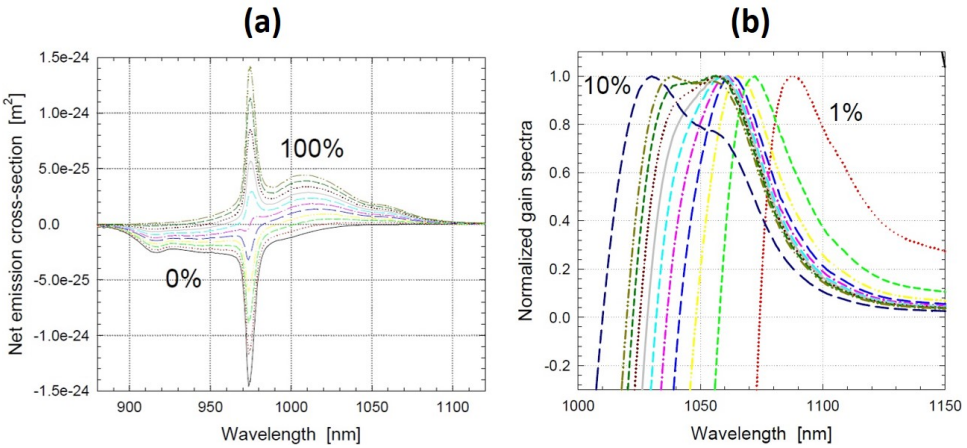

Fig. 1.4 Net emission cross-section (a) and normalized gain spectra (b) as a function of wavelength at various inversion for phospho-silicate Yb-doped fibers [28].

is directly related to the Yb gain spectra as a function of wavelength as shown in Fig. 1.4. The gain spectra can be written as [28],

$$G = \int_0^L g(z)dz \text{ and } g(z) = \Gamma N_0 \sigma_{net} \tag{1.1}$$

$$\sigma_{net}(\lambda) = \left[\sigma_e(\lambda) + \sigma_a(\lambda)\right] n_{fr} - \sigma_a(\lambda) \tag{1.2}$$

$$G_{dB}(\lambda) = 4.343 \Gamma L N_0 \sigma_{net}(\lambda) \tag{1.3}$$

where G_{dB} is the gain in dB unit, Γ is the overlap of signal mode with doped core area, L the is active fiber length, N_0 is the total number of ions (i.e. dopant concentration), σ_{net} is the net cross-section, σ_e is the emission cross-section, σ_a is the absorption cross-section, and n_{fr} is the fraction of total dopant ions averaged over the fiber, assumed to be constant along the fiber.

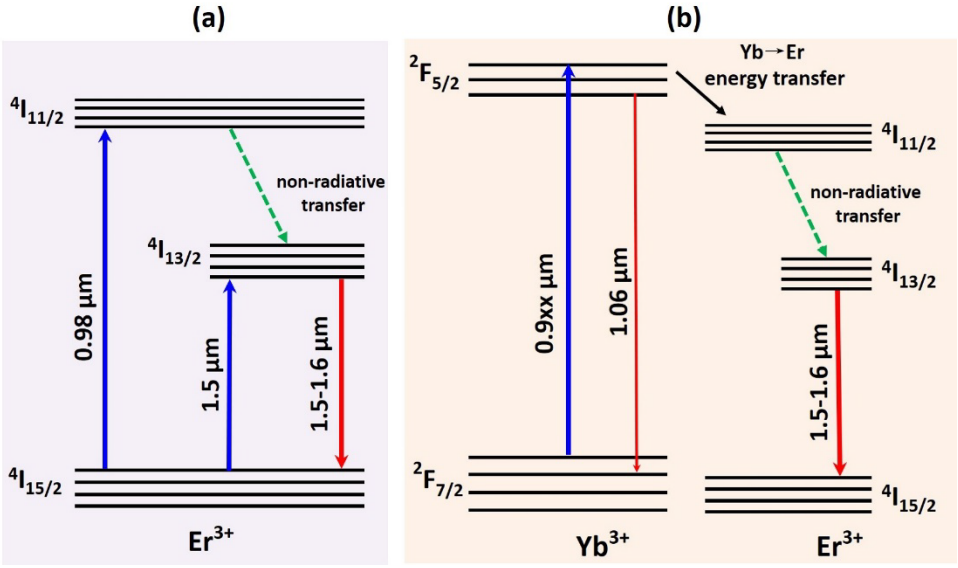

Fig. 1.5 Simplified energy level diagram of active ions in Er-doped (a) and Er/Yb co-doped (b) silica fibers. The blue and red arrows respectively show typical pumping (absorption) and laser (emission) wavelengths in each of the fibers.

Power scaling of fiber lasers operating at 1.5-1.6 µm has also been very slow compared to the ones operating at ~1.1. µm. The most common rare-earth doped fibers used for fiber lasers at this wavelength range are Er/Yb co-doped fibers or Yb-free Er doped fibers [Fig. 1.5]. Despite being one of the two most researched rare earth doped fibers together with the Nd^{3+} doped fibers in the early days of fiber laser development, the

development of Er^{3+} doped fibers for high power laser sources at 1.5-1.6 μm has lagged far behind the Yb fiber lasers at 1.1 μm due to several factors such as excessive heat load (caused by high quantum defect), low pump absorption, Er concentration quenching, etc. The highest reported average power from a diffraction limited single-mode fiber laser operating at ~1.6 μm was 207 W [29] and now it is 302 W [30] with our work to be covered in Chapter 5. The record multi-mode output power from a CW Yb-free Er-doped fiber laser was ~656 W [31]. The main issue with single-mode power scaling is the excessive ASE (or co-lasing) at ~1030 nm and limited pump absorption, respectively, for the Er/Yb co-doped fiber lasers and Yb-free Er-doped fiber lasers.

Ultimately, one needs to find the best compromise between various contradictory requirements to achieve power scaling with all the fiber lasers including single-mode fiber lasers operating ~0.98 μm and ~1.6 μm. For example, long fiber length is preferred for sufficient pump absorption and heat load mitigation, but a shorter fiber is desired for suppressing nonlinear effects. At the same time, a large core is preferred for increasing pump absorption and suppressing nonlinear effects, but core diameter is also limited by the single-mode operation requirement, i.e. $V = \frac{\pi d}{\lambda} NA \leq 2.405$, where d is fiber core diameter. In conventional large mode area (LMA) fibers, the core diameter is limited to below 20 μm in order to meet the single-mode operation requirement. A better fiber design is needed for power scaling in terms of both fiber geometry (i.e. waveguide structure) and host glass composition. Historically, improving fiber glass composition has played major role in increasing optical-to-optical efficiency, optimizing refractive index profile, and suppressing nonlinearity [19]. On the other hand, there has been much more focus on

designing fibers with better geometric structure (e.g. microstructured fibers) especially since the emergence of photonic crystal fibers (PCFs) in the late 1990s [32].

Solid-core photonic bandgap fiber (PBF) [33–35] based LMA fibers are another milestone in the power scaling of sing-mode high power fiber lasers. This kind of microstructured fibers have enabled robust single-mode operation in fibers with very large core diameters (>50 μm). In 2015, Gu *et al.* reported a novel type of all-solid Yb-doped PBF based on multiple cladding resonance (MCR) [36]design that enables robust single-mode operation with a record mode area of ~2650 μm^2 and core diameter of 100 μm [37,38]. The main advantage of the novel MCR design used in this type of PBF is to better suppress HOM by coupling HOMs from the main center core to the cladding cores. Light is guided due to the photonic bandgap effect of photonic crystal cladding in a PBF and light transmission is highly wavelength dependent. The bandgap position of the MCR-PBF can be easily scaled (by changing fiber dimensions) for ASE suppression and laser operation at different wavelengths. This types of PBF can not only act as a broadband bandpass spectral filter to suppress ASE, but also has the potential to further increase power scaling threshold of fundamental nonlinear effects such as transverse mode instability (TMI) [39,40]. We have successfully obtained record output power and efficiency in diffraction-limited Yb-doped fiber laser operating at ~980 nm [41,42]. In addition, research on the power scaling of high-power narrow-linewidth single frequency Yb-doped fiber laser operating at 1064 nm has been undergoing using a in-house fabricated MCR-PBF tailored for suppression of ASE at ~1030 nm and superior HOM suppression to increase TMI threshold above 1-kW level.

1.2 Major challenges in power scaling

1.2.1 Single-mode operation

Single-mode (i.e. diffraction-limited) operation is one of the most critical requirements of power scaling high-power fiber lasers. There are many applications as shown in Fig. 1.6 that require lasers with very good mode quality, i.e. single-mode output.

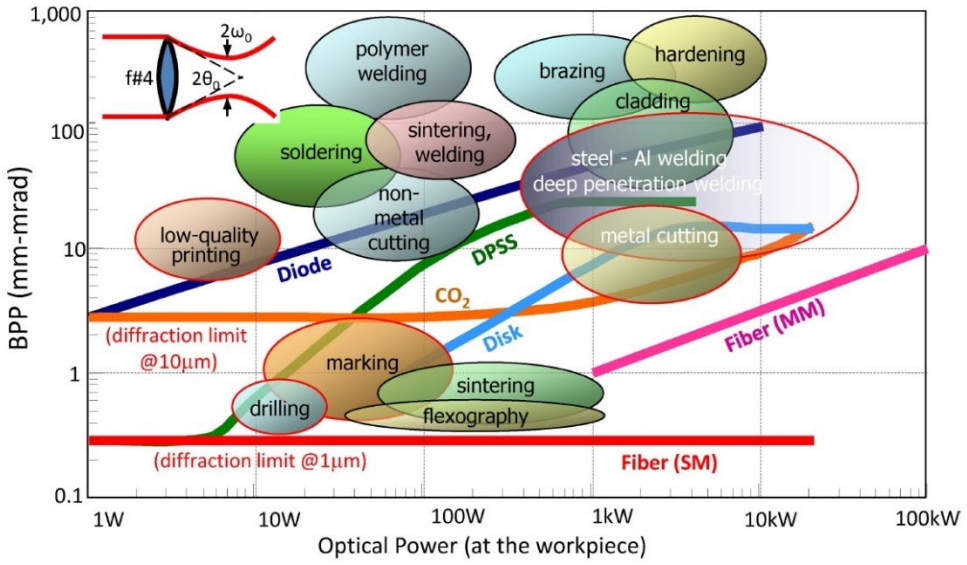

Fig. 1.6 BPP and average output power requirements for various laser application and BPP versus average output power for many industrial lasers [9].

But before we go into the details of how to optimize single-mode laser generation, it is worth clarifying the definition of single-mode and how it's characterized. The single-mode requirement for conventional fibers states that a fiber laser is operating at a single transverse mode when the V number is below the cut-off V value of LP_{01} fundamental mode, i.e. $V = \frac{\pi d}{\lambda} NA = 2.405$. In experiments, the beam quality of a laser is measured by

M^2 (pronounced as M-squared) beam quality (or beam propagation, according to A. E. Siegman [43]) factor and beam production parameter (BPP) defined as [8,44],

$$M^2 = \frac{\pi}{\lambda}\theta w_0 = \frac{\pi}{\lambda}\cdot BPP_{laser} = \frac{BPP_{laser}}{BPP_{ideal}} = \left(\frac{\theta w_0}{\theta_{ideal} w_{ideal}}\right) = \left(\frac{w_0}{w_{ideal}}\right)^2 \tag{1.4}$$

where θ is the divergence half angle of the laser beam at far field, w_0 is the beam waist radius of the laser beam, BPP_{ideal} is the BPP for an ideal Gaussian beam, and BPP_{laser} is the BPP for the measured laser beam. Both M^2 and BPP values indicate how well a laser beam can be focused or how much the measured laser beam deviates from a perfect Gaussian beam (TEM_{00}). The lower the M^2 or BPP the better the output beam quality for the measured laser. A laser beam is called diffraction-limited when beam quality is equal or close to M^2=1 (no unit) and/or $BPP_{laser} = \frac{\lambda}{\pi}$ (unit is mm-mrad). In this case the laser beam waist of the focused beam spot is the smallest it can be for a given wavelength due to diffraction of light. In industry, M^2 value is mainly used to indicate the beam quality of a single-mode laser, while BPP is given in case of multi-mode lasers such as fiber-coupled high-power diode lasers, etc. In the literatures, the term diffraction-limited and single-mode are used interchangeably to describe fiber lasers with close to perfect beam quality with $1 < M^2 \leq 1.3$. There are several different methods to obtain M^2 value by measuring beam width of a laser beam at several positions (preferably 7~10 data points) along the focused beam waist position. Among them the internationally recognized standard method ISO 11146 measures beam width based on second moment width (4Dσ) method [43]. A commonly used curve fitting equation for M^2 measurement can be written as follows [44],

$$w(z) = w_0^2 + \left(\frac{M^2\lambda}{\pi w_0}\right)^2 (z - z_0)^2 \tag{1.5}$$

where $w(z)$ is the beam radius at z distance along the beam center, z_0 is the position of the beam waist. Although M^2 is commonly used to quantify how good the laser beam is, it does not tell the exact contents of the fundamental mode and HOMs in the measured laser. Having both the mode image at the beam waist position and the corresponding curve fitted M^2 value does help further validate the beam quality of the measured laser. Nevertheless, two other alternative techniques including S^2 and C^2 are used when there is a need to better resolve the modal contents of the laser beam [10].

The use of LMA fibers in power-scaling of fiber lasers did come with several advantages such as higher pump absorption, higher pump coupling efficiency, increasing optical damage and nonlinear thresholds, etc. At the same time, conventional LMA fibers cannot always ensure single-mode operation due to large core diameter. Several techniques have been used to ensure single-mode operation in a slightly multi-mode (or so called few-mode) LMA fibers, including lowering core NA, utilizing mode-dependent bending loss with tight coils, optimizing dopant overlap for preferential gain to FM, etc. However, these approaches are somewhat limited in further single-mode power scaling. For example, small NA (<0.1) can lead to poor FM guiding in the core and mode scattering from the FM to HOMs due to small refractive index difference between the core and cladding [13]. On the other hand, significant improvement haven been achieved with the advent of micro-structured fibers with large core and broad “endlessly” single-mode operating range due to specialty waveguide design. The first of such fibers is photonic crystal fiber (PCF) which

was reported by J. C. Knight et al in 1996 [32]. Since then many variations of these specialty fibers have been developed including leakage channel fiber (LCF) [45], chirally coupled core (CCC) fiber [46], photonic bandgap fiber (BPF) [38], etc.

1.2.2 Stimulated Raman and Brillouin scattering

One of the advantages of fiber lasers over bulk crystal solid state lasers is superior heat dissipation because of the large surface area to volume ratio benefited from long fiber length. At the same time, the long fiber length is also a limitation to further power scaling due to nonlinear effects such as stimulated Raman scattering (SRS), stimulated Brillouin scattering (SBS), four-wave mixing (FWM), and self-phase modulation (SPM). Among them the SRS and SBS are the most critical limiting factor for CW high-power fiber lasers. Both SRS and SBS are related to inelastic nonlinear process and involve interaction of light with respectively acoustic waves in the fiber and phonons originated from the vibration of glass lattice. In most of the efficient high-power fiber lasers, the threshold power of SRS is much higher than SBS. The threshold powers for SRS and SBS can be estimated by the following equations [13,19],

$$P_{th}^{SRS} \approx \frac{16 A_{eff}}{g_R L_{eff}} \tag{1.6}$$

$$P_{th}^{SBS} \approx \frac{21 A_{eff}}{g_B L_{eff}} \tag{1.7}$$

where A_{eff} is the effective mode area of the guided mode, g_R is the peak Raman gain coefficient, g_B is the peak Brillouin gain coefficient, and L_{eff} is the effective fiber length.

Unlike SBS, SRS becomes a major problem in broadband lasers and the scattered signal light can propagate in both forward and backward directions. In contrast, SBS becomes a major limit in narrow-linewidth ($\Delta\nu_L \ll \Delta\nu_B$) single-frequency fiber lasers and the scattered signal light only propagates in the backward direction.

The approaches to mitigate SRS and SBS involve novel fiber designs with both new waveguide structures and optimized materials. A detailed description of mitigation methods can be find in the literatures [8,13,16,19,47]. From Eq. (1.6) and (1.7), it can be easily seen that designing novel fibers with large mode area increases threshold power for both SRS and SBS. This is where previously discussed LMA fibers (especially the micro-structured LMA fibers) with optimized waveguide structure plays a major role in mitigating nonlinear effect while ensuring single-mode operation. Large core not only lowers the laser intensity but also shortens the fiber length (hence L_{eff}) due to increased pump absorption. In addition, lowering the gain coefficients g_R and g_B by optimizing host glass composition also increases threshold powers for SRS and SBS. There are several techniques to lower g_B including tailoring acoustic velocity profile of the fiber, broadening laser linewidth, broadening Brillouin gain linewidth, optimizing gain profile of the active core, actively applying temperature and/or stress gradient along the fiber, etc.

1.2.3 Transverse mode instability

Transverse mode instability (TMI) [39,40,48–50] and SBS are the two major challenges limiting the average output power when it comes to power scaling of high-power fiber lasers. TMI is known to be a nonlinear process that leads to a sharp and rapid

beam quality deterioration above certain average power level in high-power fiber lasers, due to a phase-matched mode coupling between the fundamental mode (FM) and HOMs. This phase-matched mode coupling is in turn originated from the thermally induced refractive index change, and eventually leads to a positive feedback cycle between mode interference pattern and refractive index grating. The phenomenon was observed experimentally for the first time by Eidam et al in around 2010 [39], although the root cause of TMI is Stimulated Thermal Rayleigh Scattering (STRS) [50] which was first observed in the 1960s.

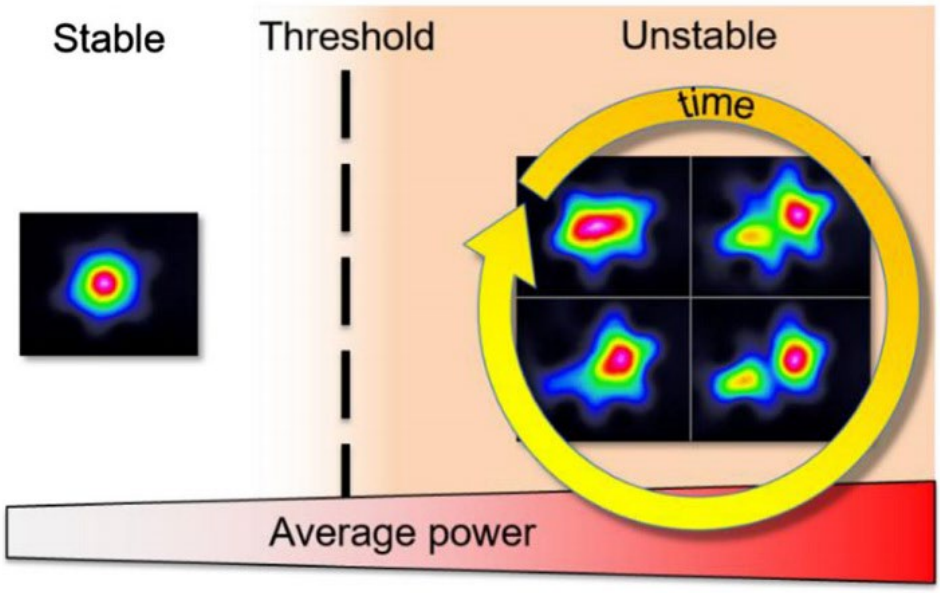

Fig. 1.7 Schematic representation of TMI [40].

TMI is a nonlinear process, but unlike SRS and SBS, it is not triggered by peak intensity of the laser but instead average power. As show in Fig. 1.7, at certain threshold average power the mode-coupling leads to time-dependent power transfer between FM

(LP_{01}) and HOM (initially LP_{11}). The fiber laser goes through three distinctive states during TMI process, including stable state, transition state and chaotic state [40]. The average power threshold power limited by TMI ranges from several 100W to multiple kW depending on the fiber design and laser configuration. In the experiment, TMI threshold is identified by steep and sharp deterioration of M^2 or standard deviation of photodiode traces of the laser output. The TMI threshold power can be estimated by the following equation [19,50],

$$P_{th}^{TMI} \propto \frac{\rho c_p}{dn/dT}\left(\frac{\lambda_s}{\lambda_p}-1\right)\mathbb{F} \tag{1.8}$$

or by another slightly different version written as [51],

$$P_{th}^{TMI} = \frac{\kappa U_\varepsilon^2\left(U_\varepsilon^2 - U_\varepsilon^2\right)}{2\pi n_{eff}\left[\eta_{heat}/(\eta_{laser}L)\right](dn/dT)}\left(\frac{\lambda_0}{d_0}\right)^2 \tag{1.9}$$

where dn/dT is the thermo-optic coefficient related to the material properties of the glass, ρ is the mass density, c_p is the specific heat and the definition of rest of the parameters can be found in [19,51]. The Eq. (1.8) and (1.9) both look rather complicated but the main limiting factors can be summarized into three aspects: host glass material, fiber waveguide design and quantum defect heat. There have been several approaches to suppress TMI and to increase TMI threshold power in high-power fiber lasers. From the material point of view, the thermo-optic coefficient dn/dT can possibly be reduced with appropriate choice of materials by combining materials with negative and positive values of dn/dT [19]. In terms of quantum defect heat, using tandem pumping rather than direct-diode pumping

does help decreasing heat load and it has been shown that TMI threshold increases in this case. Nevertheless, both approaches have certain limits and restrictions.

On the other hand, mitigating TMI with carefully designed fiber waveguide structure have been shown to be effective and promising. As noted in [19], the main factor that makes TMI a problem in fiber lasers at the first place is the compromised single-mode operation in LMA fibers which usually operate under few-mode if not multi-mode condition. In fact, it has been reported that there is no TMI effects observed in fibers with core diameter of 20 μm or less [51]. One of the key techniques that have been used to suppress TMI is to optimize HOM suppression, i.e. ensure single-mode operation, by utilizing specialty fibers such as all-solid PBF [52], etc. A new type of all-solid PBF[37,53] based on MCR design has been reported to enable further HOM suppression. The ultimate TMI threshold power on average output power of fiber lasers have been estimated to ~35 kW in case of diode pumping and ~80 kW for tandem pumping [40,51].

1.3 Outline of the dissertation

This dissertation is divided into seven chapters, which is organized into three main parts. Part I only consists of Chapter 1, Part II- consists of Chapters 2 to 6, and Part III is basically the last chapter, Chapter 7. The main findings and results of this dissertation are presented in Part II, which consists of three distinctive projects. The Chapters 2 and 3 present the results of the Project I, which is about the single-mode high-power Yb-doped fiber laser operating near 980 nm. The Chapters 4 and 5 present the results of Project II, which is about the near diffraction limited high-power Er/Yb co-doped fiber laser/amplifier operating at ~ 1560 nm. The Chapter 6 presents the latest results of the Project III, which

is about the narrow-linewidth single-frequency Yb-doped fiber laser/amplifier operating at 1064 nm. The following is a short overview of each individual chapters.

Chapter 2 starts with a short introduction of single-mode high-power three-level Yb fiber laser at ~980 nm. After a brief state-of-the-art chronological review of the previous work, the motivation of using all-solid photonic bandgap fiber (AS-PBF) design for power scaling is presented. Then it provides characterization results of the novel Yb-doped AS-PBFs, including the PM and non-PM ones. The chapter continues with the experimental results with the PM Yb-doped AS-PBF and non-PM Yb-doped AS-PBF, respectively, with 53% and ~63% output slope efficiency. The simulation overlaps fairly well with the experimental results. In addition, the chapter provides a detailed analysis of the output power, slope efficiency and mode quality facture (M^2) by comparing the PM and non-PM AS-PBF in terms of their bandgap structure (i.e. ASE suppression and single-mode guiding), Yb concentration (i.e. pump absorption), background loss, etc. Lastly, the chapter concludes with the record-breaking result of 84 W output power and slope efficiencies of 63% and 94%, respectively, with regards to the launched and absorbed pump power.

Chapter 3 describes the next half of the same project presented in Chapter 2. The same non-PM Yb-doped AS-PBF is used to build an all-fiber three-level Yb fiber oscillator operating at ~980 nm. This chapter begins with a short background and motivation of all-fiber Yb-doped fiber lasers, and it provides a brief chronological stat-of-the-art review of all-fiber three-level Yb-doped fiber lasers. Unlike the 94 W previously reported output power record from free-space (i.e. with bulk optics) three-level Yb-doped fiber lasers at ~980 nm, record results from all-fiber three-level Yb-doped fiber lasers at ~980 nm were

only ~20% slope efficiency and ~10 W output power. This was mainly due to the lack of a suitable flexible (i.e. cladding diameter ~125 μm) Yb-doped fiber for high slope efficiency and ASE suppression. With the help of readily available commercial high-power pump combiners and 200 W pump diodes at 915 nm, the same non-PM AS-PBF yields an near diffraction limited output power ~150 W which is ~15 times higher than the previous record from an all-fiber laser architecture at ~980nm.

Chapter 4 reports the numerical simulation of Er/Yb co-doped fiber lasers/amplifiers, which is part of our benchmarking study about the double clad Er/Yb co-doped fibers and near diffraction limited high-power fiber lasers operating at ~1.6 μm. It provides a short introduction and background of Er/Yb fibers in generating laser near 1.6 μm. Further, the chapter presents a brief review of modeling and experimental work which especially focuses on the resonant energy transfer process between the Er and Yb ions. The main point of interest is the role of isolated (i.e non-coupled) Yb ions in the process of continued increase of laser at ~1.6 μm even after the pump power exceeds the laser threshold of the co-lasing at ~1.1 μm due to high Yb inversion. This phenomenon was previously explained based on elevated fiber temperatures at high powers, which leads to increased re-absorption Yb emission. However, the chapter presents our new numerical model which shows that continued increase of Er emission ~1.6 μm can be better explained by incorporating the scenario of two types of Yb ions, i.e. couple Yb ions and isolated Yb ions. The simulation results also show that elevated fiber temperature plays insignificant role. Lastly, clamping of Er emission at ~1.6 μm due to Yb→Er energy transfer

bottlenecking will eventually occur in any Er/Yb co-doped fiber, albeit at much higher pump powers when the fraction of isolated Yb ions is very small.

Chapter 5 reports mostly the experimental work on the diffraction limited high-power Er/Yb fiber master oscillator power amplifier (MOPA) operating at ~1562 nm. It begins with brief review of previously reported experimental work on generating ~1562 nm laser using Er/Yb co-doped fibers and Yb-free Er-doped fibers. The amplifier was built using a double clad large mode area 25/300 μm Er/Yb co-doped fiber (LMA-EYDF-25P/300-HE) purchased from Nufern. Our experimental results show that there is negligible Yb ASE at ~1.1 μm, which means Er emission clamping threshold of this Nufern fiber is much higher than the Er/Yb co-doped fiber reported by researchers at Southampton University. This can be explained based on the new model presented in Chapter 4 and comparing the core glass composition of the Er/Yb co-doped fiber from Nufern and Southampton. Lastly, we have found that further power scaling is no longer limited by Yb ASE but fiber fuse due to excessive heat load.

Chapter 6 presents our experimental work on narrow-linewidth single-frequency Yb-doped photonic bandgap fiber (PBF) MOPA at ~1064 nm. We went through two iterations of novel ultra large core PBF based on multiple cladding resonance (MCR cladding) design. The second iteration Yb PBF has a core diameter of ~56 μm and cladding diameter of 401 μm. A detailed fiber characterization and preliminary MOPA tests show that the ASE near ~1030 nm is very well suppressed by ~45 dB. Output power of the MOPA reached ~500 W without any signs of SBS at slope efficiency of ~90% and 80% respectively corresponding to the absorbed and launched pump power. The linewidth of

the single-frequency laser did not show any broadening at high MOPA output power and it was measured to be consistently ~10 kHz which is the nominal linewidth of the seed laser. The backward power and spectrum were also monitored to detect any backward scattered SBS-shifted Stokes light. Lastly, the mode quality (M^2) were measured at various MOPA output power, and a clear dynamic mode interference between the FM and HOM were captured using high resolution camera of the M^2 device. This shows that the MOPA output was only limited by TMI at MOPA output power of 503 W or above. Further investigation on TMI dependence of seed launching, coiling diameter of the Yb PBF, fiber length, etc. will be conducted for further mitigation of TMI.

Chapter 7 begins with a brief summary of the work presented in previous chapters. Further, it presents a short overview of the scientific and engineering contribution of the work accomplished during my Ph.D. at Clemson University. Lastly, the dissertation ends with an outlook and potential application of the dissertation work.

CHAPTER TWO

FREE-SPACE YTTERBIUM PBF LASER ~980NM

This chapter presents the use of all-solid photonic bandgap fibers for efficient three-level cladding-pumped Yb fiber lasers. A new record efficiency of 62.7% has been obtained with regard to the launched pump power at ~915 nm for Yb three-level double-clad fiber lasers with a single-pass pump. The efficiency with regard to the absorbed pump power was ~94%, only limited by quantum defect. Diffraction-limited power of 84 W at ~978 nm was achieved, only limited by the available pump power at 915 nm. M^2 at ~80 W was measured to be ~1.12.

2.1 Introduction

There are two major operating wavelength regimes arise from the two energy manifolds (i.e. $^2F_{7/2}$ and $^2F_{5/2}$) for Yb fiber lasers : three-level operation regime near 970-980 nm and four-level operation regime near 1030-1200 nm [54]. In general, lasing with three-level system requires much higher pump power (i.e. higher ground state inversion) than four-level system because the ground state in this case also serves as the lower laser level of the three-level system. In fact, due to the intrinsic absorption and emission cross-sections of Yb^{3+} ions, Yb fiber lasers operating at three-level regime requires at least 50% ground state inversion to have a positive net gain, while only ~5% inversion is enough to start lasing at four-level (or quasi three-level) regime [18,55].

In the early days of fiber lasers, the main pumping technique that used for Yb doped fiber lasers was core-pumping, and the output power was only ~10 mW at ~980 nm and

~30 mW at ~1100 nm [56,57]. The watt-level output power from Yb fiber lasers came only after the invention of the cladding pumping scheme and double-clad fiber by E. Snitzer in 1988 [7]. In 1993, L. Zenteno numerically studied and predicted the possibility of obtaining tens of watts of power from laser-diode-pumped double-clad fiber lasers [58]. Unfortunately, cladding pumping scheme with conventional double-clad fibers [Fig. 2.1(a)] prefers four-level laser operation than three-level due to small overlap between the doped core and the pump cladding [59,60]. Nonetheless, core-pumping was not a viable solution for further power scaling of output power near 980 nm due to the unavailability of high power single mode pump sources near 9xx nm, although this method allows the use of very short length of Yb fiber to mitigate amplified spontaneous emission (ASE) and parasitic lasing near 1030 nm or above [60].

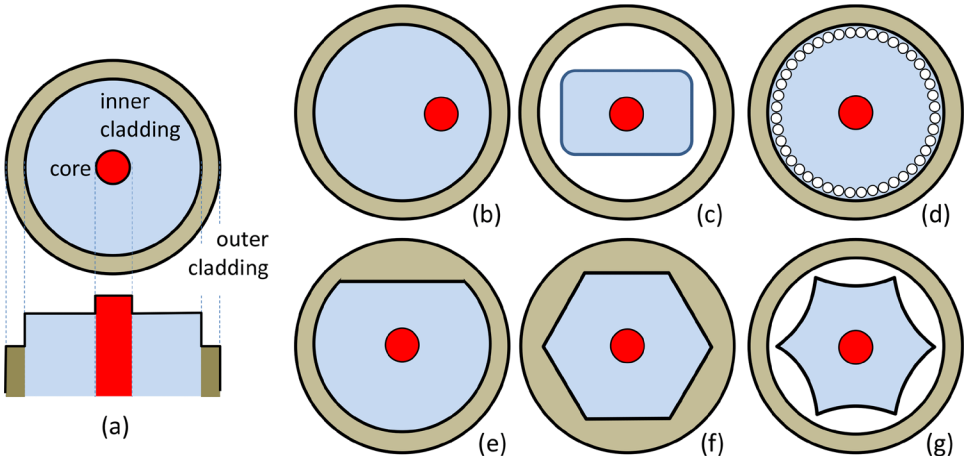

Fig. 2.1 Cladding pumped fiber cross section shapes, (a) circular cladding fiber cross-section , (b-g) various non-circular cladding shapes used for cladding perturbation to improve pump absorption [8].

In order to tackle the aforementioned problem with generating near 980 nm laser with double-clad fiber, various approaches had been used to increase pump absorption and filtering ASE near 1030 nm. There are usually two major ways to improve performance of

Yb fiber lasers: improving host glass composition and improving fiber design. Historically, the latter has played more significant role when it comes to diode laser pumped double-clad high-power fiber lasers. In order to improve cladding pump absorption in double clad fibers, various non-circular cladding fibers [Fig. 2.1 (b-g)] were used in the past [8].

However, simply increasing cladding pump absorption is not enough to realize efficient high-power single-mode fiber laser near 980 nm. There are a couple of extra factors need to be considered when it comes to improving performance of single-mode high power Yb fiber lasers near 980 nm, including mitigation of ASE, HOM, photodarkening, nonlinearities, etc. A number of different types of fiber designs were reported to address some of these issues to certain extent, including ring-doped-core fiber [59], large mode area (LMA) fiber [61], jacket air cladding (JAC) fiber [55], photonic bandgap fiber (PBF) [62], etc. Among these specialty fibers, the large-mode-area all-solid photonic bandgap fibers have unique potential to address the majority of the main challenges [63–66].

Using all-solid photonic bandgap fibers provides two major benefits. Firstly, they allow robust single-mode operation of coiled fibers at large core diameters and therefore enable a large core-to-cladding ratio. Secondly, they also provide efficient suppression of the four-level system by placing these lasing wavelengths outside the transmission bandgap. Our recent work on fiber designs has led to significant progress in robust single-mode operation at large core diameters in this type of fibers [37,38,67,68].

2.2 Motivation and background

The three-level system of Yb fiber lasers at ~980 nm has attracted much attention in the past two decades. The initial interest in the late 1990s was largely driven by the need for higher pump powers for the increasing power-demand of erbium-doped fiber amplifiers. Recent interest is mostly in pumping ultrafast solid-state and fiber lasers. Such lasers are critical for rapidly emerging micro-machining applications. Peak powers in these lasers are limited by optical nonlinearities, which can be overcome by using shorter lasers. Solid-state lasers and core-pumped fiber lasers are powerful approaches to mitigate optical nonlinearities. Diffraction-limited pump powers at ~980 nm of at least a few tens of watts are required for these applications. In addition, 980 nm fiber lasers can also be frequency-doubled to 490 nm for many other applications including pumping Ti: Sapphire lasers near their peak absorption and underwater communications and sensing.

To achieve the required power of over a few tens of watts for the abovementioned applications, cladding-pumping is necessary. The major limit to the efficient operation of cladding-pumped three-level Yb fiber lasers ~980 nm is the competing four-level systems operating at longer wavelengths of ~1030 nm as shown in Fig. 2.2. The four-level system has much higher gain at low inversions. To suppress its operation, higher inversion is required and must be maintained throughout the fiber, causing a large amount of the pump to leave the fiber. It has long been recognized that a large core-to-cladding ratio is the key to efficient three-level fiber lasers [21]. A given inversion is maintained largely due to the competing effects of pumping and stimulated emission rates, which are determined by the pump and signal intensities once the absorption and emission cross sections are fixed. A

relatively smaller pump waveguide leads to lower pump power leaving the fiber for a given pump intensity. Since single-mode operation sets an upper limit on core diameter, the need for a large core-to-cladding ratio sets an upper limit on cladding size and consequently available pump powers.

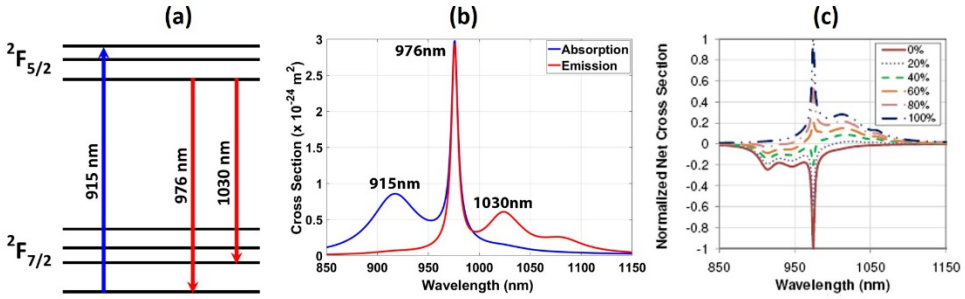

Fig. 2.2 (a) Typical energy level diagram of Yb^{3+} ions in silicate glasses , (b) typical absorption and emission cross sections of Yb^{3+} ions, (c) net cross sections of Yb^{3+} ions at various inversion levels [70].

In an early demonstration [71], 48% efficiency with regard to the coupled pump power was achieved in a Yb double-clad fiber. The core diameter was 11 μm and the pump waveguide was a rectangle of 32 μm x 16 μm. This small pump guide provided a large core-to-cladding ratio, but severely limited available pump powers, achieving only ~1 W at ~978 nm. The pump was also double passed in this case. In another demonstration [72], 4.5 W was achieved at 977 nm with an efficiency with regard to the coupled pump power of ~41%. In this case, air-cladding was used to increase the coupled pump power by increasing the NA of the 25 μm pump waveguide. In a recent demonstration [73], 25% efficiency and 5.5 W at 977 nm were achieved in a fiber with a core diameter of 28 μm and a square pump guide of 80 μm x 80 μm. In another more recent work from the same group [74], a fiber with a 20 μm core diameter and a square cladding of 80 μm x 80 μm was

tapered to 50 μm x 50 μm in the middle. 10.6 W at 976 nm and an efficiency of 18.4% was achieved. The record in both power and efficiency were set in a rod-type photonic crystal fiber with a core diameter of 80 μm and a pump waveguide diameter of 200 μm. CW output power of 94 W at 977 nm, efficiency of 48% and M^2 of 1.2 were achieved [25]. The pump was of double-pass configuration in this case. Using the same fiber, higher efficiencies of 53% and 63% were achieved for single and double pass pump respectively, but M^2 was ~1.2 only for output power below 25 W [26]. At the highest power of 95 W, the M^2 was only 2.2. This large core cannot be bent, and the fiber must be kept straight. A significant drawback of rod-type fibers is its incompatibility with monolithic fiber lasers which ensures compactness and robustness.

The use of all-solid photonic bandgap fibers for three-level Yb fiber lasers has been reported before [62]. In a core-pumped arrangement with a mode field diameter of just 3.4 μm, the output power was only ~140 mW even though the efficiency was 65.8%. In double-clad configurations, there have been reports of using Yb all-solid photonic bandgap fibers for high-power lasers above 1150 nm [75,76].

Another issue with Yb fiber lasers is photo-darkening. This can be especially bad for three-level Yb fiber lasers due to their high population inversions. A high Al to Yb ratio [74,77] or Ce and Al doping in the core [78] can be used to mitigate photo-darkening. Our active glass is made of a Yb-doped phosphosilicate glass, which has shown some of the best photo-darkening suppression [70]. We have used the same fibers for the operation at ~980 nm for a few hours daily over a few months without noticeable change in performance. Our lasers have also consistently demonstrated near quantum-limited

efficiencies versus absorbed pump powers, another testament to the low background loss, including low photo-darkening loss of our fibers.

2.3 Yb-doped all-solid photonic bandgap fiber

In all-solid photonic bandgap fibers (AS-PBFs), the cladding consists of periodically arranged high-index Ge-doped rods, and the core is firmed by omitting one or more high index rods [34,38,79]. For an active ion doped AS-PBF, the core is created by replacing the pure silica rods by rare earth doped silica rods as shown in Fig. 2.3.

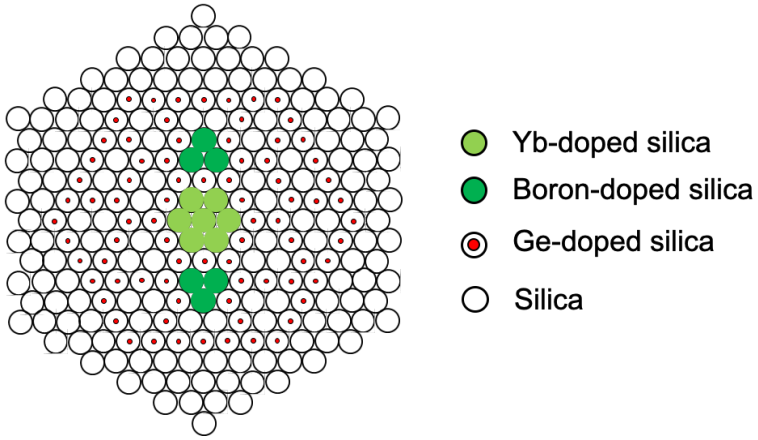

Fig. 2.3 Illustration of stack layout design of the preform for the PM AS-PBF.

We have been refining designs for single-mode large-core AS-PBFs in the past few years [37,67,68]. There are three major features of the Yb-doped AS-PBF used in this work that is worth emphasizing. First, the AS-PBF cladding design is based on the multiple cladding resonance (MCR) design [Fig. 2.4], which had previously proven to be the most effective design in introducing differential mode loss to suppress HOM and ensure single-mode operation in large mode area AS-PBF [37]. Second, the core of the AS-PBF is made from Yb-doped phosphosilicate glass with negligible photo-darkening [70]. Third, the bandgap of the AS-PBF is designed and fine-tuned such that loss near 980 nm is extremely

low while transmission loss at near 1030 nm or above is very high, which greatly increases 980 nm output efficiency and introduces sufficient ASE suppression near 1030 nm or above. That means the bandgap structure in the Yb-doped AS-PBF acts as a distributive spectral filter [35], thus eliminating the need of extra bulk optics for ASE suppression in the laser cavity.

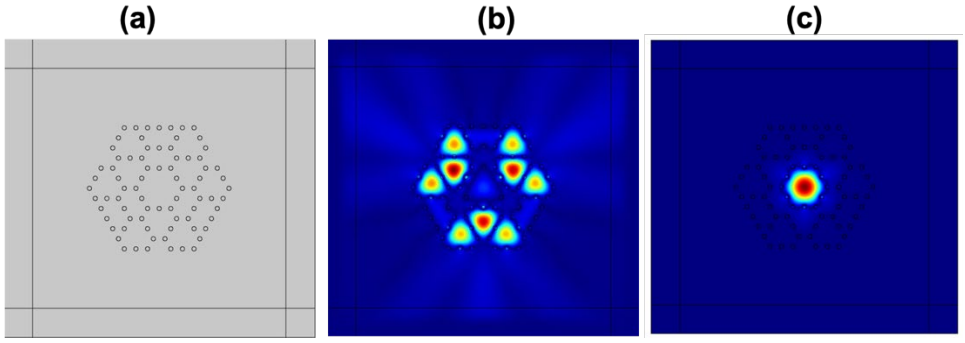

Fig. 2.4 Illustration of mode guiding in the PBF: (a) fiber cross-section for COMSOL simulation, (b) one example of the lossy HOM leaking into the cladding, (c) fundamental mode guided in the center core.

We started this project with a goal of building a lineally polarized diffraction-limited high-power Yb fiber laser near 980 nm. Thus, the first iteration Yb-doped AS-PBF has polarization maintaining (PM) structure incorporated in the microstructure cladding by introducing low-index boron-doped rods as the stress element [Fig. 2.3]. We also fabricated a second iteration PM AS-PBF from the same fiber preform, but the second batch PM fiber has smaller fiber dimensions, i.e. bandgap position is shifted towards shorter wavelength. Subsequently, a third iteration AS-PBF was drawn, but this time the PM structure was removed and higher Yb concentration core glass was used. In the end, we found that the non-PM AS-PBF performs much better than its PM counterpart, i.e. the PM AS-PBF, in terms of both efficiency and mode quality.

2.3.1 Characterization of the PM Yb PBF

In the process of optimizing fiber design and fabrication, we went through multiple iterations of passive and active fiber fabrication. The first iteration PM Yb-doped AS-PBF [Fig. 2.5(a)] has a core with corner-to-corner diameter of 26 μm and flat-to-flat diameter of 23 μm, and the cladding has a corner-to-corner diameter of 146 μm and flat-to-flat diameter of 135 μm. To study and refine the bandgap position for signal and ASE, we measured the spectral transmission [35] of the active fiber as shown in Fig. 2.5(b). The sharp dip near 980 nm is due to absorption at ~980 nm which corresponds to the peak of the absorption cross-section as in Fig. 2.2(b). This transmission spectra also shows that the long wavelength edge of the signal bandgap is 1100-1150 nm, instead we wanted the bandgap long wavelength edge positioned near 1030 nm. This is to enable low loss near 980 nm and very high loss near 1030 nm and above. Next, we aimed for smaller fiber dimensions in order to move the bandgap edge towards shorter wavelength.

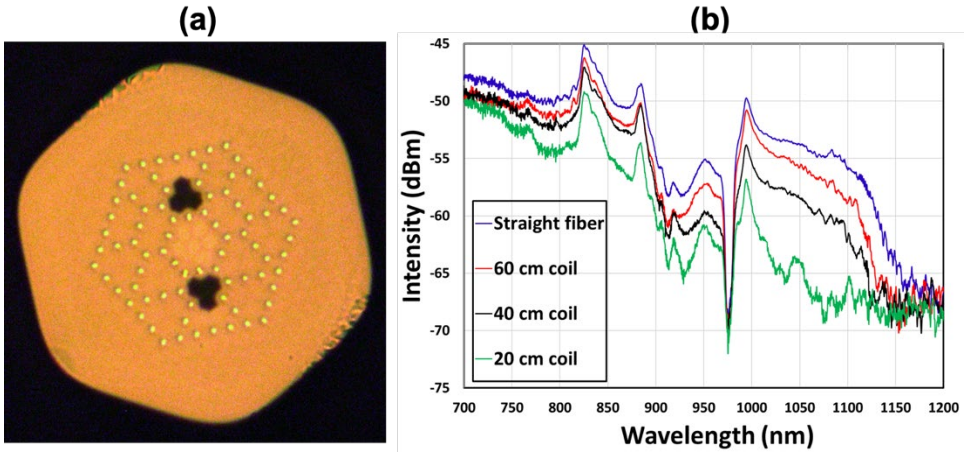

Fig. 2.5 (a) Microscope image of the first iteration PM AS-PBF cross section, (b) spectral transmission of first iteration active PM Yb-doped AS-PBF measured with low-power broadband white light source.

The cross section of the second iteration PM Yb-doped AS-PBF is shown in Fig. 2.6(a). The flat-to-flat core diameter is ~20.5 μm and flat-to-flat cladding diameter is 123μm. The same as the previous one, the fiber is polarization-maintaining (PM) by the incorporation of two boron-doped low-index stress elements. The fiber has a cladding pump absorption of ~0.7 dB/m at 915 nm and is coated with low-index acrylic to provide a pump NA of ~0.46.

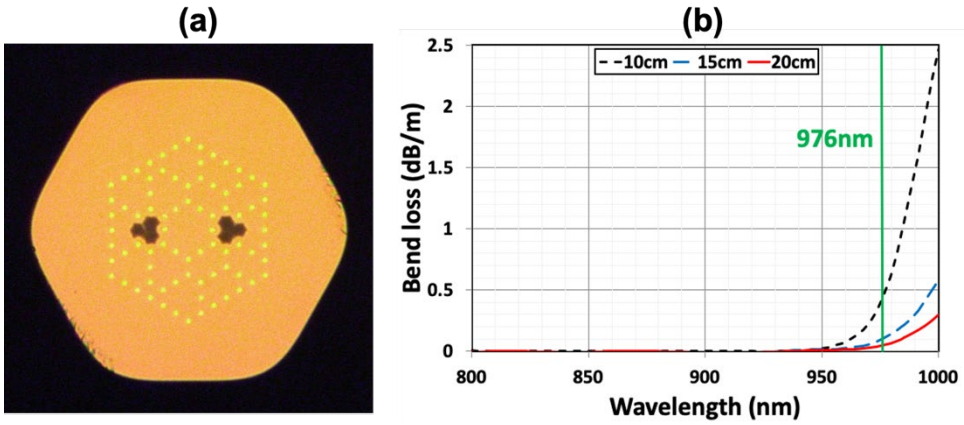

Fig. 2.6 (a) Microscope image of the second iteration PM AS-PBF cross section, (b) measured bend loss of the second iteration PM AS-PBF for coiling diameters 20 cm, 15 cm and 10 cm. The green line indicates the position of the signal wavelength.

A passive fiber with the identical fiber dimensions (i.e. same bandgap structure) and coated with high-index acrylic was also fabricated for bend-loss characterizations. The bend loss was measured by coiling ~4 m of fibers to diameters of 10 cm, 15 cm and 20 cm, shown in Fig. 2.6(b) with the laser wavelength shown as the green vertical line. The long wavelength edge of the bandgap is clearly visible. The short wavelength edge of bandgap is estimated to be around 550 nm, not covered by the PK2500 system used for this measurement. It is clear that loss can be increased significantly above 1μm by reducing the

coiling diameter. Next, we then fabricated third iteration AS-PBF without the PM structure and with slightly different fiber dimension.

2.3.2 Characterization of the non-PM Yb PBF

The cross section of the non-PM Yb-doped AS-PBF is shown in Fig. 2.2(a). The fiber has a core with corner-to-corner diameter of 24 μm and flat-to-flat diameter of 21 μm. The cladding has a corner-to-corner diameter of 131 μm and flat-to-flat diameter of 124 μm. The fiber is coated with low index acrylate to provide a pump NA of ~0.46. The pump absorption was measured to be ~1.76 dB/m at 915 nm.

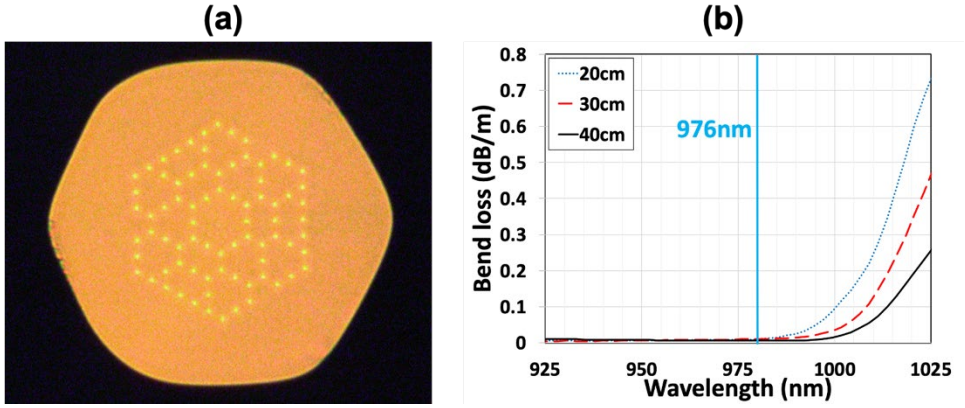

Fig. 2.7 (a) Microscope image of the non-PM AS-PBF cross section, (b) measured bend loss of the non-PM AS-PBF for coiling diameters 40 cm, 30 cm and 20 cm. The cyan line indicates the position of the signal wavelength.

A passive fiber of identical design was drawn as well. The background loss for core propagation in the passive fiber was measured to be around 20 dB/km at ~976 nm. Bend loss was also measured on the passive fiber for bend diameters of 20 cm, 30 cm and 40 cm. This is given in Fig. 2.7(b), showing negligible bend loss for coil diameters of 10 cm at the lasing wavelength of ~976 nm. The high bend loss at the longer wavelengths is related to the long wavelength edge of the bandgap, which is optimally positioned for the suppression

of the Yb four-level system (~1030 nm) without incurring significant loss on the three-level system at ~976 nm. The low-loss window [35] was measured to be around 400 nm wide in a passive fiber and the lower wavelength edge of the bandgap is just below 600 nm for the active fiber, not shown in Fig. 2.7(b).

2.4 Results and discussions

2.4.1 Experimental setup

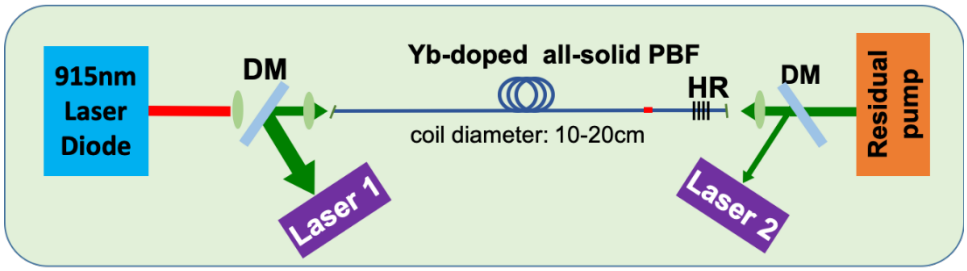

Fig. 2.8 A laser configuration used in the experiment (DM: dichroic mirror, HR: FBG with high reflectivity, >99.5%). A few other alternative arrangements were also used. 4%+4%: straight cleaves at both fiber ends, 4%+HR: straight cleave at the pump end and HR at the other end, 1%+HR: 1% FBG output coupler at the pump end and HR at the other end, angle+HR: angled cleave at the pump end and HR at the other end, angle+angle: angled cleaves at both ends.

The basic laser arrangement is a counter-pumped configuration shown in Fig. 2.8. A number of alternative laser configurations were also used, including 4%+4%, 4%+HR, 1%+HR, angle+HR, and angle+angle. The details are explained in the caption of Fig. 2.4. FBGs were written in-house using a frequency-quadrupled YAG laser at 266nm. A matching 25/125 μm photosensitive fiber was made in-house for the HR FBGs. The germanium-doped passive fiber was loaded with hydrogen first and had FBG written in them using an interferometer setup in house. The all-solid photonic bandgap fiber can be easily spliced like conventional fibers. We have used a compact tabletop fusion splicer (Fujikura 62S) in our experiments. For some arrangements, several different fiber lengths

were also tested. This was done by repeatedly cutting back the same fiber. The optimum coil diameters that yield to maximum output efficiency for the PM and non-PM fibers are, respectfully, 20 cm and 10 cm. We tried several different coil sizes and we noticed that output efficiency and ASE suppression as very sensitive to fiber coiling, as expected by the bend loss data. Outputs at both fiber ends were monitored along with residual pump. The pump was delivered in a 0.22 NA 105/125 μm fiber, i.e. the pigtail of the fiber-coupled pump diode. We started with a 100 W 915 nm pump diode, and later we were able to purchase 915 nm pump diodes with maximum 200 W output power supplied by nLight Inc. Next, we are going to present the experimental results from both the PM Yb-doped AS-PBF and non-PM Yb-doped AS-PBF separately under two subsections.

2.4.2 Results with the PM Yb PBF

In order to better understand the laser dynamics and to have a good expectation from the experiment, we simulated the efficiency of the laser using a homemade MATLAB code taking account of local pump, signal, and ASE powers in both directions as well as local inversion. All the optical powers were initially propagated forward numerically with appropriate boundary conditions at the fiber input and guessed values were used for all other parameters which could not be determined. Once the propagation reached the fiber end, only the appropriate parameters at the output end were reset by the required boundary conditions and all the optical powers propagated numerically backward. Once the input was reached, only the appropriate parameters at the input were reset by the required boundary conditions. This was repeated until numerical convergence was achieved.

The PM Yb-doped AS-PBF [Fig. 2.6] has a cladding pump absorption of ~0.7 dB/m at 915 nm and is coated with low-index acrylic to provide a pump NA of ~0.46. For the initial tests, the cavity was formed by a straight cleave at one end of the active fiber and a HR FBG spliced to the other end of the active fiber. The free end of the FBG was ~8^{o} angle cleaved to avoid back-reflection of residual light into the fiber core. The pump at 915 nm delivered in a 105/125 fiber is coupled through a dichroic mirror into the straight-cleaved end of the active fiber. The output at ~976 nm was obtained through the reflection from the dichroic mirror. The far end of the fiber was also monitored for residual pump and any laser output. Various coil diameters were tested, and the efficiency was found to decrease when the coil diameter was below the optimum coil diameters. This is consistent with the increased signal loss expected at smaller coil diameter at ~ 976 nm shown in Fig. 2.6(b). The optimum coil diameter was found to be ~20 cm for the PM Yb fiber. The measured efficiency was plotted versus active fiber length in Fig. 2.9(a) along with the simulated efficiency (see caption for details). The highest laser efficiency with respect to the launched pump power is ~52% in this case, which was obtained with a 22 m long PM Yb fiber. Excessive ASE and parasitic lasing at ~1030 nm became an issue when the fiber length goes above 22 m. Fig. 2.9(b) shows the output power versus pump power measurement of the data point marked with a red arrow in Fig. 2.9(a).

The maximum laser output exited from laser 1 (backward) is 42.7 W, corresponding to the slope efficiency data in Fig. 2.9(b). The wasted laser output from laser 2 (forward) is ~0.8 W. The laser 2 is regarded as a wasted laser output, because for a practical laser the output needs to exit only from one single end and the rest will be wasted. That means total

laser efficiency is not very helpful if the laser directionality is not good, i.e. total laser efficiency merely indicates how efficiency the fiber is in converting the 915 nm pump into laser light ~976 nm.

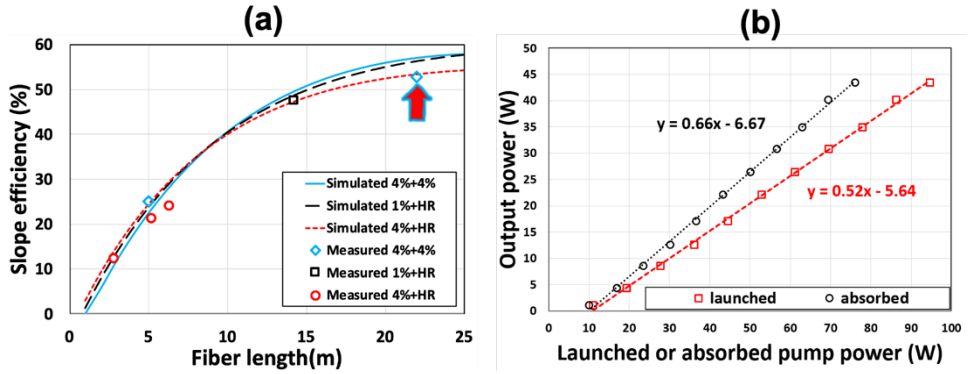

Fig. 2.9 (a) Simulated (pump loss=0.05 dB/m, signal loss=0.1 dB/m) and measured slope efficiency versus Yb fiber length, (b) maximum (red arrow) measured output power versus pump power.

The laser output spectra from laser 1 was measured at various output powers as shown in Fig. 2.10(a). Further, we also measured mode quality factor (M2) of the laser output from laser 1. For the 4%+4% cavity case, we tried to optimize mode quality but ended up measuring very bad mode quality with 22 m PM Yb fiber due to excessive cladding light. However, the mode quality with the ~5m fiber is very nice and we got M2 ~1.1 as shown in Fig. 2.10(b). We were puzzled by this mode quality result at first because the ASE ~1030 nm was suppressed by > 30 dB but we were still seeing a lot of cladding light in the mode image with the 22 m long PM Yb fiber.

Then we measured polarization extinction ratio (PER) of the laser output with various fiber lengths to identify how well the laser output is linearly polarized due to the PM structure design of this fiber. Unfortunately, the measured PER is < 1dB/m which shows that the laser output is not linearly polarized. On the other hand, this poor PER value

somewhat explains why the mode quality of the output laser with 22 m PM Yb fiber was so bad. Therefore, we suspect that this poor mode quality is mainly due to the poor PM guidance of this fiber which enhances the chance of fast axis mode easily leaking into the cladding. Thus, leading to a very poor mode quality of laser output with long PM Yb fibers, e.g. the 22 m case.

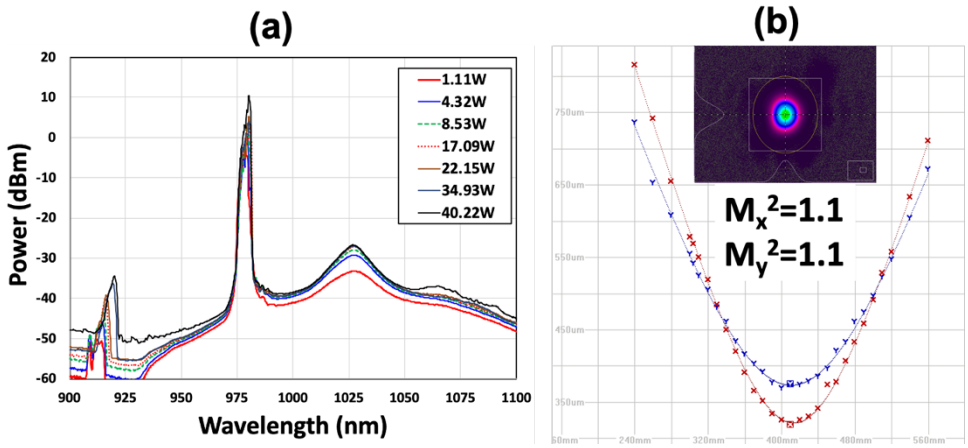

Fig. 2.10 (a) Measured laser output spectra from laser 1 at various powers, (b) measured M^2 result (mode image and fitted M^2 curves) with PM Yb fiber ~5 m.

At this point, with ~53% laser efficiency from the PM Yb fiber, we were able to demonstrate comparable laser efficiency to the previously reported ~980 nm laser with a rod-type PCF [26]. However, both the PER and M^2 are not good enough for this laser to be more competitive or be used in practical applications, e.g. core-pumping, frequency doubling, etc. Fortunately, our exploration did not stop here. Next, we are going to present the experimental results with the non-PM Yb PBF that was drawn from the same base preform but without PM structure and with higher Yb^{3+} level in the core which has pump absorption ~1.76 dB/m (i.e. ~2.5 times of the PM fiber pump absorption).

2.4.3 Results with the non-PM Yb PBF

In this section, we are presenting the experimental result for the non-PM Yb-doped AS-PBF shown in Fig. 2.7. The same MATLAB code was used for the simulation, and it was performed for 4%+4%, 4%+HR, and 1%+HR, shown in Fig. 2.11(a). It is worth mentioning that for the non-PM Yb PBF simulation we ended up using much smaller value for pump loss (0.02 dB/m) and signal loss (0.02 dB/m). This is means loss ~980 nm is 5 times lower than the case of the PM Yb PBF [Fig. 2.6]. Both outputs (i.e. total laser output) were considered for the efficiency calculations. The efficiencies are very close in these three cases. There is only a small difference, especially for shorter fibers. This is mostly due to the different total cavity losses, with lower total cavity loss leading to slightly higher efficiency.

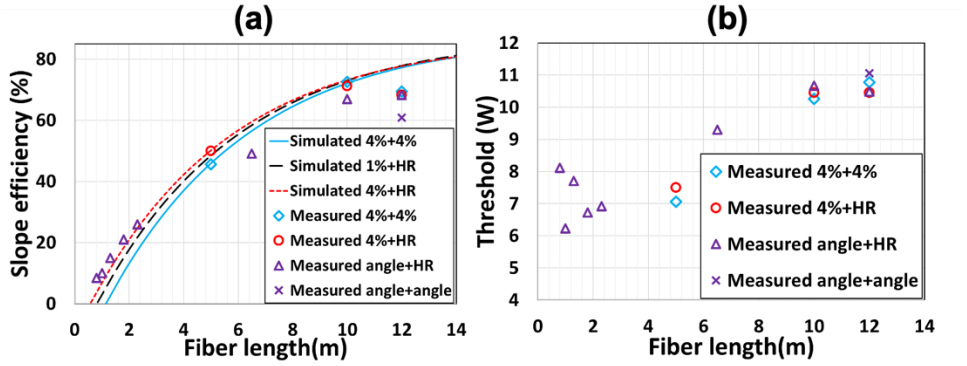

Fig. 2.11 (a) Simulated efficiency at 976 nm versus coupled pump powers at 915 nm (signal loss: 0.02 dB/m, pump loss: 0.02 dB/m) and measured efficiencies versus fiber length for a number of laser arrangements and (b) measured thresholds.

The laser efficiency was measured in a number of configurations. Laser outputs from both ends were added for the calculation of the efficiency. This is also summarized in Fig. 2.11(a). We started with 4%+4%, since this was the easiest one to test. An efficiency

of ~72.6% was achieved with 10 m fiber. Maximum output for laser 1 (pump end) was 19.9 W and laser 2 was 31.5 W in this case. The M^2 for the laser 1 (pump end) was measured to be ~1.3.

Several other configurations were also tested, including 4%+HR, angle+HR, and angle+angle. The high cavity gain is sufficient to enable lasing for schemes with not only one angled cleave but two angled cleaves, albeit with a slight efficiency reduction. The efficiency decreases beyond 10 m. This is expected when inversion falls too low far from the pump end, also evidenced by an increase in threshold with longer fibers shown in Fig. 2.11(b).

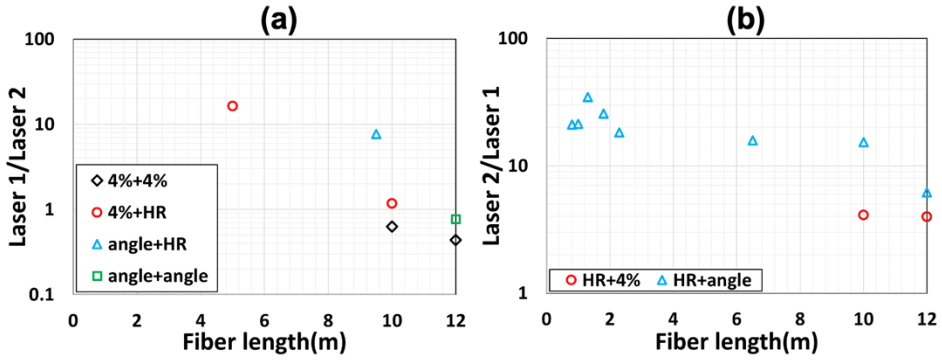

Fig. 2.12 (a) Ratio of output powers of laser 1 to laser 2 for various counter-pumping schemes, and (b) ratio of output powers of laser 2 to laser 1 for various co-pumping schemes.

We also sought to maximize the ratio of output powers of laser 1 to laser 2 for counter-pumping schemes [Fig. 2.12(a)] and the ratio of output powers of laser 2 to laser 1 for co-pumping schemes [Fig. 2.12(b)]. There are a few interesting observations. Using HR FBG with a reflectivity >99% typically over ~2 nm in wavelength, we still observed output passing through the FBG HR (laser 2). A typical laser output spectrum has a 10 dB bandwidth of 3-4 nm. The ratio of outputs of laser 1 to laser 2 is maximized using the angle+HR scheme for the counter-pumping case shown in Fig. 2.12(a). This indicates a

higher reflection at the pump end increases laser 2 output, vice versa for laser 1 output. The ratio decreases for long fiber lengths. We have also observed a significant amount of light at the laser wavelength in the cladding for laser 2 for long fibers in the counter-pumping cases shown in Fig. 2.12(a). For the co-pumping schemes in Fig. 2.12(b), the ratio of output of laser 2 to laser 1 is maximized for the HR+angle scheme, i.e. using HR at the pump end.

For an angle+HR cavity configuration with a 9 m fiber length and a 200 W 915 nm pump diode, the output powers of lasers 1 and 2 along with residual pump power are plotted in Fig. 2.13(a). In this case M^2 was measured to be 1.11 and 1.12 respectively for the two axes at 80 W for laser 1 [Fig. 2.13(b)]. M^2 was also measured at several other powers throughout the output power range and was found to change very little. The efficiency with respect to the launched pump power was 62.7% for just laser 1 output. The efficiency of the combined output powers of laser 1 and laser 2 with regard to the absorbed pump power was ~94%, at the quantum limit. For most of the lasers tested even involving fibers which were repeatedly used over many months, the efficiency of the combined (total) output powers with respect to the absorbed pump power was mostly very close to the quantum-limited efficiency, a testament to the low excess loss and photo-darkening of the fiber. The ASE at ~1030 nm was suppressed by >40 dB at high power [Fig. 2.14(a)].

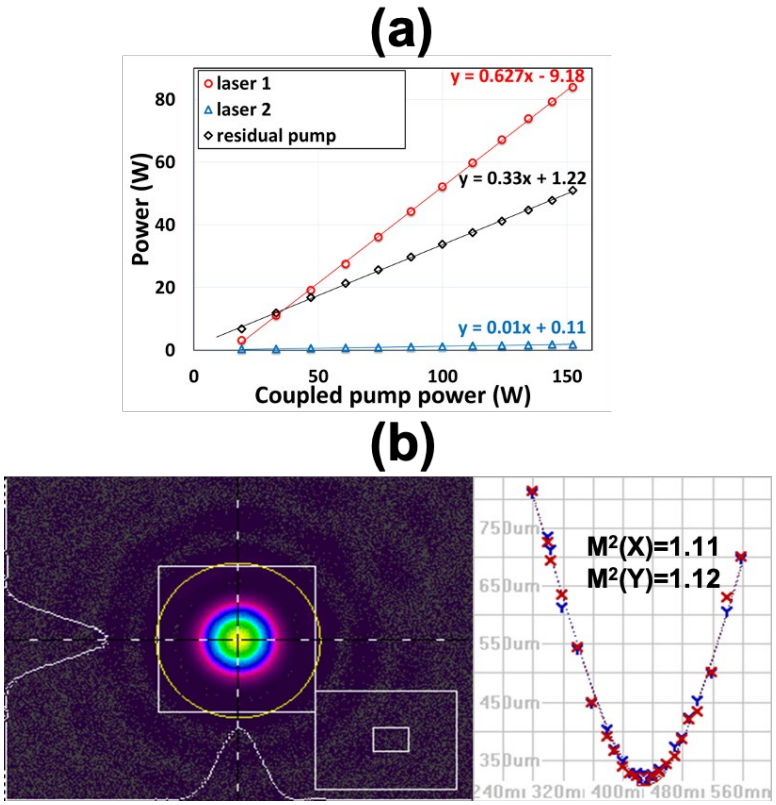

Fig. 2.13 (a) Output powers of laser 1 and laser 2 and residual pump versus coupled pump power and (b) M^2 measurement, M^2=1.11 and 1.12 respectively for x and y axis at 80 W for laser 1. The laser is in angle+HR configuration with 9 m fiber.

2.4.4 Linewidth broadening in Yb PBF

One interesting observation of the Yb three-level fiber laser is its broad spectral bandwidth [Fig. 2.14(b)]. The saturation intensity of Yb fiber lasers at ~976 nm is expected to be low due to the relatively high absorption and emission cross sections. This alone would have not caused the broad laser spectrum if the spectral linewidth of the gain were homogeneously broadened. If the spectral linewidth of the gain is dominated by inhomogeneous broadening, then gain saturation can lead to a broad laser spectrum.

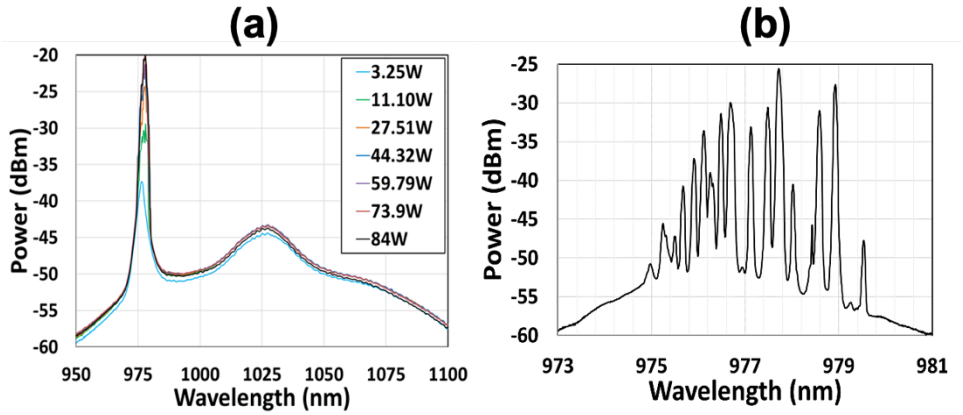

Fig. 2.14 Laser output spectra of laser 1 at various powers of the laser detailed in Fig. 2.13, (a) wide spectral range with an OSA resolution of 1nm and (b) spectrum at 84 W with an OSA resolution of 50 pm.

For erbium-doped glass, the emission at ~1550 nm was found to be mostly a homogeneously broadened line at room temperature [80]. This is due to the small Stark splitting in the order of 20-80 cm^{-1}, leading to rapid redistribution among adjacent Stark levels at room temperature in the order of pico-second (ps). Spectral hole-burning can be used to characterize homogeneous linewidth in an inhomogeneously broadened system. This was expected to be hard to see at room temperature in an erbium-doped fiber due to its homogeneously broadened nature. It was, however, observed to have a spectral width of 4-8 nm dependent on wavelength [81]. As expected for a largely homogeneously broadened system, the maximum spectral hole depth was only measured to be ~0.3 dB in this case.

On the other hand, the Stark splitting of $^2F_{5/2}$ and $^2F_{7/2}$ levels in a Yb-doped fiber is in the order of 500-700 cm^{-1}, an order of magnitude larger than that for the erbium transition at ~1550 nm, and the transition at ~976 nm originates from a single transition between the lowest Stark lines of $^2F_{5/2}$ and $^2F_{7/2}$ levels. In this system, redistribution among adjacent

Stark levels at room temperature is much slower and consequently is expected to play a much lesser role [82].

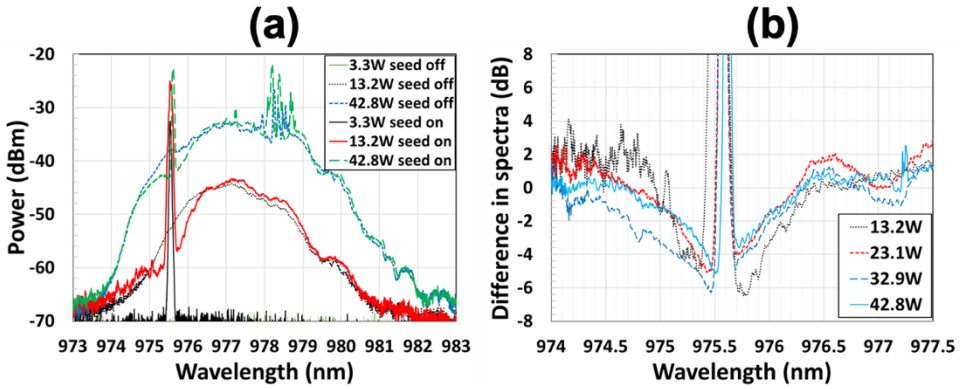

Fig. 2.15 (a) Output spectra for seed on and off at various pump powers to measure SHB with a MOPA setup seeded at 976 nm, and (b) the differential spectra at various pump powers..

In order to measure the homogenous linewidth of the transition at ~976 nm, we attempted to measure spectral hole-burning (SHB). A counter-pumped MOPA amplifier was set up using 3.5 m fiber with both ends angle-cleaved. A butterfly packaged single-mode diode laser at ~976 nm was used as the seed laser. The seed power was 519 mW just before the fiber after passing a fiber-coupled isolator. The spectral linewidth of the seed laser cannot be fully resolved by our optical spectrum analyzer (OSA, YOKOGAWA AQ6370D) at 20 pm resolution. For each pump power, two spectra were collected, one with the seed off and one with the seed on. The respective powers at the output were also measured after the pump was rejected by a dichroic mirror.

The spectra for seed on and off for three pump powers at 3.3 W, 13.2 W and 42.8 W are given in Fig. 2.15(a). At the low pump power of 3.3 W, the seed laser spectrum can be clearly seen to be resolution limited without any side bands. At pump powers of 13.2 W and 42.8 W, spectral hole-burning can be clearly seen by comparing the spectra for seed

on and off. At the pump power of 42.8 W, lasing can be seen at ~978.2 nm. The spectral difference between seed on and off are plotted in Fig. 2.15(b) for various pump powers in order to see the spectral hole-burning clearly. The FWHM of the spectral hole is ~1 nm. It is worth noting the significant depth of the spectral hole of up to 6 dB in this case, indicating the emission at ~976 nm is mostly inhomogeneously broadened. The low saturation intensity and inhomogeneous nature of the emission can easily explain our observed broad laser linewidth. This also implies a difficulty in achieving narrow linewidth and high power from this system using either an oscillator or amplifier configuration. To our knowledge, this is the first time that spectral hole-burning has been observed in a ytterbium-doped fiber.

2.5 Conclusion

We have demonstrated efficient Yb three-level fiber lasers operating at ~980 nm using Yb-doped all-solid photonic bandgap fibers. Diffraction limited single-mode (LP_{01}) operation with a record 62.7% slope efficiency with regard to the launched pump power was demonstrated for the Yb-doped three-level cladding-pumped fiber lasers with single-pass pump. The highest single-mode output power was 84 W at ~980 nm, only limited by the available pump power from the 915 nm diode laser. The laser slope efficiency with respect to the absorbed pump power was ~94%, reaching the quantum limit. In addition, we demonstrated that the Yb three-level system is mostly inhomogeneously broadened with a homogenous FWHM bandwidth of ~1 nm.

CHAPTER THREE

ALL-FIBER YTTERBIUM PBF LASER ~980NM

This chapter presents the all-fiber single-mode ~980 nm fiber laser based on the same non-PM Yb-doped all-solid photonic bandgap fiber (AS-PBF) which was previously used for the experimental demonstration of 84 W free-space-pumped single-mode Yb fiber laser at ~980 nm. Owing to the specialty AS-PBF and much stable all-fiber laser configuration combined with high-power pump/signal combiners, we have achieved a record single-mode power of 151 W at ~978 nm with an slope efficiency of 63% with respect to the launched pump power in a compact and practical monolithic laser configuration. Also, the long-term power stability of the oscillator was tested for ~60 hours, showing extremely well heat management and photodarkening-free operation of the laser system. Thus, taking it further towards becoming an industry-level prototype laser to be used outside the laboratory environment.

3.1 Introduction

Yb-doped fiber lasers have been the most successful in power scaling of all-fiber diffraction-limited transverse-single-mode (i.e. LP_{01}) high-power fiber lasers. As early as 2009 [23,83], a 10 kW all-fiber Yb-doped fiber laser based on master oscillator power amplifier (MOPA) system was reported and made commercially available by IPG Photonics. However, these record-high power outputs were realized exclusively in the long wavelength regime, i.e. ~1070nm. The development of high-power high-brightness multi-mode diode laser pumps at wavelength 9xx nm and other high-power fiber components

(e.g. pump combiners, etc.) had played a vital role in achieving this kW-level all-fiber Yb fiber lasers [Fig. 3.1]. More importantly, the laser operating wavelength at ~1.1 μm has the advantage of low quantum efficiency and lower average inversion requirement, thus relatively lower heat load along the fiber.

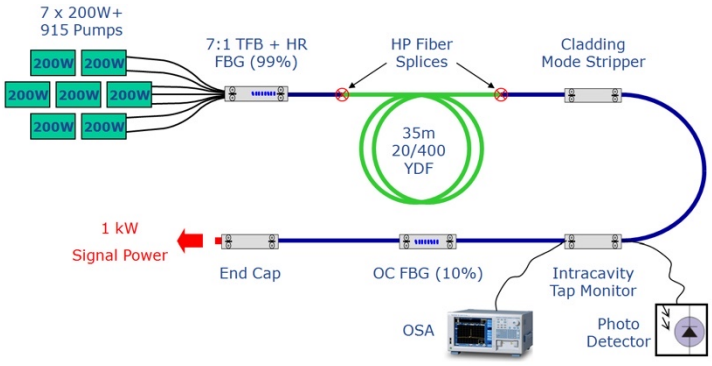

Fig. 3.1 Schematic of the 1 kW all-fiber laser oscillator [84].

On the contrary, power scaling of Yb-doped fiber lasers ~980 nm has left far behind the ~1070 nm regime. In a sharp contrast to the 10 kW report by 2009 [23,83], only 94 W by a rod-type Yb-doped PCF-based free-space-pumped fiber laser oscillator at 977 nm was reported by the end of 2008 [26]. The output power record set by this result has not been broken for the past 11 years until our work on the all-fiber Yb-doped AS-PBF laser at ~980 nm set the new record to 151 W.

3.2 Motivation and background

The use of double-cladding AS-PBFs to suppress Yb ASE at shorter wavelengths, enabling high-power lasers above 1150 nm was reported in 2009 [29,30]. In our research group at Clemson, we have previously used AS-PBFs to enable an efficient Yb fiber laser

at ~1018 nm by suppressing Yb ASE at the longer wavelengths [86]. When operating an Yb-doped fiber laser in the three-level system by suppressing the four-level system, the separation of the laser wavelength and ASE peak wavelength is only ~50nm. This is much less than the ~150 nm separation as reported in [75,76] for laser operation at 1150-1200 nm, thus it presents a much more significant challenge. The AS-PBFs used in [75,76] also had mode field diameter (MFD) of ~10 μm. This is also much smaller than what is desired in an Yb three-level system for high core to cladding ratio. In 2008, Pureur et al. [62] reported the first use of Yb-doped AS-PBF to suppress ASE ~1030 nm for laser operation at ~980 nm. However, in this case, it was a core-pumped fiber laser arrangement with an active fiber mode field diameter of just 3.4 μm, and the maximum achieved output power was only ~140 mW. This level of output power is even less than the ~1 W output power available from the commercial single-mode fiber-coupled diode lasers at ~980 nm.

The four-level Yb system has been a critical foundation for industrial high-power fiber lasers. The three-level system has only attracted a little academic interest, having been limited by poor efficiencies and low powers in practical laser configurations. Conventional methods of mitigation are almost entirely based on large core-to-cladding ratio [26,59,77]. The benefit of this design is that it lowers the intensity of the laser relative to that of the pump, therefore, allowing the required high excited state inversion to be maintained at relatively lower pump powers. This conventional approach results in reduced unabsorbed pump (i.e. residual pump), but it produces only limited performance improvements in practical high-power fiber lasers.

In a recent state-of-the-art demonstration of a monolithic fiber laser configuration, a fiber with a 20 μm core diameter and a square cladding of 80μm x 80 μm was tapered to 50 μm x 50 μm in the middle, achieving 10.6 W at 976 nm and an efficiency of 18.4% [74]. The records in both power and efficiency for Yb three-level fiber lasers were set in a rod-type photonic crystal fiber (PCF) with a core diameter of 80 μm and a pump cladding diameter of 200 μm. An output power of 94 W at 977 nm, an efficiency of 48% and an M^2 of 1.2 were achieved in a free-space bulk optics laser scheme [25]. The laser was built with a double-pass pump configuration in this case. Using the same fiber and the cavity structure, higher efficiencies of 53% and 63% were achieved for single and double pass pump respectively. However, M^2 was ~1.2 only for an output power below 25 W [26]. This large core cannot be bent, and the fiber must be kept straight. Therefore, the main disadvantage of this approach with rod-type PCF is the fiber dimensions that is not compatible with standard fiber components for monolithic all-fiber design.

There are also reports of all-fiber amplifiers ~980 nm, which was developed using non-microstructure specialty fibers with MOPA scheme. A 48 cm long LMA 35/125 μm octagonal double-clad Yb-doped fiber was used to build a MOPA seeded at 976nm and pumped by multiple diodes at 915nm, achieving 39 W output power at 976nm with an efficiency of only 19% [87]. In recent report, a 55 cm long single-mode Yb-doped fiber with 14 μm core and 40 μm pump cladding was used in combination with tapered fibers to build an all-fiber MOPA, achieving maximum output power of 13 W, slope efficiency of 31% and M^2~1.1 [88]. In both cases, the optimum length of the amplifier gain fiber was

very short to be able suppress ASE ~1030 nm, which leads to significant amount of unabsorbed pump thus limiting output efficiency.

All the above reported results were demonstrated using silica fibers, for example phospho-silicate (P_2O_5-SiO_2) fiber [70] which is known for its better photodarkening management, good rare-earth solubility and low background loss. On the other hand [89,90], it is known that rare earth dopant concertation can be 10-50 times higher in phosphate glass fibers compared to its silica glass counterpart. In 2017[91], 3.4 W power and 6.8% efficiency with a 976 nm single-frequency laser output was obtained with a 7 cm long 6 wt% Yb-doped 18/135 μm double-clad phosphate fiber. In 2018 [92], a 976 nm single-frequency linearly polarized all-fiber MOPA was demonstrated using a 29 cm long 20/130 μm 1.5 wt% Yb-doped double-clad phosphate glass fiber, achieving maximum output power of 10 W, with a slope efficiency of ~10%. It is worth noting that the slope efficiencies in the above cases [91,92] are still very low despite very high Yb concentrations. On one hand, this is due to the high background loss (~3 dB/m) in phosphate fibers and high splice loss between the silica fiber components (e.g. pump combiner) and the phosphate gain fiber, which is a manifestation of the intrinsic disadvantage of phosphate glasses. In contrast, rare earth doped silica fiber background loss is ~0.01 dB/m. On the other hand, the total pump absorption is still limited due to the fact that high inversion (≥ 50%) has to be maintained in order to suppress the ASE at ~1030nm, which is similar to the case with many conventional silica fibers without spectral filtering at long wavelength near 1030 nm or above. This shows that simply optimizing the

hos glass material will not solve the fundamental problem of inadequate total pump absorption and excessive ASE at ~1030 nm.

3.3 Results and discussions

The cross section of the all-solid photonic bandgap fiber used in this work is previously shown in Fig. 2.7 along with the measured bend loss showing the carefully engineered bandgap of the active fiber for the suppression of the Yb four-level system. The fiber can be coiled down to ~15 cm diameter without significant in-band bend loss and show strong loss above ~980 nm due to the photonic bandgap waveguide spectral filtering of the AS-PBF. It is the same active fiber as the one used in Chapter 2. The fiber has a core with a corner-to-corner diameter of 24 μm and flat-to-flat diameter of 21 μm. The cladding has a corner-to-corner diameter of 131 μm and flat-to-flat diameter of 124 μm. A multiple-cladding-resonance design is used for enhanced HOM suppression as detailed in Section 2.3 of Chapter 2. The fiber is coated with low index acrylate to provide a double-cladding fiber structure with pump cladding NA of ~0.46, and the cladding pump absorption was measured to be ~1.76 dB/m at 915 nm.

The all-fiber laser architecture is a counter-pumped monolithic configuration shown in Fig. 3.2 with two fiber-coupled pump diodes at ~915 nm (200 W, 0.22 NA 105/125 μm) spliced to a 2+1 high-power pump combiner. A piece of ~3 m long 20/105 μm Er-doped fiber with a highly Er doped core (7wt% Er^{3+}) coiled at 5 cm in diameter was used in each pump path to absorb any backward propagating leakage light at the lasing wavelength at ~978 nm. This Er fiber acts as an in-line isolator to protect the pump diode. Pump loss at ~915 nm was measured to be ~0.1 dB for the ~3 m Er fiber and ~0.46 dB for

the pump combiner. The high-reflectivity fiber Bragg grating (FBG) was written in-house using a frequency-quadrupled YAG laser at 266 nm in a 24/125 μm photosensitive fiber which was also made in-house. The FBG has a reflectivity of >99% and a FWHM bandwidth of 2 nm. The output is ~8° angle cleaved. This cavity configuration was previously found to minimize wasted laser output at the FBG end, i.e. laser 2 as marked in in Fig. 3.2, without compromising the laser efficiency [41].

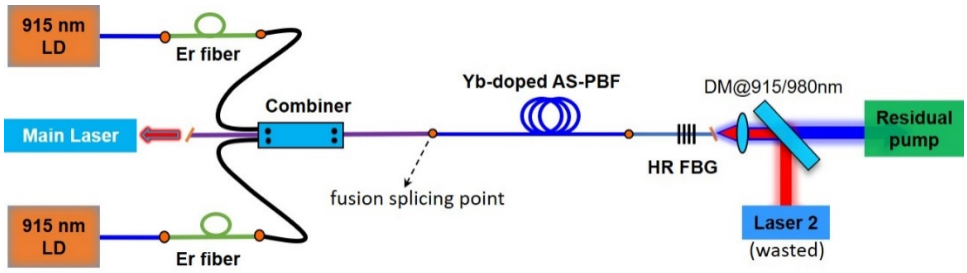

Fig. 3.2 Schematic configuration of the all-fiber Yb-doped AS-PBF laser ~ 980 nm.

We first performed length optimization of the Yb-doped AS-PBF by progressively cutting back the Yb-doped AS-PBF and fully characterizing the laser performance at each fiber length. The Yb-doped AS-PBF was coiled to 10-15cm diameter, and the residual pump light as well as wasted laser (i.e. laser 2) at ~980 nm were monitored at the far end.

Laser efficiency, total efficiency, residual pump and laser 2 are shown versus the Yb-doped AS-PBF length in Fig. 3.3. Laser efficiency (i.e. useful laser output) accounts only for the output power from the pump combiner with respect to the launched pump. Total efficiency accounts for both laser output powers (i.e. adding the output powers from combiner side and FBG side) with respect to the launched pump. The residual pump indicates the ratio of unabsorbed pump power with respect to the launched pump power,

and laser 2 is the efficiency of the wasted laser output (from the FBG side) with respect to the launched pump.

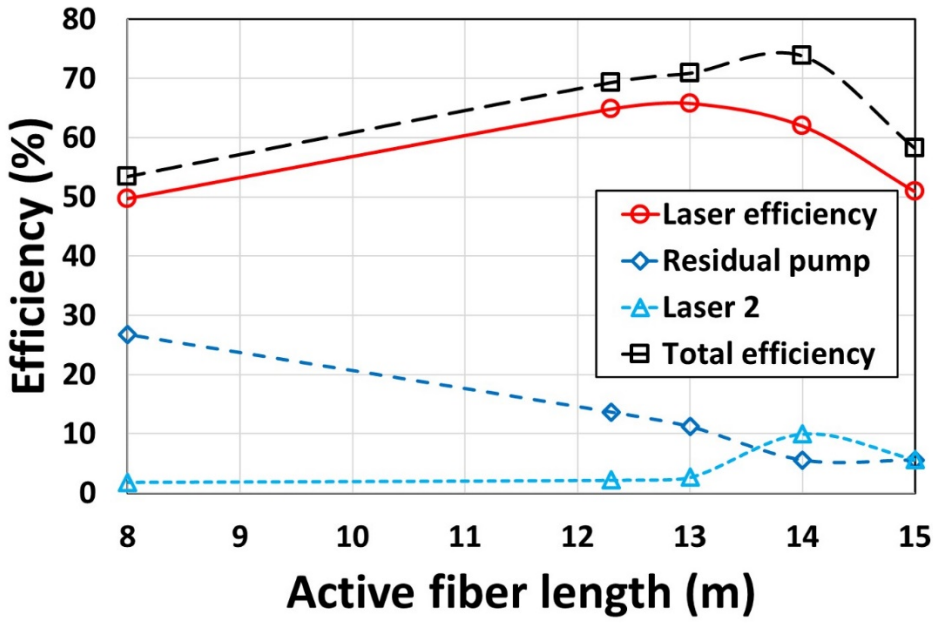

Fig. 3.3 Laser performance versus active fiber (Yb-doped AS-PBF) length.

The optimized active fiber length was determined to be ~13 m, based on active fiber length corresponding to the peak of the laser efficiency (red curve with circular mark) in Fig. 3.3. Because the laser directionality was optimized (as shown in Fig. 2.12) to obtain maximum output from the combiner end (i.e. counter propagating laser), and this output power is what really counts in a practical laser architecture. It is also worth mentioning that the actual length of the active fiber used in the last measurement for laser characterization was 12.3 m. The reason we ended up using only 12.3 m long active fiber in the final test (as in Fig. 3.4 and Fig. 3.5) is that we had been using the same piece of active fiber for

several measurements. Eventually, the active fiber got shortened during this process due to cut-back measurements and fiber cleaving. Nonetheless, we did not replace the active fiber with a new piece of Yb-doped AS-PBF because of the limited amount of Yb-doped AS-PBF left in the lab from the last draw.

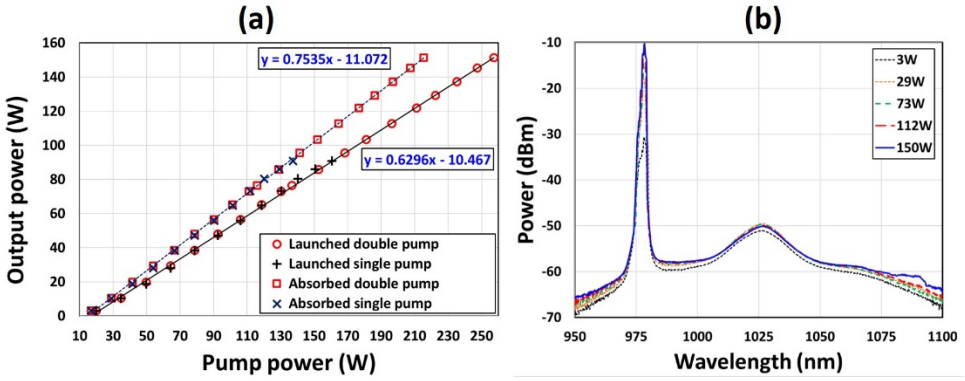

Fig. 3.4 (a) Measured output versus pump power for, respectively, with respect to the launched pump power and absorbed pump power; (b) measured laser (at combine side) output spectra for double pump case under various output power.

Output powers with a single pump and double pump configurations are shown in Fig. 3.4, with the laser output spectra at various powers. This output power does not include the output power at laser 2 (i.e. wasted laser output). A maximum output power of 90.9 W at the output was achieved with a single pump configuration and 151.4 W with double pump configuration, limited by available pump powers in both cases. The overlapping of the slopes of the output power versus pump power respectively for the single-pump and double-pump indicates that maximum the laser output is only limited by the available pump. This is, in fact, a further validation to our prediction in Chapter 2 that the output of the free-space-pumped laser with the same Yb-doped AS-PBF is only limited by available

pump. The corresponding output for the double pumping at laser 2 is 7 W, i.e. 4.4% of total power of 158.4W. With double pumping configuration, the slope efficiency was ~63% and ~75.4%, respectively, corresponding to the launched pump power after the combiner and absorbed pump power.

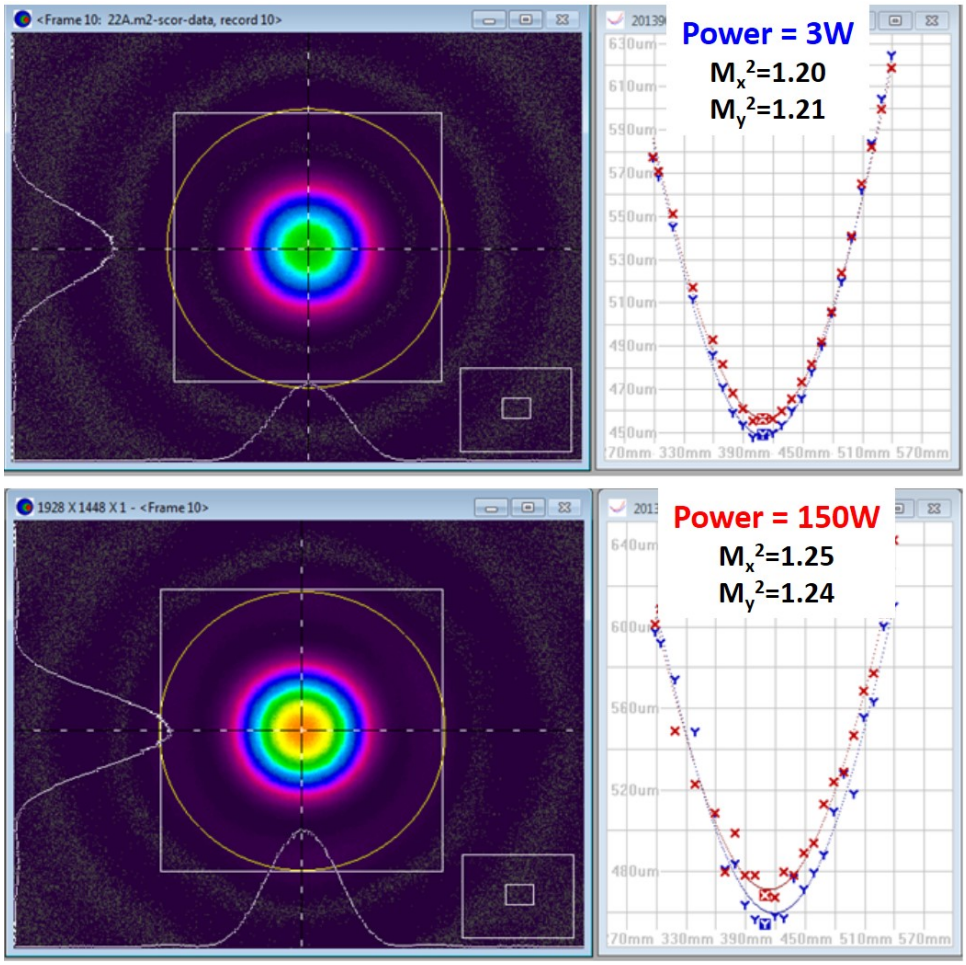

Fig. 3.5 Mode quality characterization of laser output (from combiner side) at 3 W (top) and 150 W (bottom). Near field mode images and M^2 curves with corresponding M^2 values are also included.

The slope efficiency of ~63% is at the same level as the slope efficiency of 62.7% that we achieved in a free-space bulk optics laser configuration as we covered in Chapter

2. Nevertheless, the novelty in this work covered in Chapter 3 is that we were able to achieve much higher output power using a practical monolithic all-fiber laser architecture. The ASE from the four-level system was well suppressed to below 40 dB at the highest laser output power. The M^2 at ~3 W was 1.20/1.21. The M^2 at ~150 W was 1.25/1.24 (Fig. 3.5), which was also found to be almost constant across the whole power range. This is a good indication that the laser output is near diffraction-limited single-mode (LP_{01}) and the mode quality does not degrade when output power increases to near its maximum value.

Aiming to investigate the laser output stability in terms of photodarkening, we have conducted a long-term power stability test. Photodarkening increases significantly with inversion levels in Yb fiber lasers, thus it is expected to be a severe problem for the Yb three-level system ~980 nm due to its high inversion. As mentioned before, the high inversion level (≥ 50%) is a necessary criterion for Yb lasers operating ~980 nm. It was reported in the past that optimizing core glass composition is the best approach to tackle the issue of photodarkening in Yb-doped high-power fiber lasers [78,93,94].

The Yb phosphosilicate (P_2O_5-SiO_2) core glass used in our fiber is well known for its high resistance to photo-darkening [70], and it exhibited negligible degradation of laser performance over a period of several months and numerous tests. We have conducted a long-term power stability test for about 60 hours with a single-pump configuration with the laser output power at ~75 W (Fig. 3.6). Apart from some power fluctuations in the few percent levels, most likely due to temperature changes in the lab, there was very little sign of photo-darkening. It is worth mentioning that the long-term stability test was performed

with only a single pump. This is because we wanted to be safe while running the laser continuously especially over several nights.

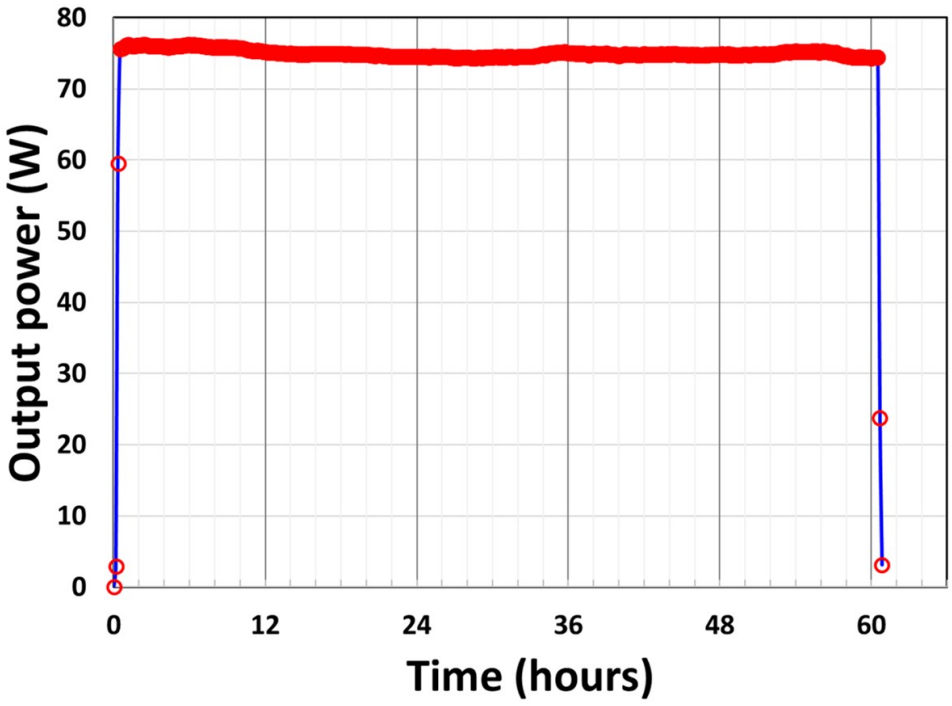

Fig. 3.6 Long-term power stability test at 75 W output for ~60 hours with one data point recorded at every 10 minutes interval.

3.4 Conclusion

We have demonstrated that the Yb three-level system at ~978 nm can be operated just like the well-established Yb four-level system in achieving single-mode high-power laser output with comparable efficiency using a Yb-doped double-clad all-solid photonic bandgap fiber with its bandgap optimized to suppress the four-level system in a practical monolithic setup. We have achieved record output power of 151.4 W, M^2 of ~1.2 at full power, and laser efficiency of 63% with respect to the launched pump power in an all-fiber monolithic Yb-doped double-clad all-solid photonic bandgap fiber laser.

Compared to the previous work with free-space bulk optics for pump and output coupling (as detailed in Chapter 2), we have increased maximum output power by a factor of ~2 while maintaining the high laser efficiency (~63%) in an all-fiber monolithic laser configuration. In addition, we have conducted long-term power stability test. Furthermore, we have experimentally validated our claim in the previous work in Chapter 2 that output power is only limited by available pump power and the active fiber (Yb-doped AS-PBF) is almost photodarkening free. This breakthrough immediately provides new tools for pumping diffraction-limited solid-state lasers and core-pumping options for fiber lasers and amplifiers, especially in core-pumped pulsed fiber lasers which are more susceptible to nonlinearity due to long gain fiber.

CHAPTER FOUR

NUMERICAL MODELING OF ERBIUM-YTTERBIUM FIBER LASER

This chapter presents a new model on numerical modeling of high-power cladding pumped Er/Yb co-doped fiber lasers and amplifiers. In this new model, we assume that the onset of Yb parasitic lasing is mostly due to the elevated population inversion of the isolated Yb ions (i.e. the Yb ions positioned too far away from Er ions), while the high energy transfer rate of the coupled Yb ions (i.e. the Yb ions positioned close to Er ions) ensures the continued growth of the output power at ~1.6 μm from Er ions long after the onset of Yb parasitic lasing at ~1.1 μm. In addition, we have also incorporated a temperature-dependent model based on thermally excited populations among Stark levels of Yb ions [82,95]. With this new model, we can successfully explain the observed behaviors of high-power cladding-pumped Er/Yb fiber lasers and amplifiers, and account for the insignificant roles that elevated temperature [96] play.

4.1 Introduction

Numerical modeling (i.e. simulation) has been very useful to study the rare earth doped fiber lasers and amplifiers. It is also an important approach to optimize laser design parameters and investigate problems that are hard to detect in an experiment. An accurate modeling of these types of fiber lasers allows us to study the signal, pump and ASE as they propagate along the fiber, which leads to better intuitive understanding of the laser dynamics and how we design lasers and amplifier for a specific application [97]. For example, modeling can help us to choose the right wavelength for the pump, optimize the

glass composition of the fiber, determine the optimum length of the gain fiber, choose the best combination of the input and output coupler reflectivity for the laser cavity, apply proper cooling strategy in the laser architecture, etc.

However, modeling results are only as accurate as the approximations and assumptions used. Modeling results may not represent the reality when the conditions and parameters are not referenced to those of the actual experiment. Further, experimental work helps validating the results obtained by theoretical modeling which in turn helps researchers to set a practical goal for the very experiment [98]. In this work, we will mainly focus on the discussion of numerical modeling of Er/Yb fiber lasers and amplifiers based on step-index fiber design approximation to the core index profile and weakly guided approximation to the optical mode distribution.

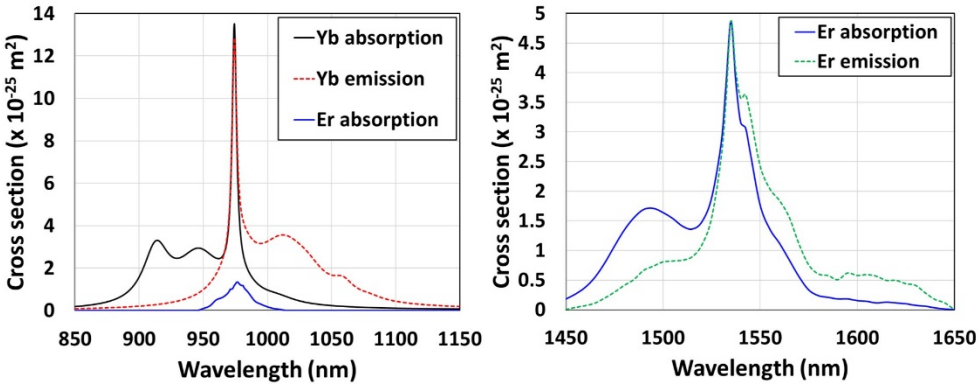

Fig. 4.1 Absorption and emission cross section of the Er^{3+} and Yb^{3+} ions of silica glass Er/Yb co-doped fiber at room temperature (T=293K).

There are several advantages in using Er/Yb co-doped fibers (i.e. Yb sensitized Er co-doped fibers) instead of Yb-free Er-doped fibers in building cladding-pumped high-power fiber lasers and amplifiers operating near 1.5-1.6 μm. First, in this case the Er ions

are indirectly pumped via resonant energy transfer from Yb ions to the Er ions. Second, the Yb ions possess broadband 900-1000 nm pump absorption which is covered by highly efficient and reliable commercial high-power diode lasers at 915 nm, 940 nm and 976 nm. Third, the large absorption cross section of Yb ions (~10 times of that of Er ions) helps significantly increasing pump absorption, thus much shorter gain fiber can be used for adequate total pump absorption. Finally, it has been also reported that co-doping with Yb helps mitigating clustering of Er ions at high concentrations [99]. Moreover, the silica glass composition of the core can be optimized for highly efficient operation of lasers and amplifiers at ~1.6 μm. The ratio of Yb to Er concentration can be optimized and the silica glass core can be co-doped with phosphorus, which can help both improving Yb→Er energy transfer and mitigating ASE (or parasitic lasing) at ~1.1 μm. In addition, the absorption spectrum of Er/Yb fiber can be flattened by using phospho-silicate glass core, which enables the use of non-wavelength-stabilized high-power pump diodes at ~ 9xx nm.

Numerical modeling on pulsed [100–102] and continuous wave (CW) [56–62] cladding-pumped Er/Yb co-doped fiber lasers and amplifiers have been reported. However, all these models assume that all the excited Yb ions are equally involved in the energy transfer process between the Yb ions and Er ions. This means that the laser emission at ~1.6 μm from Er ions will be immediately clamped (i.e. flattened) once the Yb inversion reaches its maximum level at the threshold pump power of Yb parasitic lasing at ~1.1 μm. This is, however, not what was observed in the experimental research of Er/Yb fiber lasers at high powers, where the output power at ~1.6 μm continued to grow albeit at a slower rate. It was experimentally observed [109–112] that the clamping of Er/Yb fiber laser

output at ~1.6 μm does not occur immediately after the Yb parasitic lasing at ~1.1 μm comes in, although there was laser output power roll-off (i.e. decrease in slope) at pump powers well above the threshold power of Yb parasitic lasing. In this work, we show that under high pump power the pumping rate of Er/Yb fiber laser will eventually exceed the Yb → Er energy transfer rate, leading to an energy transfer bottleneck, resulting in increasingly higher Yb inversion. Yb parasitic lasing will inevitably happen, that the Er/Yb fiber is very efficient at lower pump powers, *e.g.* highly efficient laser due to optimized Yb →Er energy transfer. This means that the output power clamping will eventually come in although the clamping threshold pump power varies depending on the quality of the Er/Yb fiber, thus, leading to all Er and Yb inversions being clamped at levels appropriate to compensate for the round-trip cavity losses for the respective Er and Yb laser. The output power at ~1.6 μm is consequently clamped by the fixed energy transfer rate at the clamped inversion levels.

In 2005, one attempt was made to explain the above-mentioned experimental phenomena using the elevated fiber temperatures at high powers, which can increase re-absorption of ytterbium emission [96]. The increased re-absorption of Yb emissions means a higher Yb inversion at Yb parasitic lasing threshold, and therefore, a higher output power at ~1.6 μm. However, in this work we have found that this re-absorption of Yb emission in [96] does not increase much with pump power, and thermal effect due to Yb absorption at high pump powers cannot justify the experimental results of un-clamped Er output at ~1.6 μm in [109,111]. Our simulation shows that incorporating the thermal effect does slightly increase the output level, but either way the Er output is eventually clamped when pump

power level is high enough above the clamping threshold which again varies depending on the quality of the Er/Yb fiber.

We have developed a new numerical model in this work to explain the observed behaviors in high-power cladding pumped Er/Yb fiber lasers and amplifiers. In this new model, we have incorporated the concept of coupled Yb ions and isolated Yb ions respectively, which was first discussed in the pioneering work [111] by researchers at the Southampton University. It is assumed here that some Yb ions are closely placed next to Er ions and their related energy transfer can be modeled by a fast energy transfer rate.

Considering the abundance of Yb ions relative to Er ions due to much higher Yb concentration, it is also possible to imagine that some Yb ions are isolated from Er ions. In other words, some Yb ions in the Er/Yb doped silica glass matrix [Fig. 4.1] are positioned too far away from the Er ions, which makes it impossible (at least very hard) to initiate the direct resonant energy transfer from Yb ions (donors) to Er ions (acceptors). The energy transfer process takes place in the form of both non-radiative and radiative transition via dipole-dipole interactions between the donor and acceptor ions [113–115]. Resonant energy transfer efficiency is proportional to $1/d^6$, where d is the distance between donor and acceptor. The radiative energy transfer to Er ions would require emission of photons and eventual re-absorption by Yb ions placed next to Er ions. Re-absorption directly by Er ions is possible but extremely unlikely (near zero probability) due to the narrow and weak erbium absorption at ~980nm. Nonetheless, direct energy transfer (or migration) between neighboring Yb ions is also possible.

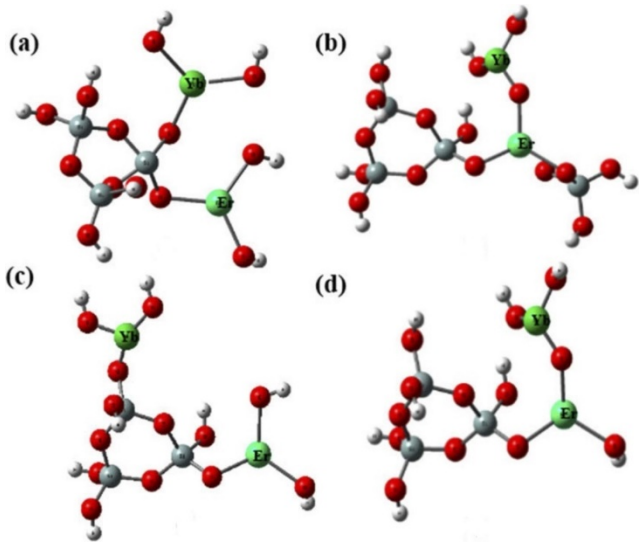

Fig. 4.2 Er/Yb co-doping structure models with different doping sites (a-d) of Er and Yb ions. The red, grey, shallow green, and dark green structures represent O, Si, Er, and Yb, respectively [116].

4.2 Theoretical model

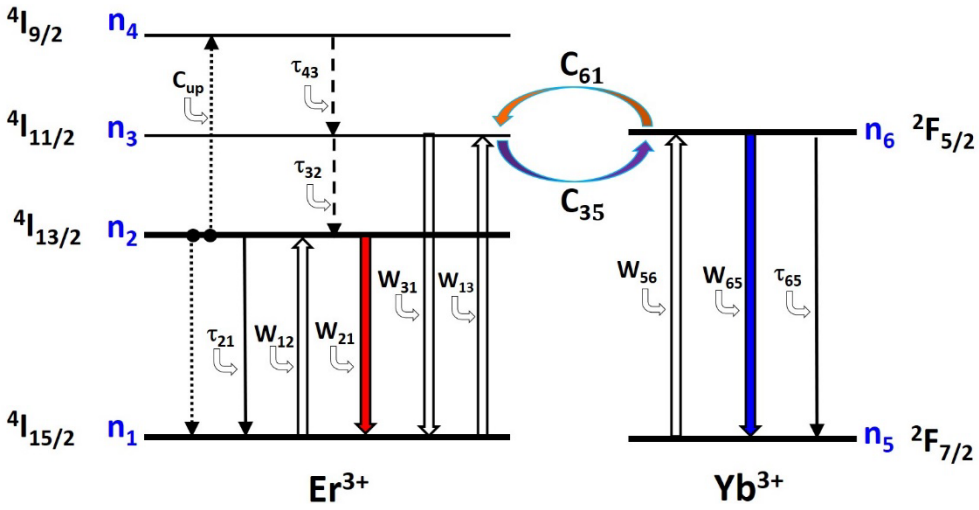

Fig. 4.3 Schematic energy level diagram of the Er^{3+} and Yb^{3+} ions of the Er/Yb co-doped system.

The simplified energy level diagram of the Er/Yb co-doped system is shown in Fig. 4.3. Transitions in Er^{3+} ions involved with energy levels $^4S_{3/2}$ and above are not included

since they are negligible. The numerical analysis is based on a rate-equations model which includes all the radiative and non-radiative transitions shown in Fig. 4.3. The stimulated transition rates are denoted as W, lifetime as τ, forward and backward energy transfer coefficients as C_{61} and C_{35}, and the upconversion coefficient as C_{up}. Two types Yb ions are assumed, respectively, the coupled (n_6^c, n_5^c) and uncoupled (n_6^{nc}, n_5^{nc}) to Er ions. The parameter f is incorporated in the Eq. (4.6) and Eq. (4.7) as the fraction of coupled Yb ions, *e.g.* f=1 is the case when 100% of the Yb ions are considered coupled to the Er ions. The cross-sections and radiative lifetime are assumed to be the same for both types Yb ions. The lifetime of the $^4I_{9/2}$ level is extremely short, therefore we assume $\tau_{43} \approx 0$ and $n_4 \approx 0$ as in a typical case [106,107,117]. The transfer rate equations describing the population density of the Er/Yb co-doped system can be written as [107],

$$\frac{\partial n_2}{\partial t} = \frac{n_3}{\tau_{32}} - \frac{n_2}{\tau_{21}} + W_{12}n_1 - W_{21}n_2 - 2C_{up}n_2^2 \tag{4.1}$$

$$\frac{\partial n_3}{\partial t} = -\frac{n_3}{\tau_{32}} + W_{13}n_1 + C_{61}n_1n_6^c + C_{up}n_2^2 - W_{31}n_3 - C_{35}n_3n_5^c \tag{4.2}$$

$$\frac{\partial n_6^c}{\partial t} = -\frac{n_6^c}{\tau_{65}} + W_{56}n_5^c + C_{35}n_3n_5^c - W_{65}n_6^c - C_{61}n_1n_6^c \tag{4.3}$$

$$\frac{\partial n_6^{nc}}{\partial t} = -\frac{n_6^{nc}}{\tau_{65}} + W_{56}n_5^{nc} - W_{65}n_6^{nc} \tag{4.4}$$

$$N_{Er} = n_1 + n_2 + n_3 \tag{4.5}$$

$$fN_{Yb} = n_5^c + n_6^c \tag{4.6}$$

$$(1-f)N_{Yb} = n_5^{nc} + n_6^{nc} \tag{4.7}$$

where N_{Er} and N_{Yb} are the Er and Yb dopant concentration of the Er/Yb co-doped fiber. Also, the two types of Yb ions are coupled through common stimulated emission rates W, which considers all pump, signal, Yb ASE and Er ASE in both directions. More explicitly, emission from one type of Yb ions can be absorbed by another type of Yb ions. Total Yb ASE gain is determined by the overall Yb inversion consisting of both types of Yb ions. In other words, both types of Yb ions contribute towards Yb ASE.

The wavelength dependent mode overlap factor between the mode field and the doped core is calculated as described on page 341 of [118]. The steady-state equations can be obtained by setting the temporal derivatives to zero for the time dependent transfer rate equations. We have further assumed that C_{61}=C_{35}, $W_{31} \approx 0$ as in all previous models [106,107,117,119].

The steady-state power evolution along the fiber for the pump, signal, Yb ASE and Er ASE are governed by the following propagation equations below.

$$\frac{\partial I_P^{\pm}}{\partial z} = \pm\left\{\Gamma_p\left[n_6\sigma_e^{Yb} - n_5\sigma_a^{Yb} - n_1\sigma_a^{Er}\right] - \alpha_p\right\} I_P^{\pm} \tag{4.8}$$

$$\frac{\partial I_s^{\pm}}{\partial z} = \pm\left\{\Gamma_s\left[n_2\sigma_e^{Er} - n_1\sigma_a^{Er}\right] - \alpha_s\right\} I_s^{\pm} \tag{4.9}$$

$$\frac{\partial I_{YbASE}^{\pm}}{\partial z} = \pm\left\{\Gamma_{YbASE}\left[n_6\sigma_e^{Yb} - n_5\sigma_a^{Yb} - n_1\sigma_a^{Er}\right] - \alpha_p\right\} I_{YbASE}^{\pm} \pm 2n_6\sigma_e^{Yb}\Delta f \tag{4.10}$$

$$\frac{\partial I_{ErASE}^{\pm}}{\partial z} = \pm\left\{\Gamma_{ErASE}\left[n_2\sigma_e^{Er} - n_1\sigma_a^{Er}\right] - \alpha_s\right\} I_{ErASE}^{\pm} \pm 2n_2\sigma_e^{Er}\Delta f \tag{4.11}$$

where $n_6=n_6^c+n_6^{nc}$. The parameters I, Γ, α and σ are respectively photon flux, mode overlap factor with the doped core, background loss and cross section. Subscript p, s, YbASE, ErASE, a, and e indicate respectively pump, signal, Yb ASE, Er ASE, absorption and emission. The ASE spectrum for Er and Yb are divided into slots of width $\Delta f = \frac{c}{\lambda^2}\Delta\lambda$.

The thermal model is based on that given in [72]. The temperature distribution is quadratic in the core and logarithmic in the cladding. It is worth noting that the thermal transport from the core to the environment is largely limited by the heat transfer process at the fiber surface. The thermal conductivity of silica glass is relatively high and the temperature at the core is typically just a few degrees higher than that at glass surface, even for hundreds of microns of cladding [95]. We have assumed that the core temperature is uniform in our model. The fiber temperature is largely determined by the heat transfer coefficient to the environment. Forced air cooling was used in [111], where the heat transfer coefficient is strongly dependent on both temperature and nature of the air flow at the fiber surface. It is reasonable to believe that fiber temperature is well below 200ºC as sustained exposure to higher temperature would lead to coating damage. The local heat load along the fiber can be calculate by considering all the emissions going in and out of the fiber segment.

The model is implemented in MATLAB. Pump, signal, Yb ASE and Er ASE in both forward and backward directions are considered. Photons are propagated forward and backward repeatedly using a standard ordinary differential equation solver (ode45) until convergence. Boundary conditions at each fiber end are set by the launched pump level and reflections (see Table 4.1). Guessed values are used as initial values for unknown

powers, and it is optimized continuously until the boundary conditions are met. The process typically converges within 50 round-trip iterations to the required tolerance.

Table 4.1 The parameters used in the numerical modeling

Parameter	**Value for** [111]	**Value for** [109]	**Notes**
Core diameter	30 μm	24 μm	[109,111]
Cladding diameter	584 μm	289.5 μm	[109,111]
Core NA	0.21	0.20	[109,111]
τ_{21}	10 ms	10 ms	[107]
τ_{65}	1.3 ms	1.3 ms	[109,111]
τ_{32}	1 ns	1 ns	[107]
$C_{61}=C_{35}$	2.98×10^{-20} m^3/s	2.15×10^{-20} m^3/s	Adjusted to fit data
C_{up}	3×10^{-24} m^3/s	3×10^{-24} m^3/s	[107]
N_{Er}	1.43×10^{25} ions/m^3	1.43×10^{25} ions/m^3	Er peak loss
N_{Yb}	2.45×10^{26} ions/m^3	1.12×10^{26} ions/m^3	Yb peak loss
N_{Yb}/ N_{Er}	17.2	7.8	
Fraction of coupled Yb ions	15%	25%	Adjusted to fit data
Loss near 1.55 μm	0.12 dB/m	0.12 dB/m	Estimated
Loss near 1 μm	0.12 dB/m	0.12 dB/m	Estimated
Thermal conductivity	1.38 W/m/K	1.38 W/m/K	[118]
Fiber length	6 m	5 m	[109,111]
Reflection at pump end	4%	4%	[109,111]
Er reflection at far end	100%	100%	[109,111]
Yb reflection at far end	5%	4%	[109,111]
Pump wavelength	975 nm	975 nm	[109,111]
Laser wavelength	1567 nm	1565 nm	[109,111]
Yb ASE wavelength	1035-1075nm in 25 steps	1035-1075nm in 25 steps	
Er ASE wavelength	1540-1590nm in10 steps	1540-1590nm in10 steps	
Temperature	20°C uniform along fiber	20°C uniform along fiber	

The refractive index and active dopant distributions are assumed to be uniform in the core. In our default case, all emission is in the fundamental mode (LP_{01}). There is only a negligible amount of Er ASE in all simulations, and it is represented at 10 equally spaced wavelengths (5 nm step size) while Yb ASE is represented at 25 equally spaced wavelengths (1.6 nm step size). This is enough to resolve any spectral features. Yb parasitic lasing can be clearly observed by significantly narrowing the Yb ASE spectrum in the simulation as expected.

4.3 Results and discussions

4.3.1 Conventional model with only coupled Yb ions (f=1)

The nominal values of all parameters used in the numerical simulations are given in Table 4.1 along with the references and explanations. In cases where values used in the model deviated from these values in Table 4.1, the new values are specified where they occur.

We first calculated the temperature dependent Yb loss and small signal gain in the core for 100% inversion of the fiber used in [111] as this is relevant to understanding the reabsorption of Yb ASE. This is given in Fig. 4.4. In general, loss at a wavelength shorter than 980 nm decreases with a temperature rise since this absorption originates from the bottom level of the Stark split of $^2F_{7/2}$ manifold level. The loss above 980 nm increases with temperature as it originates from the upper levels of the Stark splits of $^2F_{7/2}$ manifold level. The small signal gain decreases above ~1 μm with a temperature rise due to a decrease of their excited state population at the bottom level of the Stark splits of $^2F_{5/2}$ manifold level. At the peaks of gain and loss, these changes with temperature are more pronounced. Yb parasitic lasing occurred at 1067 nm in [111]. As shown in Fig. 4.4, the temperature dependence of the Yb gain and loss is very weak at this wavelength.

We then simulated the case as in the conventional model where all Yb ions are equally involved in the energy transfer and described by a single transfer coefficient, i.e. the fraction of coupled Yb ions is 100% (f=1). We studied two examples where the uniform temperature along the fiber length was set at 20°C and 500°C, and the latter is far above

what we considered realistic. The transfer coefficient C_{61} (=C_{35}) was adjusted to fit the measured Yb parasitic laser threshold in [111] at 20°C.

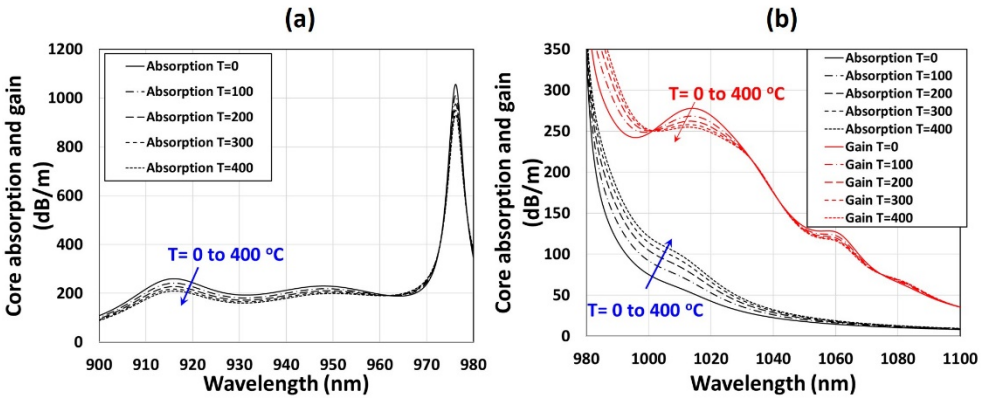

Fig. 4.4 Temperature dependence of (a) core absorption around the pump wavelength and (b) core absorption and small signal gain at 100% inversion around the ytterbium ASE wavelength from the model.

The Fig. 4.5 depicts the experimental setup described in [109], which is one of the two laser configurations used in our numerical modeling in this chapter. As shown in Fig. 4.5, the pump was launched into the fiber from free space. The cavity was formed at the pump end by straight cleaving and at the far end by butting with a dichroic mirror. The fiber was cooled by forced air.

The simulation results for modeling of laser output under different temperatures are shown in Fig. 4.6. It can be seen clearly that output powers are clamped to a fixed value in both cases, albeit that the output power is slightly higher for 500°C. This is because all the inversions are clamped to provide appropriate gains to compensate for the fixed respective

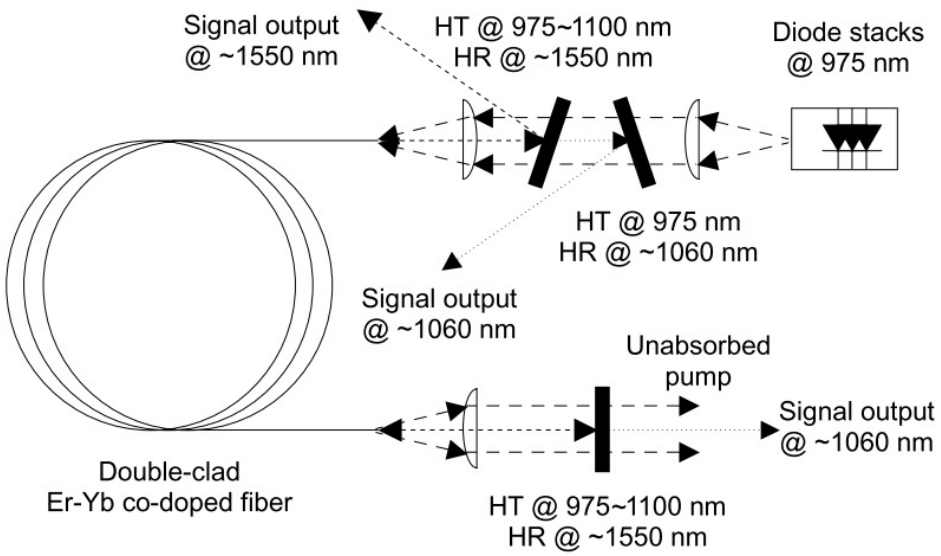

Fig. 4.5 Experimental setup of the Er/Yb co-doped fiber laser oscillator described in [109].

cavity losses for the Er and Yb emissions. This results in a fixed energy transfer rate (defined as $C_{61}n_1n_6$) from Yb to Er ions and consequently clamps the output power from the Er ions. The conventional model even with the incorporation of the temperature effect cannot explain the continued increase in output power from Er after the onset of Yb parasitic lasing observed in [109,111,121]. Additionally, the effect of temperature would be negligible for a temperature rise of just a few tens of degrees in a realistic scenario. To make matters worse, the authors in [96] used unrealistically high fiber temperature of 350°C to simulate the 103 W Er/Yb fiber laser in [109]. When scaled with the output power, this would lead to a fiber temperature of over 1000°C at 297 W output from the Er/Yb fiber laser oscillator in [111]. This is obviously not possible in a realistic scenario.

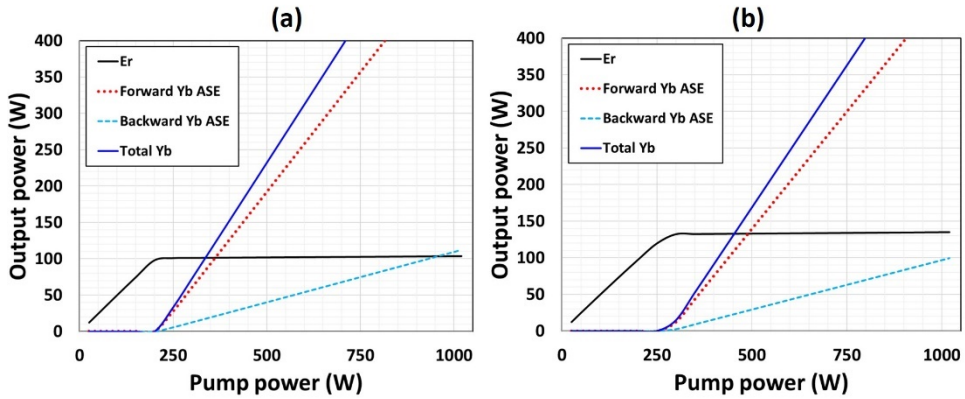

Fig. 4.6 Simulated powers from the Er/Yb fiber laser at two different temperatures predicted with the conventional model. All Yb ions are coupled to Er ions (f=1) and a uniform temperature along the fiber at (a) 20°C and (b) 500°C. The parameters C_{61}=C_{35}=1.1 × 10^{-21} m^3/s is determined by Yb threshold.

4.3.2 New model with both coupled and isolated Yb ions (f<1)

We finally studied the case where not all Yb ions are directly coupled to Er ions (f<1) with all powers in LP_{01} modes. The fraction of coupled Yb ions and the transfer coefficient C_{61} (=C_{35}) were first varied to get the best fit to the experimental data at the maximum power in [111] and the simulation was then run for the entire power range for f=0.15, 0.2, 0.4, 0.6, 0.8 and 1 as shown in Fig. 4.8.

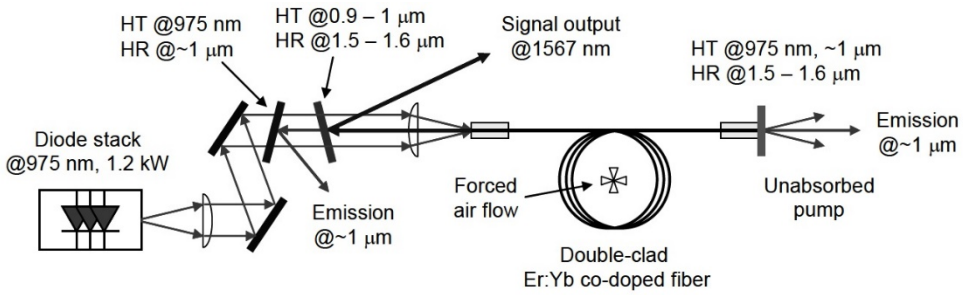

Fig. 4.7 Experimental setup of the Er/Yb co-doped fiber laser oscillator described in [111].

Output clamping is clearly seen near f=1, which needs to be lowered to get a best fit over the entire measured data range. The fraction of coupled Yb ions was determined to be 15% for the best fit. It is interesting to note that the ratio of Yb to Er ions is ~17. This indicates that, on average, one Er ion being surrounded by roughly two and half neighboring Yb ions, if 15% of the Yb ions are coupled (i.e. f=0.15).

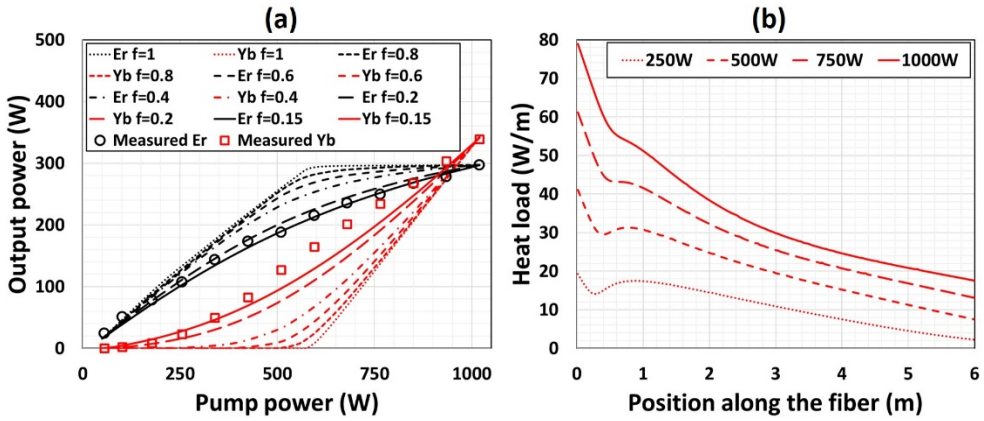

Fig 4.8 (a) Simulated Er laser output and total Yb output by assuming 15%, 20%, 40%, 60%, 80% and 100% ytterbium ions being coupled to erbium ions (f=0.15 with $C_{63}=2.98\times10^{-20}$ m^3/s, f=0.2 with $C_{63}=1.87\times10^{-20}$ m^3/s, f=0.4 with $C_{63}=7.43\times10^{-21}$ m^3/s, f=0.6 with $C_{63}=4.62\times10^{-21}$ m^3/s, f=0.8 with $C_{63}=3.36\times10^{-21}$ m^3/s, f=1 with $C_{63}=2.63\times10^{-21}$ m^3/s) and (b) heat load at various pump powers for f=0.15. Measured data is from [111].

As can be observed in Fig. 4.8 (a), a reasonably good fit was achieved especially for the output power. There is some slight discrepancy in the fit to the total Yb parasitic laser output. We modeled Yb ions using only two types of ions, those closely coupled to erbium ions and those uncoupled to erbium ions. It may be more accurate to model the system based on a continuous change in the degree of the coupling. In addition, there is non-uniformity of dopants across the core in practice which is not considered here.

The inversions along the fiber for various pump powers and inversions averaged over the entire fibers versus pump powers are shown in Fig. 4.9. It can be seen in Fig 4.9 (b) that the average Er inversion is clamped by the round-trip laser cavity loss and so is the average inversion of the uncoupled Yb ions above Yb parasitic laser threshold by the round-trip Yb cavity loss. The average inversion of the coupled Yb ions, however, continues to increase with pump power, leading to a continued increase of Yb→Er energy transfer thus leading to the increase of output power from Er ions. This increase of average inversion of the coupled Yb ions also contributes slightly towards to the gain of the Yb parasitic laser, leading to a slight decrease in the average inversion of the uncoupled Yb ions above the Yb laser threshold as shown in Fig. 4.9 (b).

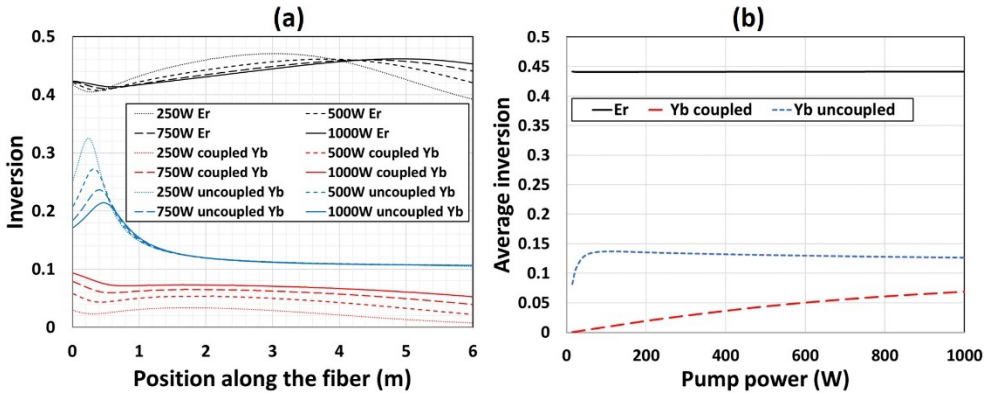

Fig 4.9 (a) Inversion along the fiber and (b) average inversion over the entire active fiber for various pump powers for case of f=0.15 in Fig. 4.8 (a).

Strong re-absorption of Yb forward ASE emission can be clearly seen by power decay during its propagation in our simulations [Fig. 4.10 (a)], previously also observed in [107]. This is true even at low pump power below the Yb parasitic lasing threshold. Pump, signal and ASE powers inside the fiber are shown for 100 W pump power in Fig. 4.10.

Even in this case of 15% coupled Yb ions, pump is mostly absorbed. There are strong ASE inside the fiber but very little of it makes to the ends as shown in Fig. 4.10(b).

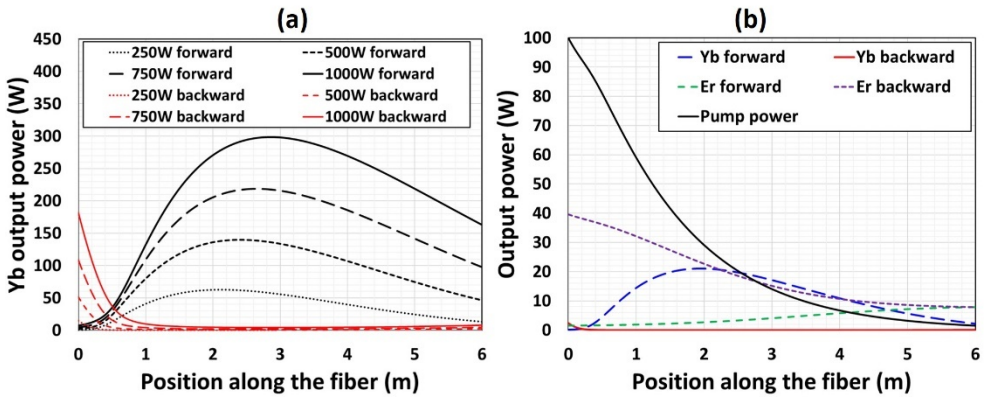

Fig. 4.10 (a) Ytterbium emission powers along the fiber at various pump powers for the model with f=0.15 in Fig. 4.7 (a); (b) pump, Er signal, and Yb emission powers in the fiber at 100 W of pump power.

According to this new model of two types of Yb ions, Yb parasitic lasing as a result of the bottleneck of Yb→Er energy transfer cannot be avoided. This will always take place at high enough pump powers when the pumping rate exceeds the energy transfer rate, i.e. $n_5{}^c W_{56} > C_{61} n_1 n_{6c}$. The energy transfer rate can be expressed as $C_{61} n_1 n_6{}^c$, where C_{61} is determined by the host glass composition; n_1 is the Er population at the ground state; and $n_6{}^c$ is the excited state population of coupled Yb ions. For the case where all Yb ions are closely coupled to Er ions (i.e. f=1), the output power is expected to be clamped above the Yb parasitic lasing threshold by the fixed energy transfer rate which can now be written as $C_{61} n_1 n_6$ where n_6 is the excited Yb population. This is because n_1 is fixed by Er round-trip cavity loss and n_6 by Yb round-trip cavity loss. This is contrary to the experimental observation in [109,111,121].

4.3.3 Brief discussion of the modeling results

Our work, for the first time, can explain the continuous growth of output at ~1.6 μm by incorporating the scenario of two types of Yb ions, those closely coupled to Er ions and those not closely coupled (i.e. isolated) to Er ions. In this case, when the above Yb parasitic lasing threshold, n_1 is still fixed, so is the population of the uncoupled Yb ions. The energy transfer rate $C_{61}n_1n_6^c$ can, however, still increase with pump power due to an increase in the population of the coupled Yb ions n_6^c, leading to a continuous increase in output power. Our model also reveals that there is a significant re-absorption of the Yb ASE by the coupled Yb ions. This is very noticeable even at low pump powers, leading to significant radiative energy transfer from the uncoupled Yb ions to the coupled Yb ions and then some to Er ions.

So, here is an interesting question. How can 40% slope efficiency be possible if only 15% of Yb ions are coupled to Er ions at low pump powers? The key to understand this is the significant amount of ASE generated in the fiber by the 85% uncoupled Yb ions which is then re-absorbed. For example, at pump power of 100 W, i.e. below Yb parasitic laser threshold, ~98.5% of the pump is absorbed in the fiber. Co-propagating ASE reaches a level of ~21 W mid-fiber, but it is mostly re-absorbed and only~2.2 W ultimately leaves the fiber [Fig. 4.10(b)]. Backward ASE is also kept low by the re-absorption until the pumping end where the Yb inversion is relatively high.

The threshold pump power for the bottleneck of energy transfer can be written as

$$P_{th} = \left(\frac{A_{pump} h\nu_p C_{61} n_1}{\sigma_a^{Yb}} \right) \frac{n_6^c}{n_5^c} \tag{4.12}$$

where A_{pump} is pump area; h is Planck's constant; ν_p is the pump frequency; $\frac{n_6^c}{n_5^c}$ is the inversion of the coupled Yb ions; and σ_a^{Yb} is the pump absorption cross section.

This threshold, however, can be increased by lowering pumping rate W_{56}. One way is by pumping at shorter wavelengths, e.g. ~915 nm or ~940 nm where the absorption cross section is much lower, i.e. lower σ_a^{Yb}. In fact, there are recent evidence for this [122,123]. The pumping rate W_{56} can be written as [124]

$$W_{56} = \frac{\sigma_a^{Yb}}{h\nu_p} I_p \tag{4.13}$$

where I_p is the pump intensity and other parameters are defined the same as in Eq. (4.12). Another way to lower pumping rate W_{56} is by lowering the pumping intensity while maintaining the same pump power. This can be achieved by using a larger inner cladding, *i.e.* higher A_{pump}.

The threshold for Yb parasitic lasing can also be adversely affected by longer lifetime of the Er $^4I_{11/2}$ level, which increases backward energy transfer. High phosphorus doping can mitigate this by providing the high phonon energy required to increase the non-radiative decay of Er $^4I_{11/2}$ level [125]. We have used very short lifetime of τ_{32}=1ns in our simulation to make it negligible as in [107]. Any increase in this lifetime can severely lower the Yb parasitic lasing threshold. A higher energy transfer rate will ease the bottleneck and raise the parasitic lasing threshold. To this end, a higher Er doping level will be beneficial to increase n_1. Clearly it needs to be kept below the clustering levels.

A fluorescence decay measurement was conducted in [111] using a Q-switched laser at 920 nm with 100 ns pulse duration as the pump. The measurement showed significant decay (50% to 70%) within the first 10 μs. This decay was believed to be caused by Yb→Er energy transfer. Roughly 2% of the ions relaxed with a time constant of 100 μs or slower. The isolated ions were estimated to be 2-5% based on this. The energy transfer time can be calculated as

$$\tau_{61} = \frac{1}{C_{61} n_1} \tag{4.14}$$

This gives τ_{61} a value of ~3 μs based on our simulation when all Er ions are in the ground state. Given the intensity of the Q-switched pump pulse of up to 30 μJ, significant amount of Yb ions were inverted. If substantial energy transfer took place, Er ions are expected to be nearly fully inverted after few hundreds of μs (noting τ_{61}depends on Er ground state population and increases as Er ions are inverted). This would have stopped any further energy transfer, leading to the decay to flat out after the initial energy transfer. This is then followed by a slower spontaneous decay.

Fluorescence decay measurements have been used in several works to evaluate energy transfer efficiencies in Er/Yb fibers [126–128]. Typically, the decay rate is used, and the magnitude of the intensity is rarely used. Low excitation is essential to avoid population saturation and ASE. The decay time of the fast decay component is typically in a range of 1-30 μs followed by slow decay component with a decay time of 500 μs to 1.3 ms [127]. >50% of decay was observed during the fast decay for Yb concentrations

exceeding 1.5wt% in [127]. These decays were not exponential especially when Yb concentration is high [126].

Non-radiative energy transfer among neighboring Yb ions can be very fast [126]. This likely also contributes towards the fast decay components when it leads to the excitation of Er ions (or loss by other mechanisms) and may also explain the observed non-exponential decays. This additional effect will make the fast decay component far more pronounced than just direct ytterbium-to-erbium transfer. Although the decay rates of this additional energy transfer can be below 100 μs, most of them are substantially slower than the few μs from the direct Yb→Er energy transfer and consequently their contribution towards the easing of the bottleneck is less significant. Clearly more accurate numerical modeling requires a better quantitative understanding of the non-radiative energy transfer process among the neighboring Yb ions. This is only possible with significant additional experimental studies.

In addition, there are also other processes which can contribute towards the fast decay component. An excited Yb ion can transfer energy to an Er ion in the long-lived $^4I_{13/2}$ level leading it to be excited to $^4I_{9/2}$ [126] and up-conversion processes can also play a part. A quantitative modeling of the fluorescence decay process can be very helpful but is only possible with additional detailed experimental studies.

In any case, if 95% to 98% Yb ions are closely coupled to Er ions derived by the proportion of fluorescence decay beyond 100 μs in [111] and considering the Yb to Er ratio of 1/0.058=~17 in this case, there will be 16 to 17 Yb ions on average neighboring to a

single Er ion. This is not physically or chemically possible unless non-radiative neighboring Yb→Yb energy transfer is considered. There can only be a maximum of 4 Yb ions next to each Er ion if rare earth ions are in the tetrahedral structure of silica. The fluorescence measurement in [111] would have included non-radiative energy transfer among neighboring Yb ions and significantly overstated the coupled Yb ions. Most of the decay processes involving energy transfer among neighboring Yb ions are significantly longer than the few μs decay time of the direct Yb→Er energy transfer and consequently play a relatively much weaker role in the bottleneck process. There may also be other effects involved in the experiments. Further experimental studies are clearly needed.

Our work for the first time establishes a quantitative value for the energy transfer coefficient based on measurements in high-power lasers, C_{61} = 2-3×10-20 m^3/s. A decay time of τ_{61}= 2-4 μs can be derived for the fluorescence decay measurement. This is consistent with the fast end of the 1-30 μs range measured in [127]. Our simulation also shows that only ~15% Yb ions are coupled to Er ions in a fiber with Er to Yb ratio of 0.058 and ~25% for a fiber with Er to Yb ratio of 0.128. Based on these results, we can also show for the first time that on average there are 2-2.5 Yb ions next to a single Er ion. From a material perspective, this is highly plausible in the tetrahedral structure of silica.

4.4 Conclusion

In conclusion, we have established a new Er/Yb model based on the existence of two types of Yb ions, those closely coupled to Er ions and those uncoupled from Er ions. We have incorporated an accurate temperature-dependent Yb cross section based on the

measured temperature-dependent Yb loss. We have validated our modeling result by comparing the simulation results and experimental data [109] and [111]. We concluded that the elevated temperatures at high powers and mode-dependent gain only play insignificant roles in the observed continuous growth of laser output from erbium after the onset of the Yb parasitic lasing. Based on the existence of two types of Yb ions, we can explain all the observed behavior in high-power Er/Yb fiber lasers in [109,111,121]. We will use the numerical modeling in this chapter as the benchmarking model for our simulation of the Er/Yb fiber MOPA that we will discuss in the next chapter.

CHAPTER FIVE

ERBIUM-YTTERBIUM FIBER MOPA ~1562NM

This chapter presents a systematic study on the Nufern Er/Yb fiber (LMA-EYDF-25P/300-HE) for further single-mode power scaling at 1562nm using a kW-level pump diode at 915 nm. A home built Er/Yb laser oscillator at 1562 nm was used as the seed (i.e. master oscillator) for the Er/Yb fiber master oscillator power amplifier (MOPA). We have obtained maximum output of 302 W single-mode power at 1562 nm with an optical efficiency record of 56%, very close to the quantum-limited efficiency of 58.6%. Also, we have found that the fiber fuse is the major limiting factor for further single-mode power scaling in this fiber rather than ASE as was previously reported. Our simulations show that off-resonance pumping at ~915 nm or ~940 nm only plays a small role in the observed negligible ASE especially at high powers. The main reason is possibly due to the high Er doping level in this Er/Yb fiber fabricated by Nufern.

5.1 Introduction

Er/Yb co-doped fiber lasers are critical for power scaling at the eye-safe wavelength of ~1.6 μm [109,111,121–123,129–132], attracting strong interest for a wide range of applications including coherent LiDAR, free-space communication, remote sensing, gravitational wave detection, etc. Despite recent progress in the demonstration of 656 W from a Yb-free Er-doped fiber laser in a multimode beam with an M^2 of 10.5 [31], the weak pump absorption of Er ions requires very large cores in double-clad fibers for sufficient pump absorption over practical fiber lengths of under few tens of meters limited by fiber

background loss. This would limit potential power scaling of single-mode operation due to the limited core size. Using a 34 μm-core, 75 W single-mode power was achieved in [133] and 103 W in [134]. Higher power is possible with the higher pump brightness available now, but significant further power scaling will be limited for Yb-free Er-doped fiber.

The previous power record from an Er/Yb co-doped fiber was set over a decade ago with 297 W at 1567 nm and an M^2 of 3.9 [111]. The average slope efficiency was ~40% at low powers and decreased to ~19% at high powers. The main limit was identified as Yb parasitic lasing. In fact, the total output from the Yb parasitic laser was 337 W at 1067nm, higher than the 297 W laser output at 1567 nm in [111]. In-band pumping of Er/Yb fiber has been proposed to overcome this. Indeed, 264 W at 1585 nm was demonstrated by pumping at ~1535 nm with an average slope efficiency of 74% [132]. The pump was, however, from a combination of 36 individual Er/Yb fiber lasers, each with an output of 11 W at 1535 nm. Commercial high-power diodes are not widely available at ~1535 nm, severely limiting this approach. Several attempts have been made to control the Yb parasitic lasing by using an auxiliary seed or positive feedback at the Yb emission wavelength [135–137]. Very little progress towards high-power, however, was made with any of these approaches.

5.2 Motivation and background

There have been some recent developments in single-mode power scaling of Er/Yb fiber lasers pumped by 9xx nm pump diodes. Single-mode single-frequency power of 207 W at 1560 nm was demonstrated with a MOPA configuration in [122]. The pump was at ~940 nm in a counter-pumping configuration. This is the current single-mode power record

from an Er/Yb fiber pumped by 9xx nm diodes. What is notable with this demonstration is the much higher efficiency and almost total absence of Yb amplified spontaneous emission (ASE) especially at high powers. The average slope efficiency was 50.5% and optical efficiency was 49.3%. These are record efficiencies, significantly higher than the ~40% in previous works.

The key breakthrough is the new 25/300 fiber from Nufern [Fig. 5.1]. The authors in [29] also conducted a comparison study with pump diodes at 976 nm. The fiber length was significantly shortened in this case to provide the same amount of pump absorption of 12 dB as in the 5 m fiber for the 940 nm case. An average slope efficiency of 40.2% and an optical efficiency of 35.6% were achieved, much lower than those for the 940 nm pump. Using 5.5 m of the same fiber with a MOPA counter-pumped at 940 nm, 111 W at 1556 nm and an optical efficiency of 46% was achieved in [8]. A simulation was also conducted in [8], showing much higher Yb ASE for 976 nm pumping in comparison to pumping at 915 nm or 940 nm in the case where the total pump absorption is the same.

The 25/300 μm Er/Yb co-doped fiber has a doped core with 9.1 wt% P, 1.6 wt% Al, 4.9 wt% Yb and 0.44 wt% Er. The cladding pump absorption at 915 nm is ~2.6 dB/m and core absorption at 1535 nm is ~85dB/m. The fiber has a pedestal design with a core NA of ~0.09. Pump cladding NA is ~0.46. The first use of the early version of this Nufern developed large mode area (LMA) pedestal design Er/Yb co-doped fiber was reported in 2006 by Tankala et al. [138]. The key benefit of the pedestal structure is to ensure core NA<0.1, which supports much lower number of modes in the large diameter doped core. Without the pedestal design, the refractive index difference between the doped core and

the cladding is much higher with core NA ~0.2. For a 25 μm core diameter, the V-number will be ~4.5 for NA=0.09 and ~10 for NA=0.2. Thus, the active fiber is a few-mode fiber rather than a highly multi-mode fiber thanks to the pedestal.

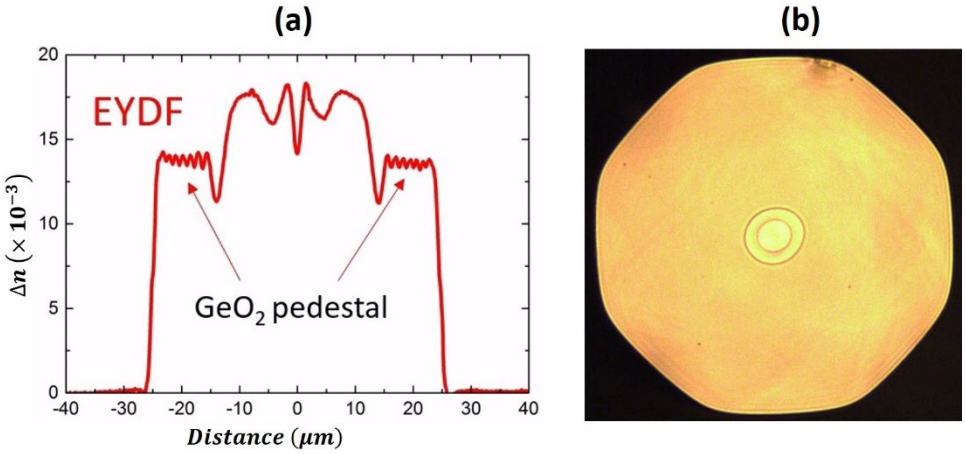

Fig. 5.1 (a) Refractive index profile of the 25/300 μm Er/Yb co-doped fiber from Nufern.[139] (b) Microscopic image of the Nufern Er/Yb fiber cross-section.

5.3 Results and discussions

The experimental setup is shown in Fig. 5.2. It is a MOPA counter-pumped by a 915 nm multi-mode diode laser module delivering up to 1.5 kW for the power amplifier. The 25/300 Nufern Er/Yb fiber was spliced at both ends to matching passive fibers (LMA-GDF-25/300) also from Nufern. The reason for the passive fiber splice is twofold: to allow the entire active fiber to be immersed in water for cooling and to ensure launching of fundamental mode seed into the core of the pedestal designed Er/Yb fiber. The ends of the passive fibers were angle cleaved. Various active fiber lengths were tested to find the optimum fiber length. The master oscillator was built with a 10/128 CorActive Er/Yb fiber

(DCF-EY-10/128), which, at one end, was spliced to a home-made high-reflectivity fiber Bragg grating (FBG) at 1562 nm and straight-cleaved at the output end.

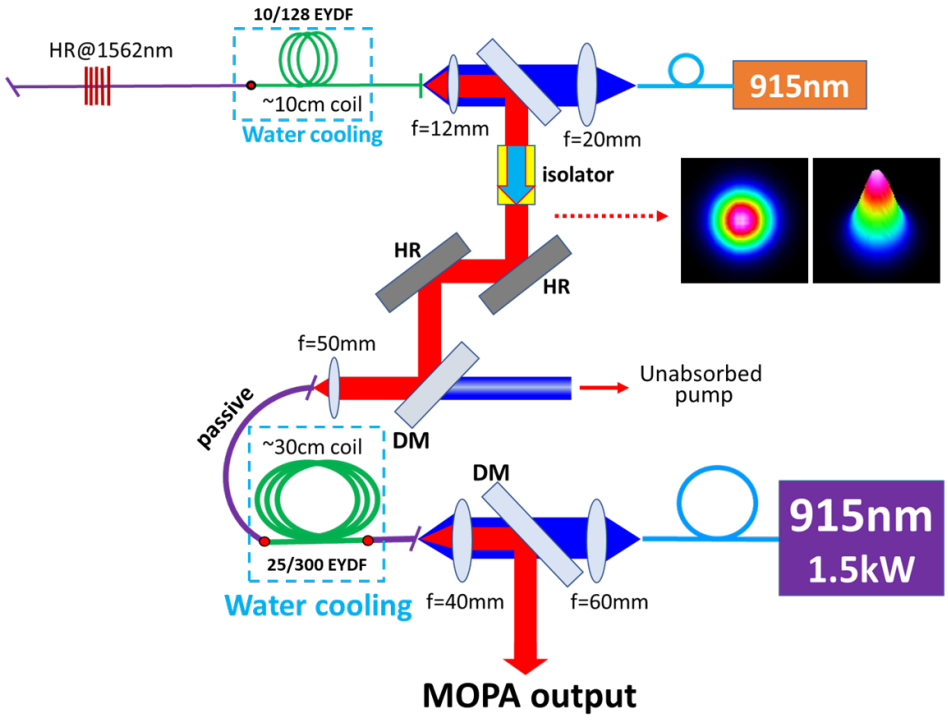

Fig. 5.2 Experimental MOPA setup (DM, dichroic mirror; HR, high reflectivity mirror).

Both active fibers were fully immersed in water for cooling and the coiling diameters of the Er/Yb fibers for the seed laser and power amplifier were, respectively, 10 cm and 30 cm. The master oscillator was also pumped at 915 nm and was followed by an isolator. The M^2 of the seed was measured to be 1.17/1.12 (see inset in Fig. 5.2 for its mode image) and ~1.9 W was launched into the power amplifier. The laser mode quality factor (M^2 value) of both the seed output from the master oscillator and MOPA output was

measured using a scanning slit beam quality measurement system (BP209IR2) from Thorlabs. All the M^2 tests were performed in accordance with ISO 11146 standard.

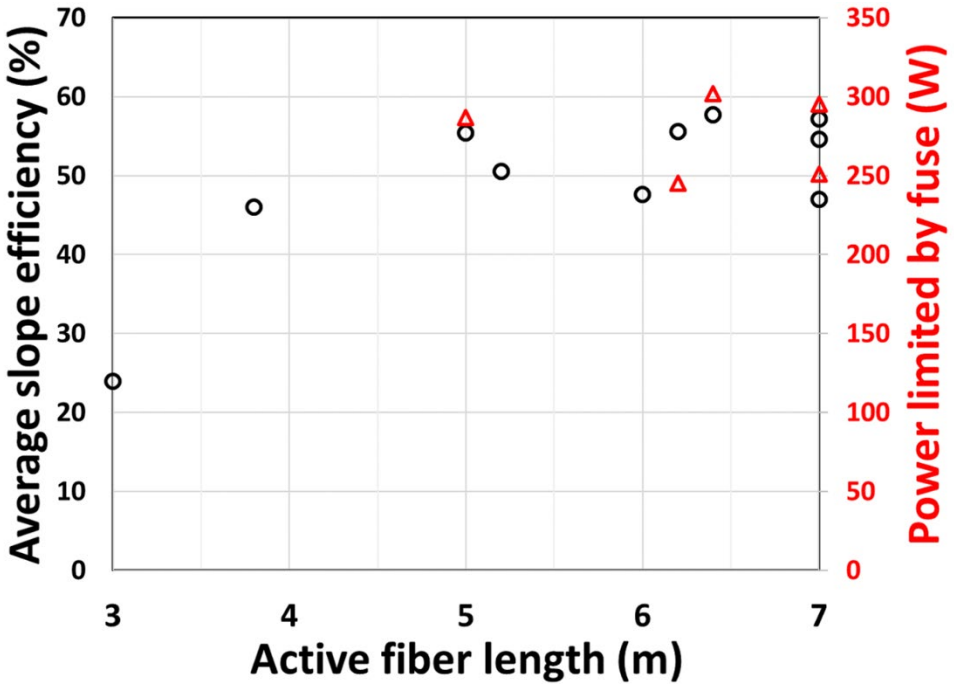

Fig. 5.3 Average slope efficiency versus active fiber length in the MOPA and the maximum output powers where fiber fuse occurred.

We systematically studied several fibers of various lengths. Typically, the slope efficiency varied with pump power (more on this later). We plotted the average slope efficiency versus active fiber length in Fig. 5.3. Higher than 50% average slope efficiency was regularly achieved for active fiber length between 5 m and 7 m. In addition, in most cases, the maximum power was limited by fiber fuse which starting between 0.2 m to 0.4 m away from the splice at the pump end. Those maximum powers were also plotted in Fig. 5.3, typically between 250 W to 300 W with a maximum of 302 W. In a few exceptional

cases, the maximum power was limited by fiber damage at the pump end. Hardly any Er or Yb ASE was observed in any case.

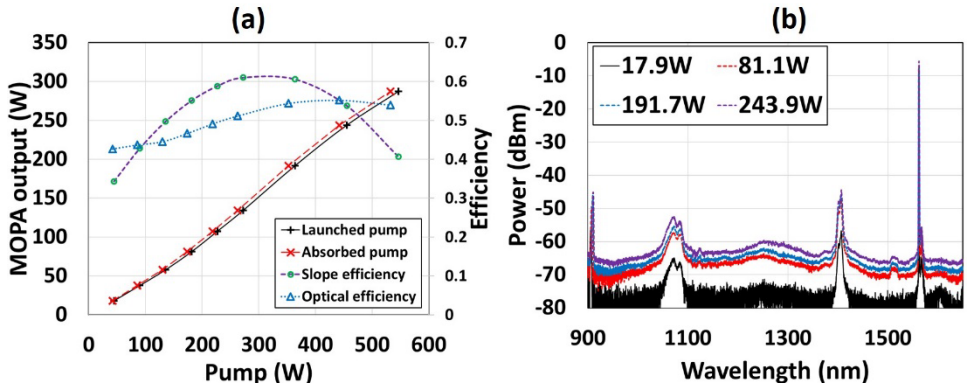

Fig. 5.4 (a) MOPA output power versus launched (and absorbed) pump power with slope and optical efficiency; (b) optical spectra at various output powers for the run with an active fiber length of 5m.

The experimental measurement with 5 m Er/Yb fiber is described in more detail in Fig. 5.4. The output power is plotted against both launched and absorbed pump power in Fig. 5.4(a). The two curves almost overlap, indicating near total absorption of the pump. The slope efficiency calculated by taking the derivative of a polynomial fit to the output versus launched pump is also plotted. It generally shows an increase with the pump at low pump powers and a slight decrease towards the maximum output power. Optical efficiency calculated as output divided by the absorbed pump is also plotted, showing similar trend. The optical spectra at various output powers are also shown in Fig. 5.4(b). The peak at ~1.4 μm appeared in both the seed and MOPA outputs is not identified, possibly an artifact from high order reflections of the grating built in the commercial optical spectrum analyzer (AQ6370D). There is in general hardly any ASE from either Er or Yb. M^2 versus MOPA output power is plotted in Fig. 5.5(a). This shows a general decrease in M^2 at high powers,

typical of a pedestal design due to the stronger gain competition at higher powers. M^2 was 1/1.08 at an output power of 244 W (see mode image in Fig. 5.5(b) and the related M^2 measurement in Fig. 5.5(a)). There was not enough time to take an M^2 measurement at the maximum output power of 302 W.

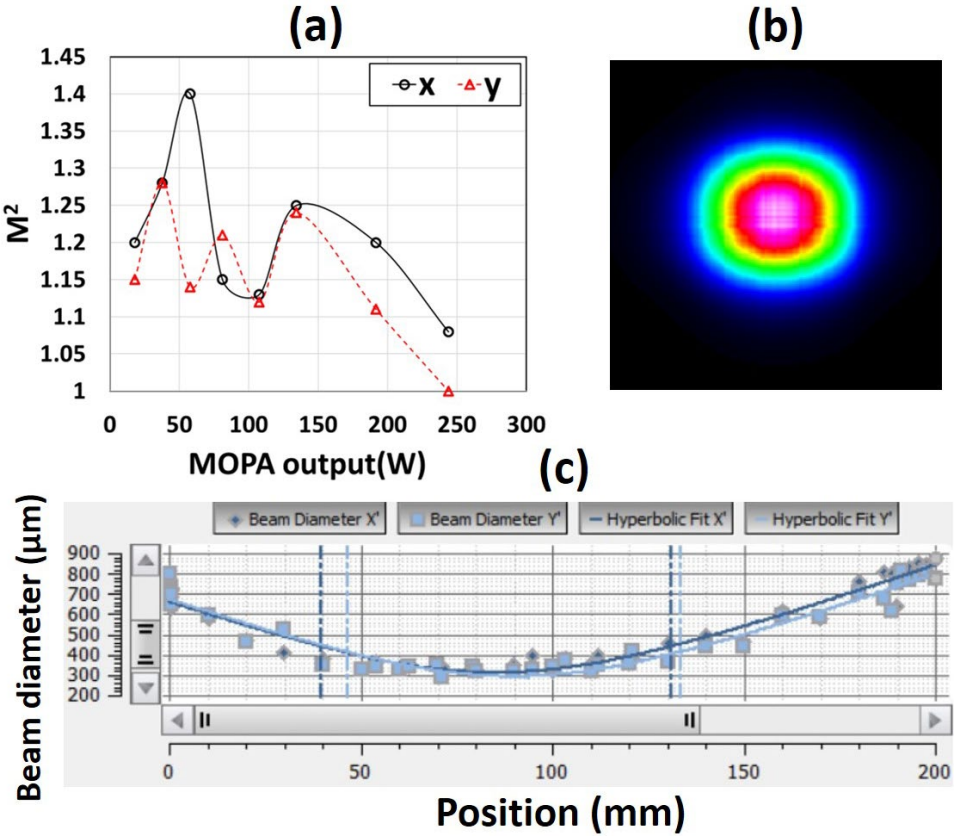

Fig. 5.5 (a) M^2 value at various output powers; (b) mode image and (c) its M^2 measurement at 244 W output for the run described in Fig. 5.3.

The measurement with 6.4 m Er/Yb fiber is detailed in Fig. 5.6. The output power versus launched and absorbed pump are plotted in Fig. 5.6(a) along with the slope efficiency and optical efficiency. A record power of 302 W was measured in this test. The maximum slope efficiency was ~64% at ~360 W of pump power. A record optical

efficiency of 56% was also measured, very close to the quantum-limited efficiency of 58.6%. The M^2 was measured to be 1.27/1.35 at an output power of 250 W in this case.

In order to understand the onset of fiber fuse, we simulated the heat load in this case using a home-made Er/Yb fiber numerical model like that described in [140]. The model is implemented in MATLAB based on a model described in detail previously in Chapter 4. Pump, signal, Yb ASE and Er ASE in both directions are considered in order to evaluate local inversion. This allows all the powers to propagate repeatedly forward and backward with appropriated boundary conditions applied at the fiber ends until convergence. Local heat load is calculated by the difference of all optical powers flowing into and out of a small segment of fiber. Key fiber parameters are given in Table 5.1.

The calculated heat load at various pump powers is shown in Fig. 5.6(b). The highest heat load occurs at the pumping end of the active fiber in this counter-pumped case, where z=0 is the seed coupling end and z=6 is the pump coupling end. A maximum heat load of ~100 W/m is expected at our maximum pump power.

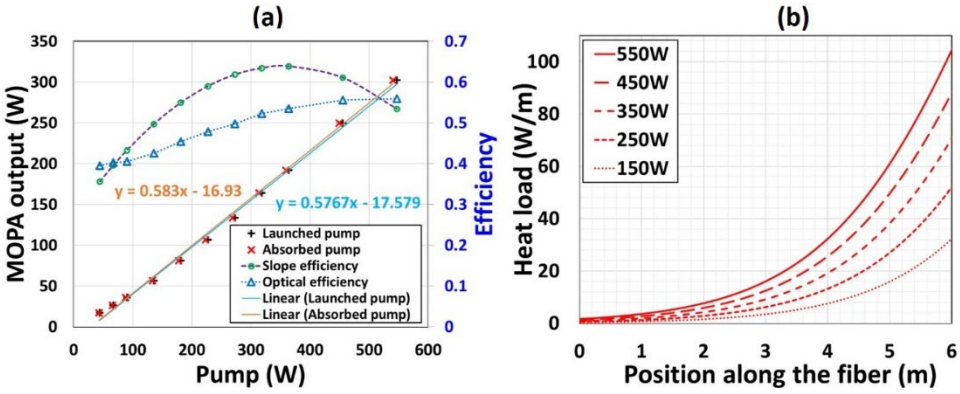

Fig. 5.6 (a) MOPA output power versus launched (and absorbed) pump power with slope and optical efficiency; (b) simulated heat load at various pump powers for the run with an active fiber length of 6.4m.

The fiber fuse in our experiments typically started between 0.2 m to 0.4 m away from the splice point in the active fiber at the pump end. Coating discoloration/degradation near the splice at the pump end was also observed in [29]. This is interesting because the fiber burn does not initiate at the splice point between the 25/300 μm matching passive fiber and the Er/Yb fiber, where the maximum temperature due heat load was expected as shown in Fig. 5.6(b). Instead the fiber burn usually occurs certain distance away from the splice point. During our experiments, we spent considerable amount of time to optimize the splicing quality of the fusion splice [Fig. 5.7(b)]. Nevertheless, the splice might have scattered some pump light into the coating, leading to its over-heating and damage. This coating damage could have initiated the fiber fuse and could have also been responsible for the decreasing of slope efficiency near the maximum output power.

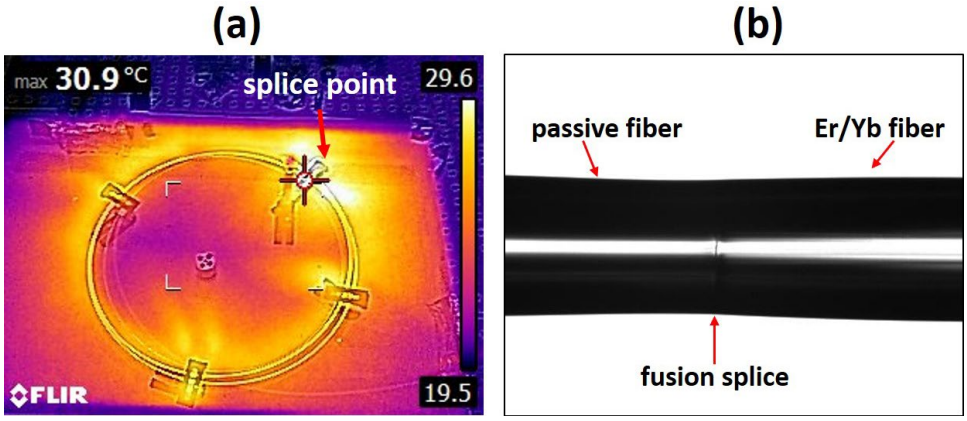

Fig. 5.7 (a) Thermal image of the Er/Yb fiber with ~30 cm coil diameter in the water bath under counter-pump high power test; (b) fusion splice between the 25/300 μm matching passive fiber and Er/Yb fiber.

We then simulated the co-pumped case and found the heat load is also close to ~100 W/m near the pump end, so there is no benefit for trying co-pumping scenario. We have also simulated the fiber laser in [111] which achieved the previous power record of 297 W.

In this case, the maximum heat load is expected to be 60 W/m at the pump end (see Chapter 4 for more details). The much lower heat load is due to the oscillator nature of the demonstration. In an oscillator, heat load is more broadly distributed along the fiber, unlike that in an amplifier where it is narrowly distributed near the pumping end.

The efficiency difference between ~976 nm pumping and that for ~915 nm and ~940 nm pumping can generally be understood by an energy transfer bottleneck in an Er/Yb fiber which happens when the pumping rate of Yb ions exceeds the rate of Yb→Er energy transfer. The Yb pumping rate is proportional to the product of the Yb absorption cross-section at the pumping wavelength σ_p, pump photon density I_p, and Yb ground-state population n_5, i.e. $\sigma_p I_p n_5$. The energy transfer rate is Rn_6n_1 (see [140] for example), i.e. proportional to the product of the energy transfer coefficient R, the population of the excited Yb ions n_6 and the population of the Er ions at the ground state n_1. The bottleneck condition can be written as $\sigma_p I_p n_5 > Rn_6n_1$. The energy transfer coefficient R is determined

Table 5.1 Comparison of fiber parameters

Parameter	Southampton	Nufern
Core diameter (μm)	30	25
Cladding diameter (μm)	600	300
Core NA	0.21	0.09
N_{Er} (ions/m^3)	1.43×10^{25}	4.22×10^{25}
N_{Yb} (ions/m^3)	2.45×10^{26}	3.35×10^{26}
N_{Yb}/ N_{Er}	17.24	7.94
Fiber length (m)	6	5-7
Pump wavelength (nm)	975	915/940
Laser wavelength (nm)	1567	1562

by the host glass composition. The higher absorption cross-section σ_p at ~976 nm will increase Yb ASE due to its much higher pumping rate. The higher efficiency with pumping at ~915 nm was first observed by Nilsson et al. [129].

The biggest mystery is what is the key difference between the new Nufern fiber with negligible Yb ASE at high powers and the Southampton fiber used in [111] which was severely limited by Yb parasitic lasing. The key parameters of the two fibers are listed in Table 5.1. The Er and Yb dopant concentrations are calculated from the absorption data provided in [111] and by Nufern. In the case of the Nufern fiber, we also measured the dopant levels by scanning electron microscope (SEM) since we have access to the fiber, which confirmed the calculated data in Table 5.1. The SEM data shows 0.44 wt% of Er, 4.9 wt% of Yb, 9.1 wt% of P and 1.6 wt% of Al in the Nufern fiber.

An oscillator configuration pumped at 975 nm was used in [111]. In order to see if this is a major factor, we have conducted extensive modeling of the Southampton fiber and the details are discussed previously in Chapter 4. In summary, we observed in our simulations that the Southampton fiber would still be ASE limited in a similar MOPA configuration pumped at 915 nm.

Energy transfer efficiency η of Er/Yb fibers has been shown to correlate with their slope efficiency at low powers, $\eta = (\tau_{Yb} - \tau_f)/\tau_{Yb}$, where τ_{Yb} and τ_f are, respectively, Yb lifetime without and with the presence of Er ions. For a good Southampton Er/Yb fiber, η was measured to be 0.84 [126]. The Nufern fiber was measured to have η =0.9 in [141]. Our measurement of the Nufern fiber at low power gave a slope efficiency of ~43% for the

915nm pump (see Fig. 5.4 (a)), which is similar to that of Southampton fibers [129], indicating that the energy transfer efficiency η predicts slope efficiency reasonably well at low powers. The near quantum-limited efficiency achieved in the Nufern fiber with 1.6 wt% of Al is contrary to the conclusion reached in [142] regarding the detrimental effect of Al on slope efficiency.

The increased slope efficiency with pump power observed in this work is consistent with that seen in [29]. If we can assume the main loss mechanisms are fiber loss and Yb ASE, the contribution from loss is independent of pump powers and does not explain the pump-dependent slope efficiency. At higher pump powers, the increase of signal power with an increase in pump power is expected to overwhelm the increase of Yb ASE due to an increase in Yb inversion below Yb parasitic lasing threshold, which we had not reached even at the highest pump power in our case. This may explain the increase of slope efficiency at higher pump powers. The drop of the slope efficiency near the maximum powers may be due to the onset of fiber coating damage which eventually initiated fiber fuse.

The near quantum-limited optical efficiency achieved at high powers indicates negligible overall loss from all loss mechanisms. Comparing to [29], our modeling work shows that our MOPA operates at very similar conditions. The slightly different seed power and pump wavelength do not seem to play a major role. We have tested many pieces of fibers purchased over 1-2 years and have not seen significant variations. The improved efficiency may be due to the qualities of the splices which we spent months to perfect and

the more efficient cooling techniques used, i.e. water immersion in our case versus cold plate in [29].

The biggest question is why parasitic lasing observed at high powers in the Southampton fiber in [111] but not in the current Nufern fiber. When pumping rate exceeds this energy transfer rate, i.e. $\sigma_p I_p > Rn_1\left(\frac{n_6}{n_5}\right)$, a bottlenecking would arise, leading to higher Yb inversion and consequently parasitic lasing. This will eventually happen in any Er/Yb co-doped fiber at high enough pump power. The question is why the parasitic lasing thresholds differ so much in the Southampton and Nufern fibers.

Both the cladding and core sizes of the Southampton fiber are larger than that of the Nufern fiber. This is, in fact, favors the control of ASE. Because the larger cladding size reduces the pump intensity and consequently lowers the Yb pumping rate. The larger core lowers Yb ASE intensity and therefore reduces Yb ASE. One of the key factors for the near absence of the Yb ASE in the Nufern fiber is likely its much higher Er doping level. This will increase the energy transfer rate, i.e. Rn_6n_1, by the much larger Er population at the ground state n_1. There are more Er ions to transfer energy to, i.e. more acceptors. In addition, the energy transfer coefficient R is dependent on the host glass composition and it increases with the higher N_{Er}/N_{Yb} ratio found in the Nufern fiber as a result of the much higher Er doping level [126,141]. Pumping at wavelengths with smaller absorption cross-section $\sigma_p$also helps.

5.4 Conclusion

We have demonstrated a new power record of 302 W in single-mode Er/Yb fiber lasers using a counter-pumped MOPA configuration. A near quantum-limited new record optical efficiency of 56%. This single-mode power is a new record for any lasers at this wavelength range and the efficiency is also a new record for Er/Yb fiber lasers, demonstrating the power scaling potential of Er/Yb operating at very high efficiency. Slope efficiency was found in general to increase with pump power at lower powers and to decrease before the maximum power. The maximum slope efficiency achieved was a record 64%. Further, the experimental results also show that fiber fuse is the primary limit to further power scaling in the 25/300 LMA Er/Yb fiber, not Yb ASE as was previously expected. We found Yb ASE to be negligible in all cases we tested. The new breakthrough is mostly a combination of more efficient Er/Yb fiber from Nufern and off-resonant pumping at 915 nm which eases the bottlenecking of Yb→Er energy transfer. Since fiber fuse can be mitigated by lowering the heat load, a longer Er/Yb fiber with a lower pump absorption can be used to further power scaling. Our results provide significant new insights into power scaling at ~1.6 μm and optimizing the Er/Yb fiber fabrication especially for future home-made Er/Yb fiber based on all-solid photonic bandgap design to suppress Yb parasitic lasing [143].

CHAPTER SIX

SINGLE-FREQUENCY YTTERBIUM FIBER LASER ~1064NM

This chapter presents the experimental study on power scaling of narrow-linewidth single-frequency high-power Yb-doped photonic bandgap fiber (PBF) laser based on a counter-pumped MOPA configuration. We focus on optimizing a novel Yb-doped fiber design to demonstrate a ~50/400 μm core/clad diameter PBF based on multiple cladding resonance (MCR) cladding microstructure design which was proven to be very successful in suppressing HOM even with very large core diameter fibers as discussed in Chapter 1 and 2 of this dissertation and in [37,38]. Previously, a single-frequency Yb-doped fiber laser operating at 1064 nm using 50/400 μm all-solid PBF based on a different PBF design was reported to be only limited by TMI near 400 W signal average output power [52]. Our simulation also shows SBS threshold is above 1-kW level with this novel Yb doped PBF. The preliminary experimental results show that the MOPA operates TMI-free up to signal output power of ~500 W with an M^2 of ~1.3 and linewidth of ~10 kHz. Our goal is to power scale the output power of 1064 nm single-frequency Yb PBF laser to near 1-kW by further suppressing the TMI thus increasing TMI limit to ~1-kW using this Yb PBF in which we incorporated the previously proven successful MCR design.

6.1 Background and introduction

6.1.1 Limits and mitigation techniques

In recent years, single-frequency fiber lasers have attracted increasing interests over the past decade due to the advantages of low noise, narrow linewidth, and long coherent

length of high power single-frequency lasers in many applications, such as coherent beam combination, high resolution spectroscopy, nonlinear frequency conversion, coherent communication, active laser remote sensing, gravitational wave detection, etc. The demand for narrow-linewidth high-power fiber lasers is especially strong for direct energy weapons application in defense. However, the maximum CW output power from sub-MHz narrow-linewidth single-frequency fiber lasers still hover ~800 W [144,145]. The output power has been limited mainly due to nonlinear effects such as SBS [19] and TMI [40], which were previously discussed in detail in Section 1.2.2 of Chapter 1. In general, SBS has the lowest threshold among all the nonlinear effects involved in limiting the output power of narrow-linewidth single-frequency fiber lasers.

The SBS is a two-step process which is driven by electrostriction and it involves the coupling of backward scattered signal wave (initially starts with spontaneous Brillouin scattering), forward signal wave, and forward acoustic wave. As the pump power reaches near certain threshold power level, there is a strong interference between the forward signal wave and the backward scattered Stokes wave, which leads to the increase of forward acoustic wave through electrostriction. Thus, evolving from a spontaneous Brillouin scattering to stimulated Brillouin scattering (SBS). Eventually the acoustic wave acts as a strong reflector grating and reflects large portion of the forward signal wave, thus limiting the output power of the fiber lasers. The threshold power is reached when the power of back scattered Stokes light is equal to the forward signal output. As shown in Eq. (1.7), the threshold power for SBS is proportional to acousto-optic effective mode area A_{eff}, and it is inversely proportional to peak Brillouin gain coefficient (BGC) g_B and effective

nonlinear interaction length L_{eff}. The three main parameters that involve in the estimation of SBS threshold power can be written as following [10,19],

$$A_{eff} = \frac{\left(\iint_A IdA\right)^2}{\iint_A I^2 dA} \approx \pi w_m^2 \tag{6.1}$$

$$g_B = \frac{2\pi n^7 p_{12}^2}{c\lambda_0^2 V_a \rho \Delta\nu_B} \tag{6.2}$$

$$L_{eff} = \int_0^L \frac{P(z)}{P_{out}} dz = \frac{1}{\alpha}\left[1 - \exp(-\alpha L)\right] \tag{6.3}$$

where w_m is the optical mode field radius, $\Delta\nu_B$ is the Brillouin gain linewidth, $\Delta\nu_L$ is the laser linewidth, V_a is the acoustic velocity, p_{12} is the transverse photoelastic coefficient, ρ is the density of the host glass, α is the optical attenuation coefficient with a unit of m^{-1}, and the BGC g_B scales with $\frac{\Delta\nu_B}{\Delta\nu_L + \Delta\nu_B}$ when $\Delta\nu_L \gg \Delta\nu_B$. Also, the frequency shift of the Stokes wave (i.e. the backward scattered light) can be derived from the energy and momentum conservation of forward optical wave, backward scattered Stokes wave and the forward traveling acoustic wave as following,

$$\nu_B = \frac{2n_{eff}V_a}{\lambda_L} \tag{6.4}$$

where n_{eff} is the effective mode index and λ_L is the wavelength of the forward signal laser, i.e. the seed laser in the case of a MOPA amplifier. The maximum Brillouin frequency shift

is wavelength dependent, and it is ~10 GHz at 1.5 μm and ~16 GHz at 1 μm. In the experiment of single-frequency MOPA at 1064 nm, both the backward scattered power and optical spectrum are monitored, and usually the optical spectrum shows a Rayleigh scattering peak at the signal frequency and SBS shifted Stokes frequency at ~16 GHz, i.e. ~0.06 nm shifted from 1064 nm towards longer wavelength.

Over the years, various mitigating techniques have been reported to suppress SBS, including increasing core diameter while decreasing NA (i.e. increasing mode area A_{eff}) [52], laser gain competition [145,146], phase modulation [147], increasing pump absorption (i.e. decreasing L_{eff}), applying thermal or stress gradient along the fiber, tailoring acoustic velocity of the fiber by optimizing the dopant and other material properties [148,149], etc. Among these approaches, quite many of them are focused on reducing the Brillouin peak gain, i.e. the g_B. As can be seen from the Eq. (6.2), the BGC can be altered via engineering so many parameters of the fiber most of which are related to the material properties [19] of the fiber core glass such as acoustic velocity, density, refractive index, photoelastic coefficient, and Brillouin gain linewidth. In many cases, one or multiple of the mitigation techniques are used to suppress SBS. But eventually it comes to how efficient and practical the mitigation techniques are for specific applications. For example, the waveguide design and fiber material related approaches are usually very stable and free from environment instabilities that hinder the practicality of the single-frequency laser. On the other hand, applying thermal or stress gradient along the fiber may not be the case.

Table 6.1. A list of common techniques to suppress SBS, effectiveness in increasing SBS threshold, and potential limitations. [150]

Mitigation strategy	P_{th}^{SBS} **increase**	**Potential limits**
Large core (A_{eff} ↑) [150]	> 100 x	SM operation & TMI
Acoustic tailoring (g_B ↓)	10 x	Optical homogeneity
Lower intrinsic BGC (g_B ↓)) [151]	100 x	Fiber fabrication
Thermal/stress gradient ($\Delta\nu_B$ ↑)	7 x	Fiber failure
Higher Yb concentration (L_{eff} ↓)	1.5-2 x	Photodarkening &TMI
Phase modulation ($\Delta\nu_L$ ↑) [150]	> 100 x	Beam combinability

Table 6.1 shows a list of common SBS suppression techniques with its effectiveness and potential drawback or limitations in practical applications and fiber fabrication. Among them, the large core and phase modulation approaches have the greatest impact on suppressing the SBS, thus the scalability of the output power. Material optimization can potentially also have a great impact [19]. Although the phase modulation technique involves in broadening the laser linewidth, so it is not the best way to go especially for MHz or kHz level narrow-linewidth applications. The Brillouin gain bandwidth $\Delta\nu_B$ is on 10s or 100s of MHz level (~50 MHz in silica fibers [10]) and the SBS becomes a main limitation only when $\Delta\nu_L \ll \Delta\nu_B$. But this is also the linewidth regime that certain applications require. That means utilizing VLMA fibers with large core diameter is not

only very efficient but also a straightforward way to mitigate SBS for ultra-narrow-linewidth single-frequency fiber laser systems. Unfortunately, mode quality degradation due to the large core is one of the main reasons behind TMI, the other major limiting factor of output power from high-power single-frequency fiber amplifiers.

The physical origin behind TMI is not as well understood as SBS, given that SBS was theoretically predicted by L. Brillouin in 1924 and experimentally discovered first by C. H. Towns et al. in 1964 [152] very shortly after the invention of lasers, and SBS is very common not only in high power fiber lasers and amplifiers but also in many other laser architectures involving high optical intensity, long gain medium, etc. On the other hand, TMI was experimentally observed for the first time only about 10 years ago around 2010 [39,48]. Nevertheless, TMI is generally regarded as the result of two factors: excessive heat load and poor mode quality. When the output power exceeds certain TMI threshold, the TMI leads to output beam fluctuation as a result of phase-matched mode interference and energy (or power) transfer between the fundamental mode (i.e. LP_{01}) and one or more HOMs. More details on TMI can be found in Section 1.2.3 of Chapter 1 of this dissertation as well as in a very recently published tutorial/review article by Jauregui et al. [40].

As shown in Eq. (1.8) and (1.9), the TMI can be mitigated by optimizing the waveguide design, quantum defect between pump and signal, and host material composition (e.g. thermo-optic coefficient, thermal conductivity, etc.). Jauregui et al. [40] reported that there are also some other fiber parameters that affect TMI threshold, such as rare-earth dopant concentration, photodarkening loss, active fiber length, signal linewidth, etc. Among these mitigation techniques, the optimizing fiber waveguide design to improve

mode quality is one of the most effective and somewhat intuitive approaches to increase TMI threshold by reducing the mode interference between the FM and HOMs.

6.1.2 Brief review and motivation

The utilization of photonic bandgap fibers (PBF) [35,38,63], a special type of very large mode area (VLMA) fibers, combined with intrinsic thermal gradient along the fiber at high output power has the potential to be an effective method to mitigate both SBS and TMI for further scaling the average output power from narrow-linewidth single-frequency fiber laser systems. In 2007, Liu [149] proposed in a modeling study of SBS threshold mitigation that a single-frequency fiber amplifier can generate up to 1 kW output power with 60 kHz narrow linewidth without the onset of SBS in a VLMA fiber with core diameter ~ 40 μm, and the temperature gradient plays very important role in suppressing SBS. In 2007, Jeong et al [148] reported a 500 W single-frequency output power at 1060 nm using a 25 μm core and 380 μm cladding diameter Yb-doped fiber of ~6.5 length through a MOPA configuration counter-pumped at 975 nm. In the same year, Gray et al [153] reported a 502 W single-frequency output at 1064 nm using a 8.5 m long Yb-doped fiber with 39 μm core and 420 μm cladding diameter through a multi-stage MOPA configuration bi-directionally pumped at 976 nm. In the same study, Gray et al also conducted a numerical modeling of SBS suppression using the same 39 μm core but under counter-pumped MOPA configuration, and it was predicted that up to 2 kW of SBS-free single-frequency output power can be generated mainly due to the fact that counter-pumping configuration leads to much greater temperature gradient (i.e. the temperature difference between the coolest and hottest position along the fiber) and the signal was

treated as perfectly linearly polarized. In real experiments, most of the LMA fibers are not PM so the polarization of the signal is far from a perfect linear polarization. In fact, the Eq. (1.7) that estimates the threshold power of SBS can be multiplied by a factor of 2 for the case of a perfectly linear polarized signal light. That means practical estimation of SBS threshold in this case is also near 1 kW. Nevertheless, all the aforementioned studies showed that temperature gradient due to quantum defect heating at the output end of the fiber in a counter-pumped MOPA configuration can help further mitigating the SBS threshold. The SBS threshold increase due to high temperature gradient can be explained by the temperature dependent Brillouin gain broadening, thus decreasing the Brilloiun gain coefficient g_B. By this time, quite a lot of research and study were done to mitigate SBS in single-frequency laser and amplifiers, and significant progress was made to increase SBS threshold over 1 kW. Then, TMI was observed in around 2010 [39] and it has since then been the major limiting factor in further power scaling of single-frequency fiber amplifiers especially in the cases where a VLMA fibers (e.g. PCF, PBF, etc.) were used since the large core significantly increases the SBS threshold but deteriorated mode quality because of large core (even in the case of strong HOM suppression) leads to TMI at certain power level before it reaches the SBS threshold.

In 2011, Robin et al [154] from the Air Force Research Laboratory (AFRL) reported a 500 W SBS-free output power from a counter-pumped MOPA using a 40 μm core and 300 μm inner cladding diameter Yb-doped PCF (provided by NKT Photonics) with a segmented transverse acoustic tailored core design for SBS suppression. The output power was eventually limited by TMI near 500 W. In 2014 [144], the same research group

reported a 811 W record output power using a PCF which has a specially designed core to suppress both SBS and TMI, i.e. gain tailored for TMI suppression (by reducing the coupling between LP_{01} and LP_{11} modes) and acoustic tailored for SBS suppression (by introducing segmented acoustic index of refraction using dopants comprised of F, Al, and Ge). They used a 9.2m long PCF with a core diameter of 38 μm (MFD~30 μm) and cladding diameter of 400 μm, which had an estimated pump absorption of 1.6 dB/m at 976 nm. The MOPA output was eventually limited by SBS near 811 W, which was indicated by >0.1% ratio of backward scattered power to signal output power. Although the TMI was mitigated in this case, but it came with a price of a very complex core design and much smaller core diameter of only 38 μm which played a major role in leading to lower SBS threshold.

In 2014 [52], a collaboration research work between the AFRL and our group at Clemson University led to an output power of 400 W from a single-frequency MOPA using a Yb-doped all-solid photonic bandgap fiber (PBF) with very large flat-to-flat core diameter of 52 μm and flat-to-flat cladding diameter of 431 μm. Later, a further study on SBS characterization with this Yb PBF were conducted and it revealed that g_B was ~ 6×10^{-11} m/W which is about a factor of 2 lower than the g_B of the NKT fiber in [144,154]. Compared to the PCF with air holes in the cladding, the all-solid PBF has many advantages such as easy to splice for future monolithic all-fiber amplifier architecture. In addition, the low loss bandgap region of the PBF can be engineered to operate at various wavelength regimes that suffer from high ASE at ~1030 nm in conventional PCFs.

In this chapter, we will present our experimental work on power scaling of ultra-narrow-linewidth single-frequency fiber MOPA operating at 1064 nm using a double-clad Yb-doped all-solid PBF through a MOPA configuration counter-pumped at 976 nm. The all-solid PBFs we have used in our present work are very similar to the PBF used in terms of fiber dimensions and glass composition (e.g. g_B). Except the slightly different fiber dimensions of the new PBF, the major difference is the new microstructure cladding design based on multi-cladding resonance (MCR) PBF which was previously showed superiors HOM suppression [37,38]. So far, we have gone through two iterations of bandgap position engineering by draw a second fiber with slightly larger fiber dimensions in order to move the short wavelength edge of the low loss bandgap near the signal wavelength at1064 nm. We have conducted detailed fiber characterizations and tests to study the SBS and TMI thresholds. By the time this dissertation was written, we have obtained ~500 W output power and 10 kHz linewidth single-frequency output power before it was limited by TMI threshold.

6.2 Experimental setup and results

The experimental setup of the all-solid Yb-doped PBF MOPA is shown in Fig. 6.1. The seed laser is a JDSU manufactured CW linearly polarized single-frequency laser (NPRO M126N-100-1064-100) with a maximum free-space output power of 100 mW and a nominal linewidth of ~ 5 kHz. The output of the NPRO seed was free-space coupled into the input signal fiber of the multi-stage amplifier system (YAR-50K-LP-SF) manufactured by the IPG. The NPRO seed signal was amplified through the IPG amplifier and then delivered to the main amplifier fiber (i.e. the Yb PBF) after transmitted through multiple

free space optics, including the built-in isolator (ISO1) at the output end of the IPG amplifier, the half-wave plate (HWP), the external free space isolator (ISO2) and the long-pass dichroic mirror (DM2) that transmits 1064 nm and reflects unabsorbed pump at 976 nm plus some very low power ASE ~1030 nm. The power of the amplified seed laser before the coupling lens (after DM2) is ~18W when the IPG amplifier was running at 90% output. The length of the Yb PBF was 7~9 m for adequate pump absorption and high slope efficiency of the MOPA output. The main amplifier was counter-pumped at 976 nm by a DILAS diode laser with a maximum output power of 1.5 kW.

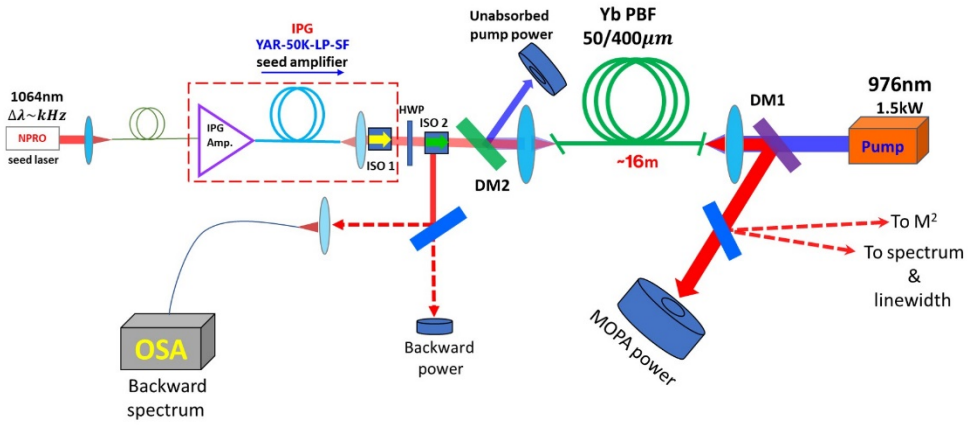

Fig. 6.1 Experimental setup of the single-frequency Yb fiber laser system based on a counter-pumped MOPA configuration.

The output of the MOPA was reflected by DM1 and majority of the power was measured using a water-cooled 1.5 kW rated thermal power meter (L1500W-BB-50) manufactured by Ophir Photonics. A wedge mirror was used to obtain a small amount of the tap power for MOPA output diagnostics including mode quality (M^2), output spectrum, and linewidth measurement. The ISO2 is used for both protecting the seed amplifier from

back reflected signal and extract the backward power from the MOPA. Then another wedge mirror was used to split the small amount of tap power for monitoring backward spectrum, while the main backward power was measured using a power meter. A YOKOGAWA AQ6370 optical spectrum analyzer (OSA) was used to measure output spectrum of the MOPA output and the backward propagating power extracted via IOS2.

The first iteration of the all-solid PBF (fiber number DA00816) has flat-to-flat (F-F) core diameter of 53.5 µm and F-F cladding diameter of 383 µm. Pump absorption is ~2.3 dB/m at 976 nm. Although the fiber dimensions are much larger, this fiber has a similar MCR design as the 25/125 µm all-solid Yb PBF [41,42] that was used for the ~ 980 nm fiber laser which was previously covered in Chapter 1 and Chapter 2 of this dissertation. The microscopic cross-section image of the fiber and its bend loss [35] measurement can be seed in Fig. 6.2.

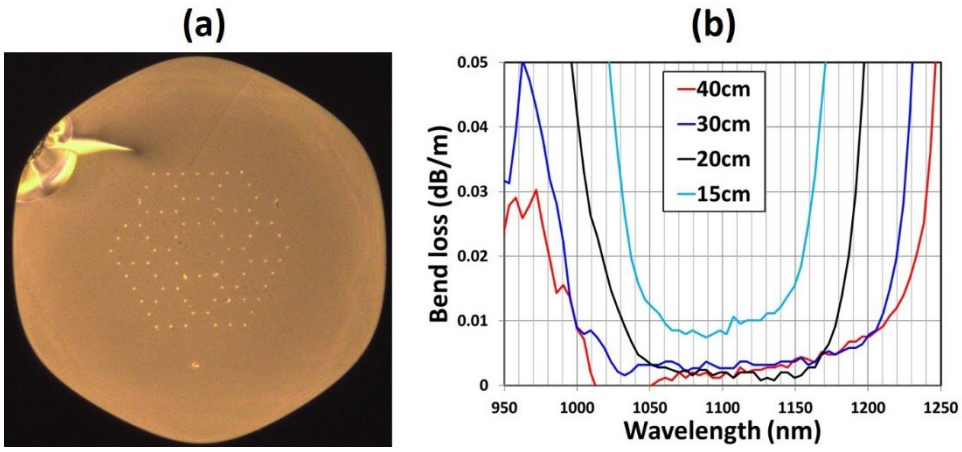

Fig. 6.2 (a) The microscopic image of the fiber cross-section of the first iteration all- solid Yb-doped PBF (DA00816) with F-F core diameter of 53.5 µm and F-F cladding diameter of 383 µm, (b) the transmission spectrum of the fiber at various bending diameters as the legend shows.

We carried out systematic tests to characterize the first iteration fiber for single-frequency MOPA operating at 1064 nm. With a coiling dimeter of ~33 cm and fiber length of ~7.5 m, we obtained maximum output slope efficiency of ~70% and ~87% with respect to the launched pump power and absorbed pump power for an estimated 80% coupling efficiency of the multi-mode pump at 976 nm into the cladding of the Yb-doped PBF. The

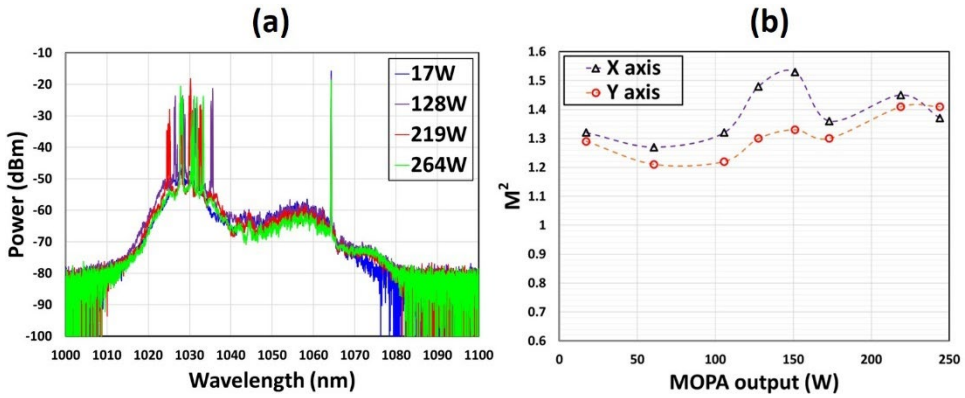

Fig. 6.3 (a) MOPA output spectrum at various output power, (b) Measured M2 at various output power.

M^2 was measured at various output power as shown in Fig. 6.2 (b). However, the output spectrum shows very strong ASE/co-lasing near 1030 nm as in Fig. 6.2(a). The short wavelength edge of the bandgap position was not well positioned to introduce high bending loss to suppress ASE ~1030 nm. Without any spectral filtering, the gain peaks near 1030 nm in a phospholipase Yb fiber.

The second iteration all-solid Yb-doped PBF (fiber number DC27920) was drawn from the same preform as the first iteration (DA00816). The new fiber dimension was scaled up by ~5% compared to the original Yb PBF to move the short wavelength edge of the low loss bandgap to the right to be close enough to the signal wavelength at 1064 nm. Fig. 6.4(a)

shows the calculated position of the of the new fiber transmission at 30 cm coil diameter. As the red solid line indicates the signal wavelength at 1064 nm, the short wavelength edge of the low loss bandgap moves closer to the signal wavelength after the fiber dimension was scaled up by ~5%. Fig. 6.4(b) is the microscopic image of the drawn second iteration Yb-doped PBF which has a F-F core diameter of 56 μm and F-F cladding diameter of 401 μm. The pump absorption is still 2.3 dB/m at 976 nm.

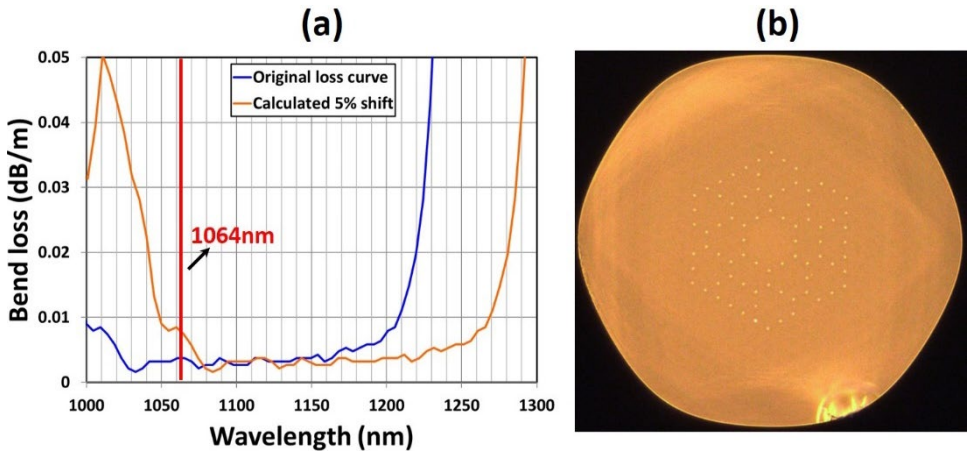

Fig. 6.4 (a) Measured transmission loss at 30 cm coiling diameter (blue) and the same measured data points scaled by 5% (orange), (b) microscopic image of the fiber cross-section of the new fiber scaled up ~5% (DC27920) with F-F core diameter of 56 μm and F-F cladding diameter of 401 μm.

The fiber used for the final test was ~9 m and it was coiled at a coiling dimeter ~32 cm. The MOPA output power as a function of pump power is shown in Fig.6.5. The maximum output power before the onset of TMI is ~503 W. The output power was plotted respectively as a function of absorbed pump power and launched pump power. The coupling efficiency of the 976 nm pump into the inner cladding of Yb PBF was estimated as 80 %. The slope of efficiency with respect to the absorbed pump power is ~90%, which

indicates a very low background loss considering the quantum efficiency of 91.7%. The slope efficiency with respect to the launched pump power is ~80%. The difference between

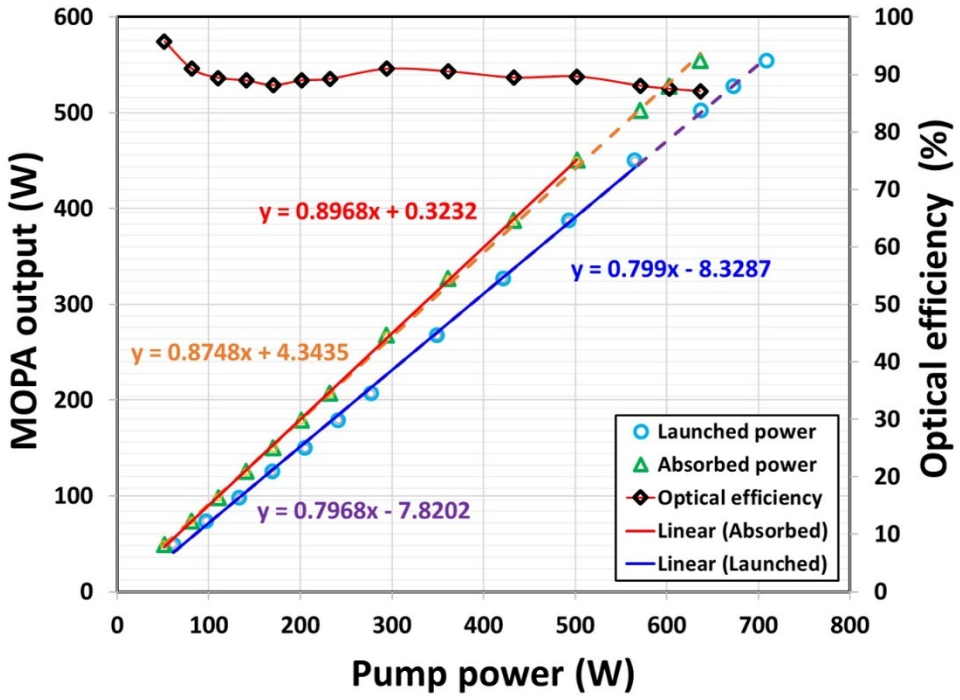

Fig. 6.5 MOPA output power versus pump power (left vertical axis). The slope efficiency with respect to absorbed pump power and launched pump power are indicated by the linear fit to the measured data points as indicated by the circle and triangle markers, respectively. Optical efficiency versus absorbed pump power (right vertical axis).

the two slope efficiencies are due to the unabsorbed pump power that exits the fiber from the seed end of the amplifier reflected by the DM2 as shown in the experimental setup [Fig. 6.1]. The optical efficiency is plotted was calculated via dividing the MOPA output power by the absorbed pump power. The optical efficiency is ~90% at various output powers, which is another indication of very efficient process of pump photon conversion into the signal photon benefited from low background loss.

The MOPA output spectrum was monitored at various output power as we increased the pump power as shown in Fig. 6.6. By comparing this to the output spectrum

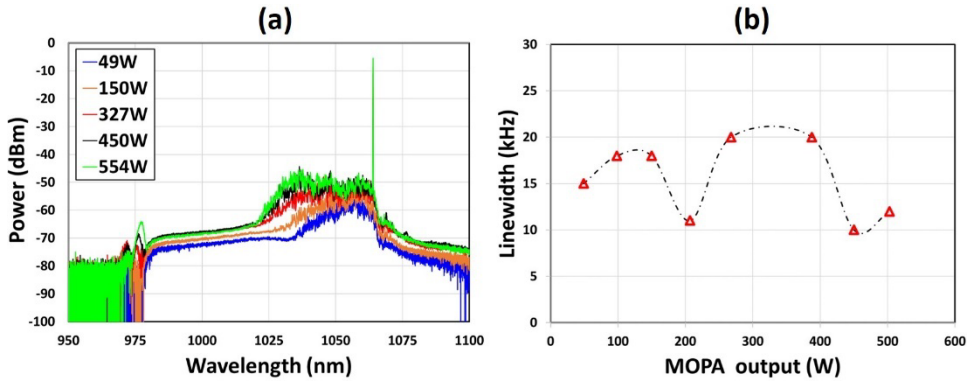

Fig. 6.6 (a) Measured optical spectrum of MOPA output at various output power, (b) measured linewidth of MOPA output at various output power.

in Fig. 6.3(a), we can tell that the low loss bandgap of the new Yb PBF moved to the right, i.e. towards the longer wavelength. The ASE peak moved to near ~1060 nm and it was very well suppressed by ~45 dB in this case. The high slope efficiency and the low ASE both indicate that the bandgap of the new fiber was fine-tuned very precisely to where we wanted, i.e. introducing high bend loss to ASE below 1064 nm but not too close to the signal wavelength so that background loss at 1064 nm is still kept low to guarantee high slope efficiency.

The linewidth of the MOPA output was monitored as well at various output powers as shown in Fig. 6.6(b). Fig. 6.7 shows the setup for the heterodyne detection technique to measure linewidth of MOPA output by beating the output of an identical single frequency laser (NPRO2) with the output of the MOPA which seeded with NPRO1. In the experiment, the central frequency of the NPRO2 was slightly shifted by applying a ~6V

DC voltage (i.e. via temperature-tuning of the NPRO crystal), in order to move the beat frequency away from the 0 Hz position on the RF spectrum analyzer (RFSA). The sweep

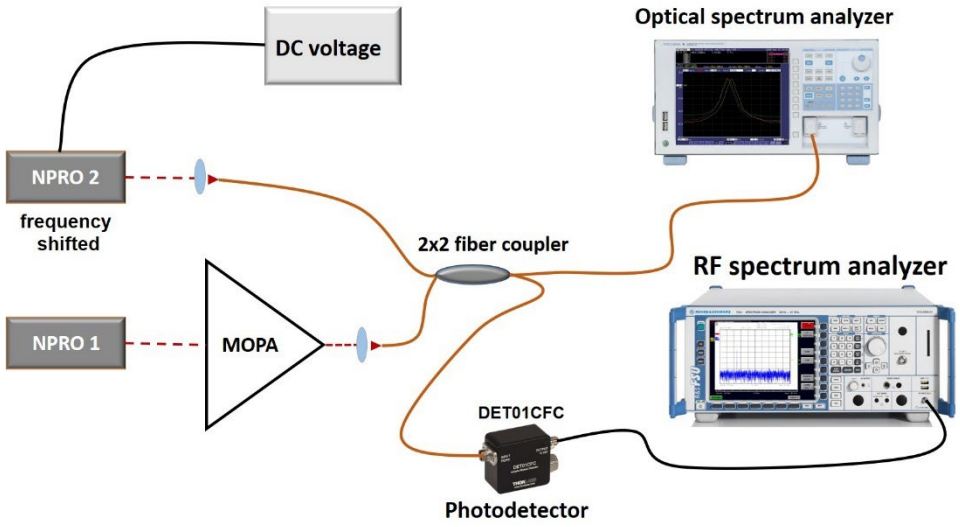

Fig. 6.7 Schematic of the setup for optical heterodyne linewidth measurement of the MOPA output.

time (SWT), video bandwidth (VBW), and resolution bandwidth (RBW) were respectively set to 100 ms, 10 kHz, and 10 kHz. The linewidth of lasers is often defined in terms of 3dB linewidth of the measured RF spectrum bandwidth. In the case of a heterodyne detection, the real linewidth of the laser is half of the measured linewidth of the beat frequency. The fluctuation in the measured linewidth data points at various powers are within the acceptable uncertainty due to frequency noise and resolution of RFSA. The purpose of linewidth measurement is to monitor if there is any linewidth broadening due to SBS onset.

At the same time, power and spectrum of the backward propagating light was monitored using high resolution optical spectrum analyzer (OSA). If the SBS effect comes in, the spectrum will show a Stokes frequency shift by ~16 GHz, i.e. shifted by ~0.06 nm

towards longer wavelength. Fig. 6.8 shows the measured spectrum of the backward propagating light at MOPA output power of ~503 W, and it does not show any signs of

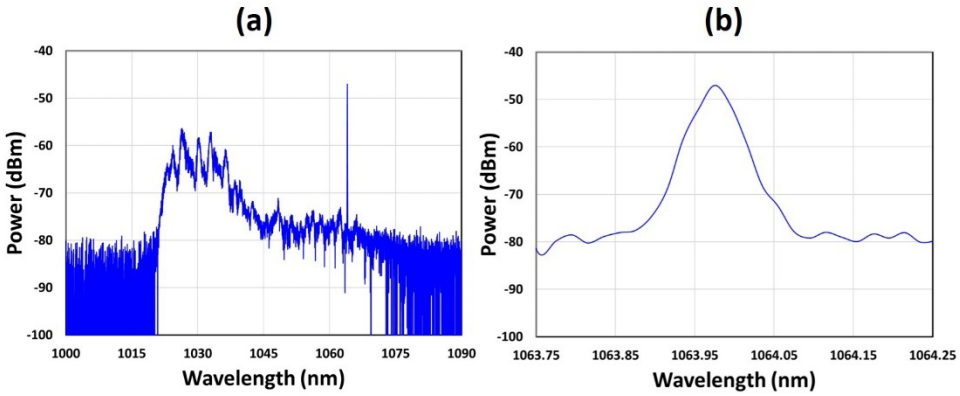

Fig. 6.8 (a) Optical spectrum of the backward propagating light from the MOPA, (b) zooming in around the peak of signal wavelength with the OSA resolution set to 0.02 nm.

SBS. This indicates that the MOPA output was not limited by SBS whatsoever. The high SBS threshold could be explained by the ultra large core and dopant composition which led to very low Brillouin gain in a previous PBF used by the AFRL [52,155]. According to Dragic et al [156] , Yb doped phosphosilicate glass core composition, which is also present in this PBF, can help lowering the peak Brillouin gain g_B.

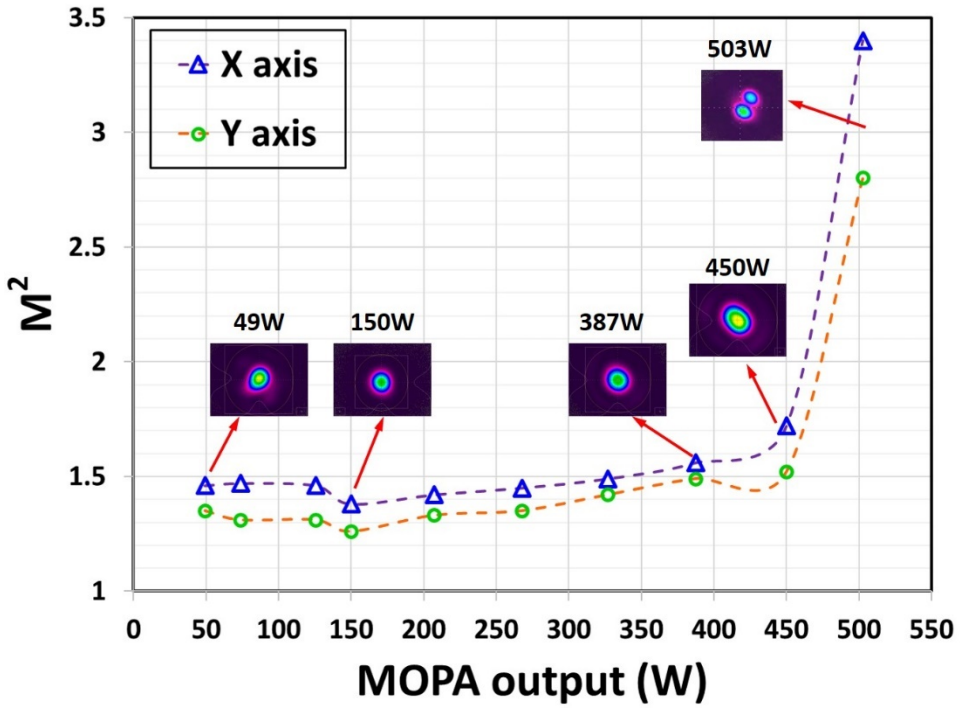

Fig. 6.9 Measured M^2 (along X axis and Y axis) at various MOPA output powers. The inset also shows the mode profile corresponding to a few data points.

The mode quality (M^2) of the MOPA output was measured at various output powers as shown in Fig. 6.9. The M^2 was ~1.3-1.4 before it reached the TMI threshold power at 503 W. When the MOPA output power increased form 450 W to 503 W, a clear time-dependent mode fluctuation was recorded with fast camera of the M^2 device (Ophir Photonics M200s-FW), similar to the dynamic mode fluctuation observed in the by Eidam et al [39]. A small aperture was placed at the center of the beam path before it enters the M^2 device, to remove the unwanted cladding light for consistent mode quality measurement. A second CCD camera was used to measure the mode profile of the MOPA output at various output power as shown in Fig. 6.10. The CCD camera was slightly

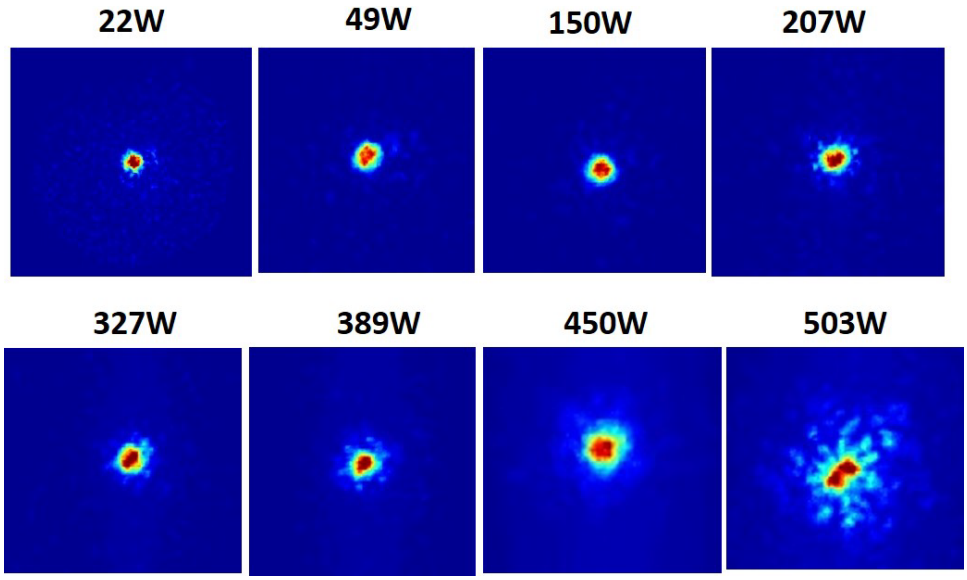

Fig. 6.10 Mode profile of the MOPA output measured with a separate CCD camera than the mode profile shown in Fig. 6.9.

saturated, the LP_{11} mode can be seen clearly in the last mode profile at 503W as shown in Fig. 6.10. In the experiment, it was noticed that the mode quality of MOPA output could be improved by optimizing the seed launching, coiling diameter, and the fiber holding block which introduces excessive stress on the fiber that will lead to deterioration of fundamental mode guided in the core. This was mostly caused by the free-space coupling optics of the amplifier system. Better mode quality (e.g. M^2~1.2) should help increasing the TMI threshold.

6.3 Conclusion

We have presented our preliminary experimental results of power scaling narrow-linewidth single-frequency Yb-doped all-solid PBF MOPA operating at 1064 nm. The low-loss photonic bandgap of the all-solid PBF was fine-tuned through careful characterization

and subsequent scaling of the fiber dimensions. The maximum SBS-free output power was ~500 W, which was eventually limited by TMI onset. The ASE suppression at maximum output power was ~45 dB. Output slope efficiency was ~90% and 80% with respect to the absorbed and launched pump power. The good SBS suppression may be due to the advantages of the fiber and amplifier configuration, including large core, low BGC core composition, temperature gradient from quantum defect heat and counter-pumping scheme, etc.

6.4 Future work

This work has not been completed yet. A more detailed study on the TMI threshold dependence on coil diameters, seed power, seed launching condition, fiber length, etc. needs to be conducted in the future experiments. Further investigation on improving mode quality of the MOPA output could result in a much higher TMI threshold.

CHAPTER SEVEN

SUMMARY AND OUTLOOK

7.1 Summary of the dissertation

This dissertation work covers the research on three separate but also related projects about power scaling of diffraction-limited high-power rare earth doped fiber lasers and amplifiers, including single-mode high-power Yb-doped three-level fiber laser operating at ~980 nm, near diffraction-limited high-power Er/Yb co-doped fiber MOPA operating at ~1562nm, and narrow-linewidth single-frequency high-power Yb-doped fiber MOPA operating at ~1064 nm. These are three distinctive projects but with all of them we utilized specialty LMA fibers based on silica host glass to achieve further power scaling of direct diode pumped single-mode high-power fiber lasers for specific applications at these wavelengths.

The research in this work focused mainly on improving laser performance by optimizing the photonic bandgap fiber design, including both waveguide structure and host glass material. Yb-doped silica glass fiber lasers have become the most popular choice for high-power fiber lasers for many applications including industry, medical, aerospace, scientific, etc. Driven by the increasing need for applications in material processing and so on, single-mode high-power Yb fiber lasers system operating at wavelength near 1.1 μm with 10 kW average output power had already become a commercial product in around 2010. At around the same time, further power scaling of high-power fiber lasers met with

several critical limitations and challenges such as TMI, SBS, photodarkening, and thermal lensing, to name a few.

The first part of this Ph.D. dissertation research (in Chapter 2 and 3) has focused on addressing several key issues with power scaling of Yb fiber lasers at ~980 nm which operates as three-level system unlike the conventional high-power Yb fiber laser operating at ~1070 nm which operates as four-level system. Efficient cladding pumped three-level Yb fiber lasers are difficult to achieve due to the competing four-level system and high inversion (>50%) criterion to obtain net gain in three-level systems. The demand for single-mode high-power fiber lasers at ~980 nm has increased substantially in the past two decades or so. This kind of single-mode lasers can be used for pumping core-pumped fiber lasers and bulk solid-state lasers to generate high peak power ultrafast pulses. At least a few tens of watts of single-mode (near diffraction limited) lasers at ~980 nm are required for such applications. Unfortunately, output power from single-mode diode lasers operating at ~980 nm is limited to only ~1 W. Cladding pumping is necessary for power scaling single-mode laser output to the required tens of watts. In the past, a number of cladding pumped Yb fiber lasers based on various LMA fibers have been reported but the results are somewhat limited in terms of either in output efficiency and power or mode quality.

One of the major issues with this type fiber lasers is suppressing ASE/co-lasing at ~1030nm due to the competing four-level operation. There are two ways to mitigate this problem: one is to incorporate high spectral loss at ~1030nm in the laser cavity and the other one is to ensure operation at high inversion along the fiber since the four-level system

has much higher gain at low inversions. Free-space bulk optics (e.g. dichroic mirrors) have been used in many previous demonstrations to introduce high (>30dB) spectral loss at ~1030nm, which makes it impossible to build an alignment-free all-fiber compact fiber laser system. To overcome this, we have proposed to utilize a ~25/125 μm core/clad diameter Yb-doped specialty all-solid photonic bandgap fiber (AS-PBF) based on multi-cladding resonance (MCR) micro-structured cladding design.

The novel MCR design of the AS-PBF not only enables high ASE suppression at~1030 nm but also ensures high HOM suppression which is the key to obtaining diffraction-limited mode quality in LMA fibers. In an AS-PBF, the modes are guided by the photonic bandgap effect, i.e. due to anti-resonance of cladding photonic crystal lattice. After multiple iterations of fine tuning the bandgap position of AS-PBF, we were able to fabricate the right fiber with long wavelength edge of the AS-PBF transmission band carefully engineered to be next to the ~980 nm laser signal wavelength. This enabled suppression of ASE at ~1030 nm with SNR>40dB and keep background loss at 977 nm to be as low as 0.02 dB/m at coiling diameter of ~10 cm. Among the several iterations of slightly different Yb-doped AS-PBF, the non-PM Yb fiber with 1.7 dB/m small signal pump absorption and signal loss of 0.02 dB/m showed the best performance in terms slope efficiency and mode quality (M^2). The high pump absorption means that much shorter fiber can be used thus ensuring high inversion all along the fiber. It's also worth mentioning that the high-inversion operation criterion also comes with two issues. One is that photodarkening becomes a sever limiting factor in high-inversion fiber lasers. Another is the high unabsorbed (i.e. residual) pump that intrinsically limits the laser slope efficiency

with respect to the launched pump power. Nevertheless, we have demonstrated an all-fiber monolithic Yb fiber laser at ~980 nm with record high 151 W average output power at near diffraction limited beam quality of M^2~1.2. The slope efficiency with respect to absorbed and launched pump power were, respectively, 94% (only limited by quantum defect) and 63% which is also a new record for all-fiber laser schemes operating at ~980 nm. In addition, the long-term power stability of the all-fiber Yb fiber laser was tested for ~60 hours, showing extremely well heat management and photodarkening-free operation of the phosphorsilicate glass core fiber laser.

The second part of this Ph.D. dissertation research (in Chapter 4 and 5) has focused on theoretical modeling and experimental demonstration of single-mode high-power Er/Yb co-doped fiber laser system based on MOPA configuration. Yb sensitized Er/Yb co-doped fibers are preferred for generating laser in wavelength range 1.5-1.6 μm, due to much higher active dopant concentration without clustering and large Yb absorption cross-section at pump wavelength at ~9 xx nm. There has been very little progress in power scaling of Er/Yb fiber lasers in the past decade or so. There are two major challenges with power scaling of single-mode Er/Yb fiber lasers operating at ~1.6 μm: one is the Yb→Er energy transfer bottleneck which results in Yb ASE (or parasitic lasing) at ~1.06 μm and output power clamping (i.e. flattening) at certain threshold pump power, the other one is ensuring single mode operation that yields near diffraction-limited beam quality (M^2). In several previous experimental reports, it was observed that the ~1.6 μm output power clamping does not occur immediately after the onset of the Yb parasitic lasing. This phenomenon in high-power Er/Yb fiber lasers cannot be explained by the conventional

model which dictates that all Yb ions are equally involved in the Yb→Er energy transfer process.

In this work, we proposed a new model of simulating the Er/Yb fiber laser dynamics in order to explain the abovementioned experimental behaviors. According to this new model, we assume that there are two kinds of Yb ions involved in the Er/Yb co-doped fiber, including coupled Yb ions which are in close proximity with Er ions, and un-coupled (i.e. isolated) Yb ions which are positioned too far away from Er ions. Also, the onset of Yb parasitic lasing is mostly due to the elevated population inversion of the isolated Yb ions, while the high energy transfer rate of the coupled Yb ions ensures the continued growth of the output power at ~1.6 μm from Er ions long after the onset of Yb parasitic lasing at ~1.1 μm. Our simulation shows that the threshold pump power to output power clamping increases as the fraction of coupled Yb ions increase, although the output is eventually clamped at certain pump power even in the case when the fraction of coupled Yb ions is set to be 100%. This threshold pump power is reached when pumping rate exceeds the Yb →Er energy transfer rate.

Then, we conducted an experimental study on power scaling of single-mode Er/Yb fiber laser using a commercial few-mode Er/Yb fiber (LMA-EYDF-25P/300-HE) from Nufern. Other than the Yb→Er energy transfer bottlenecking and mode quality, excessive heat load due to high quantum defect is a major challenge in Er/Yb high-power fiber lasers. To mitigate heat load, we have used 915 nm kW-level diode as the pump which enabled us using active fiber about three times longer compared to the case with pumping at 976

nm. We have obtained a maximum of 302 W single-mode power at 1562 nm with an optical efficiency record of 56%, very close to the quantum-limited efficiency of 58.6%. Also, we have found that the fiber fuse is the major limiting factor for further single-mode power scaling in this fiber rather than ASE as was previously reported. This could be mitigated by lowering heat load, e.g. utilizing a longer active fiber with lower pump absorption. Our simulations show that off-resonance pumping at ~915 nm or ~940 nm only plays a small role in the observed negligible ASE especially at high powers. The experimental results show that the main reason is most likely due to the high Er doping level in this Nufern Er/Yb fiber compared to the Southampton Er/Yb fiber from a previous demonstration. This will lead to a higher energy transfer rate $R(n_6/n_5)n_1$, which increases the output clamping threshold pump power, e.g. $P_{th} \propto (A_{pump}Rn_6n_1)/(n_5\sigma_p)$ where R is the energy transfer coefficient. Thus, possible ways to increase threshold power include optimizing glass composition for higher energy transfer rate, using pump wavelength with smaller absorption cross-section, and obviously larger pump cladding if possible.

The last part of this Ph.D. dissertation research (in Chapter 6) has focused on power scaling of narrow-linewidth single-frequency Yb-doped fiber laser system based on MOPA configuration operating at 1064 nm. The motivation behind this works was to incorporate the novel MCR design based PBF into the ultra-large-core Yb-doped PBF for single-frequency fiber laser system operating at 1064 nm. Two iterations of fiber characterization and optimization led to the successful fabrication of a new MCR based Yb-doped PBF with core/clad diameter of 56/401 μm. Preliminary experimental results have shown that the single-frequency MOPA operates at output power of ~500 W and linewidth of ~10 kHz,

without any signs of SBS effect although the TMI comes in at output power of ~503 W. In addition, the ASE near 1030 nm was very well suppressed by ~45 dB. The slope efficiency of the MOPA output was ~90% and 80% with respect to the absorbed and launched pump power. Both the good ASE suppression and high slope efficiency indicate that the low loss bandgap region of the new VLMA Yb PBF has been fine-tuned very close to the ideal position that we wanted. Further experiments to be continued to investigate the dependence of TMI threshold on MOPA configurations such as coiling diameter of fiber, fiber length, seed launching condition, seed wavelength, etc.

7.2 Innovations and contributions

The major scientific and engineering contributions of this dissertation work is summarized as following.

1. A novel Yb-doped all-solid photonic bandgap fiber for highly efficient single-mode three-level fiber laser operating at ~980 nm was designed and optimized over many iterations of characterization, test and fabrication. This has paved the way for using new types fiber designs on the research field of power scaling three-level Yb fiber lasers at ~980nm.

2. Experimentally demonstrated record power scaling performance by AS-PBF based all-fiber monolithic Yb fiber laser operating at ~980 nm with 151 W average output power, 63% output slope efficiency, and near diffraction-limited mode quality of M^2~ 1.2.

3. The new monolithic laser was characterized in terms of coil diameters, ASE suppression, optimum fiber length, linewidth broadening, photodarkening and long-term

power stability. A robust all-fiber prototype laser of this kind could become a new powerful tool for many turn-key laser-based applications such as pumping ultrafast bulk or fiber based solid state lasers, etc.

4. The major limiting factors of high-power Er/Yb fiber lasers were analyzed and numerically modeled for the first time based on the new model of two types of Yb ions, i.e. coupled Yb ions and un-coupled (isolated) Yb ions. This can help explaining the physics behind the observed behaviors of Yb→Er energy transfer bottlenecking and various output power clamping thresholds in Er/Yb fibers with different Er to Yb ratios.

5. A record average output power of 302 W and near quantum efficiency limited optical-to-optical efficiency of 56% were demonstrated from single-mode Er/Yb fiber MOPA laser system using a commercial Er/Yb fiber from Nufern. The experimental results show that fiber fuse due to excessive heat load is the major limit for further power scaling unlike the Yb parasitic lasing at ~1.06 μm as was previously had been reported.

6. Designing and optimizing of a novel all-solid PBF has been explored for power scaling of narrow-linewidth single-frequency Yb fiber laser operating at 1064 nm. An SBS-free output power of ~500 W with ASE suppression of ~45dB and linewidth of ~10 kHz was achieved. Further power scaling experiments to be continued.

7.3 Outlook

Significant progress has been made in power scaling of rare earth doped high-power fiber lasers and amplifiers. Ensuring single mode operation and power scaling always comes with tremendous challenges. Novel all-solid PBF based on MCR design

demonstrated significant potential in further power scaling at wavelength regimes which previously legged behind, such as ~0.98 μm and ~1.6 μm.

The record high power all-fiber laser demonstrated by the work of this dissertation can be turned into a new series of tabletop commercial products to be used for pumping ultrafast lasers. In addition, the same knowledge that acquired from developing the novel PBF can be easily expanded to other wavelength regimes such as 1.5-1.6 μm. Combining the newly discovered mitigation approaches such as Yb → Er energy transfer, ASE suppression, heat load treatment, etc., the new all-solid PBF could be used for further power scaling single-mode Er/Yb co-doped fiber lasers in the future.

Ultra large core all-solid PBF based MCR design demonstrated in this work could pave the way for further scaling the SBS and TMI free output power of the single-frequency fiber amplifiers for applications such as coherent beam combining, direct energy weapon systems, etc. This novel fiber design can incorporate many features of previously demonstrated fibers which were designed for SBS and TMI suppression, such as gain tailoring, acoustic tailoring, etc.

APPENDICES

Appendix A

List of Publications

Journal Papers

1. Turghun Matniyaz, Wensong Li, Monica Kalichevsky-Dong, Thomas W. Hawkins, Joshua Parsons, Guancheng Gu, and Liang Dong, "Highly efficient cladding-pumped single-mode three-level Yb all-solid photonic bandgap fiber lasers," Opt. Lett. **44**(4), 807-810 (2019)

2. Wensong Li, Turghun Matniyaz, Saddam Gafsi, Monica T. Kalichevsky-Dong, Thomas W. Hawkins, Joshua Parsons, Guancheng Gu, and Liang Dong, "151W monolithic diffraction-limited Yb-doped photonic bandgap fiber laser at ~978nm," Opt. Express **27**(18), 24972-24977 (2019)

3. Liang Dong, Turghun Matniyaz, Monica Kalichevsky-Dong, Johan Nilsson, Yoonchan Jeong, "Modeling Er/Yb fiber lasers at high powers," Opt. Express **28**(11), 16244-16255 (2020)

4. Turghun Matniyaz, Fanting Kong, Monica Kalichevsky-Dong, Liang Dong, "302W single-mode power from an Er/Yb fiber MOPA," Opt. Lett. **45**(11), 3021-3021 (2020)

Conference Proceedings

5. Turghun Matniyaz, Monica T. Kalichevsky-Dong, Thomas W. Hawkins, Joshua Parsons, Guancheng Gu, Wensong Li, Max Faykus, Bradley Selee, Jonathan A. Dong, and Liang Dong, "Single-mode Yb-doped Double-clad All-solid Photonic Bandgap Fiber Laser Generating 27.8W at 976nm," in Laser Congress (ASSL), paper **AM6A.28** (2018) [**Poster**]

6. Turghun Matniyaz, Monica T. Kalichevsky-Dong, Thomas W. Hawkins, Joshua Parsons, Guancheng Gu, Wensong Li, Max Faykus, Bradley Selee, Jonathan A. Dong, Liang Dong “Diffraction-limited Yb-doped double-clad all-solid photonic bandgap fiber laser at 976 nm,” Proc. SPIE **10897**, 108970V (2019) [**Invited talk**]

7. Turghun Matniyaz, Wensong Li, Saddam Gafsi, Monica Kalichevsky-Dong, Thomas W. Hawkins, Joshua Parsons, Guancheng Gu, and Liang Dong, "A monolithic single-mode Yb three-level fiber laser at ~978nm with a record power of ~150W," CLEO, paper **JTh5A.7**, San Jose (2019) [**Post-deadline talk**]

8. Turghun Matniyaz, Wensong Li, Monica Kalichevsky-Dong, Thomas W. Hawkins, Joshua Parsons, Guancheng Gu, Liang Dong "Efficient High-power Single-mode Yb Three-level Cladding-pumped All-solid Photonic Bandgap Fiber Lasers at ~978nm," CLEO, paper **SM4L.2**, San Jose (2019)

9. Turghun Matniyaz, Fanting Kong, Monica T. Kalichevsky-Dong, and Liang Dong, " Record high power single-mode erbium-ytterbium fiber amplifier with a near quantum-limited optical efficiency," in Laser Congress (ASSL), paper **ATh1A.8** (2020)

Patents

10. Liang Dong and Turghun Matniyaz, “Three-Level System Fiber Lasers Incorporating an All-Solid Photonic Bandgap Fiber,” Filed on Sep. 21, 2020 (U.S. Patent Application No. 17/026,760)

Reference

1. "Fiber Laser vs. Thin Disk and CO2 | JMTUSA," http://jmtusa.com/fiber-laser-vs-thin-disk-and-co2/.
2. E. Snitzer, "Optical maser action of Nd+3 in a barium crown glass," Phys. Rev. Lett. **7**(12), 444–446 (1961).
3. E. Snitzer, "Glass Lasers," Appl. Opt. **5**(10), 1487 (1966).
4. C. J. Koester and E. Snitzer, "Amplification in a Fiber Laser," Appl. Opt. **3**(10), 1182 (1964).
5. H. Injeyan and G. D. Goodno, *High-Power Laser Handbook*, 1st ed. (McGraw-Hill Education, 2011).
6. D. N. Payne, L. Reekie, R. J. Mears, S. B. Poole, I. M. Jauncey, and J. T. Lin, "Rare-earth doped single-mode fiber lasers, amplifiers, and devices," in *Conference on Lasers and Electro-Optics (1986)* (The Optical Society, 1986), p. FN1.
7. E. Snitzer, H. Po, F. Hakimi, R. Tumminelli, and B. C. McCollum, "DOUBLE CLAD, OFFSET CORE Nd FIBER LASER," in *Optical Fiber Sensors (1988)* (The Optical Society, 1988), p. PD5.
8. M. N. Zervas and C. A. Codemard, "High power fiber lasers: A review," IEEE J. Sel. Top. Quantum Electron. **20**(5), (2014).
9. Y. Jeong, J. K. Sahu, D. N. Payne, and J. Nilsson, "Ytterbium-doped large-core fiber laser with 1.36 kW continuous-wave output power," Opt. Express **12**(25), 6088 (2004).
10. L. Dong and B. Samson, *Fiber Lasers: Basics, Technology, and Applications*, 1st ed. (CRC Press, 2016).
11. P. Even and D. Pureur, "High-power double-clad fiber lasers: a review," in *SPIE Proc.* , M. J. F. Digonnet, ed. (SPIE, 2002), **4638**(14), pp. 1–12.
12. P. Dupriez, J. Nilsson, Y. Jeong, J. K. Sahu, C. A. Codemard, D. B. S. Soh, C. Farrell, J. Kim, A. Piper, A. Malinowski, and D. J. Richardson, "Current progress in high-power fiber lasers and amplifiers," in *Optics InfoBase Conference Papers* (Optical Society of America, 2005), p. TuD1.
13. J. Limpert, F. Röser, S. Klingebiel, T. Schreiber, C. Wirth, T. Peschel, R. Eberhardt, and A. Tünnermann, "The rising power of fiber lasers and amplifiers," IEEE J. Sel. Top. Quantum Electron. **13**(3), 537–544 (2007).
14. D. J. Richardson, J. Nilsson, and W. A. Clarkson, "High power fiber lasers: current status and future perspectives [Invited]," J. Opt. Soc. Am. B **27**(11), B63 (2010).
15. J. Zhu, P. Zhou, Y. Ma, X. Xu, and Z. Liu, "Power scaling analysis of tandem-pumped Yb-doped fiber lasers and amplifiers," Opt. Express **19**(19), 18645 (2011).
16. C. Jauregui, J. Limpert, and A. Tünnermann, "High-power fibre lasers," Nat. Photonics **7**(11), 861–867 (2013).
17. P. Zhou, H. Xiao, J. Leng, J. Xu, Z. Chen, H. Zhang, and Z. Liu, "High-power fiber lasers based on tandem pumping," J. Opt. Soc. Am. B **34**(3), A29 (2017).
18. J. O. White, "Parameters for quantitative comparison of two-, three-, and four-level laser media, operating wavelengths, and temperatures," IEEE J. Quantum

Electron. **45**(10), 1213–1220 (2009).
19. P. D. Dragic, M. Cavillon, and J. Ballato, "Materials for optical fiber lasers: A review," Appl. Phys. Rev. **5**(4), (2018).
20. D. J. Richardson, J. Nilsson, and W. A. Clarkson, "High power fiber lasers: current status and future perspectives [Invited]," J. Opt. Soc. Am. B **27**(11), B63 (2010).
21. V. Dominic, S. MacCormack, R. Waarts, S. Sanders, S. Bicknese, R. Doble, E. Wolak, P. S. Yeh, and E. Zucker, "110 W Fiber Laser," in *CLEO* (1999).
22. Y. Jeung, J. K. Sahu, D. N. Payne, and J. Nilsson, "Ytterbium-doped large-core fibre laser with 1 kW of continuous-wave output power," Electron. Lett. **40**(8), 470–472 (2004).
23. M. O'Connor, V. Gapontsev, V. Fomin, M. Abramov, and A. Ferin, "Power Scaling of SM Fiber Lasers toward 10kW," in *Conference on Lasers and Electro-Optics/International Quantum Electronics Conference (2009), Paper CThA3* (The Optical Society, 2009), p. CThA3.
24. "IPG Photonics Corporation," https://www.ipgphotonics.com/en/whyIpg/GetIpgLaserData.
25. J. Boullet, Y. Zaouter, R. Desmarchelier, M. Cazaux, F. Salin, J. Saby, R. Bello-Doua, and E. Cormier, "High power ytterbium-doped rod-type three-level photonic crystal fiber laser," Opt. Express **16**(22), 17891 (2008).
26. F. Roser, C. Jauregui, J. Limpert, and A. Tünnermann, "94 W 980 nm high brightness Yb-doped fiber laser," Opt. Express **16**(22), 17310 (2008).
27. T. Matniyaz, W. Li, S. Gafsi, M. Kalichevsky-Dong, T. W. Hawkins, J. Parsons, G. Gu, and L. Dong, *A Monolithic Single-Mode Yb Three-Level Fiber Laser at ~978nm with a Record Power of ~150W* (2019).
28. J. Nilsson, "High power fiber sources," in *Short Course SC748 (SPIE Photonics West)* (2019).
29. D. Creeden, H. Pretorius, J. Limongelli, and S. D. Setzler, "Single frequency 1560nm Er:Yb fiber amplifier with 207W output power and 50.5% slope efficiency," in *Proc. SPIE*, J. Ballato, ed. (SPIE, 2016), **9728**(11), p. 97282L.
30. T. Matniyaz, F. Kong, M. Kalichevsky-Dong, and L. Dong, "302W single-mode power from an Er/Yb fiber MOPA," Opt. Lett. **45**(10), 2910–2913 (2020).
31. H. Lin, Y. Feng, Y. Feng, P. Barua, J. K. Sahu, and J. Nilsson, "656 W Er-doped, Yb-free large-core fiber laser," Opt. Lett. **43**(13), 3080 (2018).
32. J. C. Knight, T. A. Birks, P. S. J. Russell, and D. M. Atkin, "All-silica single-mode optical fiber with photonic crystal cladding," Opt. Lett. **21**(19), 1547 (1996).
33. O. N. Egorova, S. L. Semjonov, A. F. Kosolapov, A. N. Denisov, A. D. Pryamikov, D. A. Gaponov, A. S. Biriukov, E. M. Dianov, M. Y. Salganskii, V. F. Khopin, M. V. Yashkov, A. N. Gurianov, and D. V. Kuksenkov, "Single-mode all-silica photonic bandgap fiber with 20-μm mode-field diameter," Opt. Express **16**(16), 11735 (2008).
34. T. A. Birks, G. J. Pearce, and D. M. Bird, "Approximate band structure calculation for photonic bandgap fibres," Opt. Express **14**(20), 9483 (2006).
35. T. A. Birks, F. Luan, G. J. Pearce, A. Wang, J. C. Knight, and D. M. Bird, "Bend loss in all-solid bandgap fibres," Opt. Express **14**(12), 5688 (2006).

36. T. Murao, K. Saitoh, M. Koshiba, J. C. Knight, F. Luan, G. J. Pearce, A. Wang, T. A. Birks, D. M. Bird, A. K. George, T. D. Hedley, and P. J. St Russell, *Multiple Resonant Coupling Mechanism for Suppression of Higher-Order Modes in All-Solid Photonic Bandgap Fibers with Heterostructured Cladding References and Links* (2011), **45**(8).
37. G. Gu, F. Kong, T. W. Hawkins, M. Jones, and L. Dong, "Extending mode areas of single-mode all-solid photonic bandgap fibers," Opt. Express **23**(7), 9147 (2015).
38. L. Dong, F. Kong, G. Gu, T. W. Hawkins, M. Jones, J. Parsons, M. T. Kalichevsky-Dong, K. Saitoh, B. Pulford, and I. Dajani, "Large-Mode-Area All-Solid Photonic Bandgap Fibers for the Mitigation of Optical Nonlinearities," IEEE J. Sel. Top. Quantum Electron. **22**(2), (2016).
39. T. Eidam, C. Wirth, C. Jauregui, F. Stutzki, F. Jansen, H.-J. Otto, O. Schmidt, T. Schreiber, J. Limpert, and A. Tünnermann, "Experimental observations of the threshold-like onset of mode instabilities in high power fiber amplifiers," Opt. Express **19**(14), 13218 (2011).
40. C. Jauregui, C. Stihler, and J. Limpert, "Transverse mode instability," Adv. Opt. Photonics **12**(2), 429 (2020).
41. T. Matniyaz, W. Li, M. Kalichevsky-Dong, T. W. Hawkins, J. Parsons, G. Gu, and L. Dong, "Highly efficient cladding-pumped single-mode three-level Yb all-solid photonic bandgap fiber lasers," Opt. Lett. **44**(4), 807 (2019).
42. W. Li, T. Matniyaz, S. Gafsi, M. T. Kalichevsky-Dong, T. W. Hawkins, J. Parsons, G. Gu, and L. Dong, "151W monolithic diffraction-limited Yb-doped photonic bandgap fiber laser at ~978nm," Opt. Express **27**(18), 24972 (2019).
43. A. E. Siegman, "How to (Maybe) Measure Laser Beam Quality," in *Optical Society of America Annual Meeting* (1997).
44. T. S. Ross and W. P. Latham, "Appropriate measures and consistent standard for high-energy laser beam quality," J. Dir. Energy **2**, 22–58 (2006).
45. L. Dong, X. Peng, and J. Li, "Leakage channel optical fibers with large effective area," J. Opt. Soc. Am. B **24**(8), 1689 (2007).
46. C. H. Liu, G. Chang, N. Litchinitser, A. Galvanauskas, D. Guertin, N. Jabobson, and K. Tankala, "Effectively single-mode chirally-coupled core fiber," in *Advanced Solid-State Photonics* (Optical Society of America (OSA), 2007), p. ME2.
47. J. Ballato and P. Dragic, "Rethinking optical fiber: New demands, old glasses," J. Am. Ceram. Soc. **96**(9), 2675–2692 (2013).
48. C. Jauregui, T. Eidam, H.-J. Otto, F. Stutzki, F. Jansen, J. Limpert, and A. Tünnermann, "Physical origin of mode instabilities in high-power fiber laser systems," Opt. Express **20**(12), 12912 (2012).
49. A. V. Smith and J. J. Smith, "Mode instability in high power fiber amplifiers," Opt. Express **19**(11), 10180 (2011).
50. L. Dong, "Stimulated thermal Rayleigh scattering in optical fibers," Opt. Express **21**(3), 2642 (2013).
51. M. N. Zervas, " Transverse mode instability, thermal lensing and power scaling in

Yb 3+ -doped high-power fiber amplifiers ," Opt. Express **27**(13), 19019 (2019).
52. B. Pulford, T. Ehrenreich, R. Holten, F. Kong, T. W. Hawkins, L. Dong, and I. Dajani, "400-W near diffraction-limited single-frequency all-solid photonic bandgap fiber amplifier," Opt. Lett. **40**(10), 2297 (2015).
53. F. Kong, G. Gu, T. W. Hawkins, M. Jones, J. Parsons, M. T. Kalichevsky-Dong, B. Pulford, I. Dajani, and L. Dong, "~1 kilowatt Ytterbium-doped all-solid photonic bandgap fiber laser," in *Proc. SPIE*, C. A. Robin and I. Hartl, eds. (SPIE, 2017), **10083**, p. 1008311.
54. P. Zeil and F. Laurell, "On the tunability of a narrow-linewidth Yb-fiber laser from three- to four-level lasing behaviour," Opt. Express **19**(15), 13940 (2011).
55. R. Selvas, J. K. Sahu, L. B. Fu, J. N. Jang, J. Nilsson, A. B. Grudinin, K. H. Ylä-Jarkko, S. A. Alam, P. W. Turner, and J. Moore, "High-power, low-noise, Yb-doped, cladding-pumped, three-level fiber sources at 980nm," Opt. Lett. **28**(13), 1093 (2003).
56. J. R. Armitage, R. Wyatt, B. J. Ainslie, and S. P. Craig-Ryan, "Highly Efficient 980nm Operation of an Yb3+-Doped Silica Fibre Laser," Electron. Lett. **25**(5), 298–299 (1989).
57. D. C. Hanna, R. M. Percival, I. R. Perry, R. G. Smart, P. J. Suni, and A. C. Tropper, "An ytterbium-doped monomode fibre laser: Broadly tunable operation from 1.010 μm to 1.162 μm and three-level operation at 974 nm," J. Mod. Opt. **37**(4), 517–525 (1990).
58. L. Zenteno, "High-Power Double-Clad Fiber Lasers," J. Light. Technol. **11**(9), 1435–1446 (1993).
59. J. Nilsson, J. D. Minelly, R. Paschotta, A. C. Tropper, and D. C. Hanna, "Ring-doped cladding-pumped single-mode three-level fiber laser," Opt. Lett. **23**(5), 355 (1998).
60. L. A. Zenteno, J. D. Minelly, M. Dejneka, and S. Crigler, "0.65 W single-mode Yb-fiber laser at 980 nm pumped by 1.1 W Nd:YAG," in *Advanced Solid State Lasers (2000), Paper MD7* (The Optical Society, 2000), p. MD7.
61. N. G. R. Broderick, H. L. Offerhaus, D. J. Richardson, R. A. Sammut, J. Caplen, and L. Dong, "Large mode area fibers for high power applications," Opt. Fiber Technol. **5**(2), 185–196 (1999).
62. V. Pureur, L. Bigot, G. Bouwmans, Y. Quiquempois, M. Douay, and Y. Jaouen, "Ytterbium-doped solid core photonic bandgap fiber for laser operation around 980 nm," Appl. Phys. Lett. **92**(6), 061113 (2008).
63. J. C. Knight, J. Broeng, T. A. Birks, and P. S. J. Russell, "Photonic band gap guidance in optical fibers," Science (80-.). **282**(5393), 1476–1478 (1998).
64. F. Luan, A. K. George, T. D. Hedley, G. J. Pearce, D. M. Bird, J. C. Knight, and P. S. J. Russell, "All-solid photonic bandgap fiber," Opt. Lett. **29**(20), 2369 (2004).
65. S. Février, D. D. Gaponov, P. Roy, M. E. Likhachev, S. L. Semjonov, M. M. Bubnov, E. M. Dianov, M. Y. Yashkov, V. F. Khopin, M. Y. Salganskii, and A. N. Guryanov, "High power photonic-bandgap fiber laser," Opt. Lett. **33**(9), 989–991 (2008).
66. E. M. Dianov, M. E. Likhachev, and S. Février, "Solid-core photonic bandgap

fibers for high-power fiber lasers," IEEE J. Sel. Top. Quantum Electron. **15**(1), 20–29 (2009).
67. F. Kong, K. Saitoh, D. Mcclane, T. Hawkins, P. Foy, G. Gu, and L. Dong, "Mode area scaling with all-solid photonic bandgap fibers," Opt. Express **20**(24), 26363 (2012).
68. G. Gu, F. Kong, T. Hawkins, J. Parsons, M. Jones, C. Dunn, M. T. Kalichevsky-Dong, K. Saitoh, and L. Dong, "Ytterbium-doped large-mode-area all-solid photonic bandgap fiber lasers," Opt. Express **22**(11), 13962 (2014).
69. S. S. Aleshkina, T. L. Bardina, D. S. Lipatov, K. K. Bobkov, M. M. Bubnov, A. N. Gur'yanov, and M. E. Likhachev, "Factors reducing the efficiency of ytterbium fibre lasers and amplifiers operating near 0.98 μm," Quantum Electron. **47**(12), 1109–1114 (2017).
70. S. Suzuki, H. A. McKay, X. Peng, L. Fu, and L. Dong, "Highly ytterbium-doped silica fibers with low photo-darkening," Opt. Express **17**(12), 9924 (2009).
71. L. A. Z. Lawrence C. Hughes, Xingsheng Liu, Donnell T. Walton, Chung-En Zah, "Cladding-pumped quasi 3-level fiber laser/amplifier," (November 10, 2005).
72. D. B. S. Soh, C. Codemard, J. K. Sahu, J. Nilsson, V. Philippov, C. Alegria, and Y. Jeong, "A 4.3 W 977 nm Ytterbium-doped Jacketed-Air-Clad Fiber Amplifier," in *Advanced Solid-State Photonics* (The Optical Society, 2004), p. MA3.
73. S. S. Aleshkina, M. E. Likhachev, D. S. Lipatov, O. I. Medvedkov, K. K. Bobkov, M. M. Bubnov, and A. N. Guryanov, "5.5 W monolitic single-mode fiber laser and amplifier operating near 976 nm," in *Proc. SPIE, Fiber Lasers XIII: Technology, Systems, and Applications*, J. Ballato, ed. (SPIE, 2016), **9728**, p. 97281C.
74. S. S. Aleshkina, A. E. Levchenko, O. I. Medvedkov, K. K. Bobkov, M. M. Bubnov, D. S. Lipatov, A. N. Guryanov, and M. E. Likhachev, "Photodarkening-free Yb-doped saddle-shaped fiber for high power single-mode 976-nm laser," IEEE Photonics Technol. Lett. **30**(1), 127–130 (2018).
75. A. Shirakawa, H. Maruyama, K. Ueda, C. B. Olausson, J. K. Lyngsø, and J. Broeng, "High-power Yb-doped photonic bandgap fiber amplifier at 1150-1200 nm," Opt. Express **17**(2), 447 (2009).
76. C. B. Olausson, A. Shirakawa, M. Chen, J. K. Lyngsø, J. Broeng, K. P. Hansen, A. Bjarklev, and K. Ueda, "167 W, power scalable ytterbium-doped photonic bandgap fiber amplifier at 1178nm," Opt. Express **18**(16), 16345 (2010).
77. S. S. Aleshkina, M. E. Likhachev, D. S. Lipatov, O. I. Medvedkov, K. K. Bobkov, M. M. Bubnov, and A. N. Guryanov, "5.5 W monolitic single-mode fiber laser and amplifier operating near 976 nm," in *Fiber Lasers XIII: Technology, Systems, and Applications*, J. Ballato, ed. (SPIE, 2016), **9728**, p. 97281C.
78. P. Jelger, M. Engholm, L. Norin, and F. Laurell, "Degradation-resistant lasing at 980 nm in a Yb/Ce/Al-doped silica fiber," J. Opt. Soc. Am. B **27**(2), 338 (2010).
79. L. Dong, "A vector boundary matching technique for efficient and accurate determination of photonic bandgaps in photonic bandgap fibers," Opt. Express **19**(13), 12582 (2011).
80. S. Zemon, G. Lambert, W. J. Miniscalco, L. J. Andrews, and B. T. Hall, "Characterization Of Er3+-Doped Glasses By Fluorescence Line Narrowing," in

Proc. SPIE 1171, Fiber Laser Sources and Amplifiers, M. J. F. Digonnet, ed. (SPIE, 1990), **1171**, p. 219.
81. A. K. Srivastava, J. L. Zyskind, J. W. Sulhoff, J. D. Evankow, and M. A. Mills, "Room temperature spectral hole-burning in erbium-doped fiber amplifiers," in *Optical Fiber Communication, OFC* (Institute of Electrical and Electronics Engineers Inc., 1996), pp. 33–34.
82. X. Peng and L. Dong, "Temperature dependence of ytterbium doped fiber amplifiers," J. Opt. Soc. Am. B **25**(1), 126–130 (2008).
83. E. Stiles, "New developments in IPG fiber laser technology," in *Proceeding of the 5th International Workshop on Fiber Lasers* (2009).
84. Y. Xiao, F. Brunet, M. Kanskar, M. Faucher, A. Wetter, and N. Holehouse, "1-kilowatt CW all-fiber laser oscillator pumped with wavelength-beam-combined diode stacks," Opt. Express **20**(3), 3296 (2012).
85. X. Fan, M. Chen, A. Shirakawa, K. Ueda, C. B. Olausson, J. K. Lyngsø, and J. Broeng, "High power Yb-doped photonic bandgap fiber oscillator at 1178 nm," Opt. Express **20**(13), 14471 (2012).
86. F. Kong, G. Gu, T. W. Hawkins, M. Jones, J. Parsons, M. T. Kalichevsky-Dong, S. P. Palese, E. Cheung, and L. Dong, "Efficient 240W single-mode 1018nm laser from an Ytterbium-doped 50/400μm all-solid photonic bandgap fiber," Opt. Express **26**(3), 3138 (2018).
87. N. Valero, C. Feral, J. Lhermite, S. Petit, R. Royon, Y.-V. Bardin, M. Goeppner, C. Dixneuf, G. Guiraud, A. Proulx, Y. Taillon, and E. Cormier, "39 W narrow spectral linewidth monolithic ytterbium-doped fiber MOPA system operating at 976 nm," Opt. Lett. **45**(6), 1495 (2020).
88. L. Kotov, V. Temyanko, S. Aleshkina, M. Bubnov, D. Lipatov, and M. Likhachev, "Efficient single-mode 976 nm amplifier based on a 45 micron outer diameter Yb-doped fiber," Opt. Lett. (2020).
89. N. Boetti, D. Pugliese, E. Ceci-Ginistrelli, J. Lousteau, D. Janner, and D. Milanese, "Highly Doped Phosphate Glass Fibers for Compact Lasers and Amplifiers: A Review," Appl. Sci. **7**(12), 1295 (2017).
90. M. Franczyk, R. Stępień, B. Piechal, D. Pysz, K. Stawicki, B. Siwicki, and R. Buczyński, "High efficiency Yb 3+-doped phosphate single-mode fibre laser Related content," Laser Phys. Lett. **14**(10), 105102 (2017).
91. J. Wu, X. Zhu, V. Temyanko, L. LaComb, L. Kotov, K. Kiersma, J. Zong, M. Li, A. Chavez-Pirson, R. A. Norwood, and N. Peyghambarian, "Yb^3+-doped double-clad phosphate fiber for 976 nm single-frequency laser amplifiers," Opt. Mater. Express **7**(4), 1310 (2017).
92. J. Wu, X. Zhu, H. Wei, K. Wiersma, M. Li, J. Zong, A. Chavez-Pirson, V. Temyanko, L. J. LaComb, R. A. Norwood, and N. Peyghambarian, "Power scalable 10 W 976 nm single-frequency linearly polarized laser source," Opt. Lett. **43**(4), 951 (2018).
93. M. Engholm and L. Norin, "Preventing photodarkening in ytterbium-doped high power fiber lasers; correlation to the UV-transparency of the core glass," Opt. Express **16**(2), 1260 (2008).

94. Y. Li, K. Peng, H. Zhan, S. Liu, L. Ni, Y. Wang, J. Yu, X. Wang, J. Wang, F. Jing, and A. Lin, "Yb-doped aluminophosphosilicate ternary fiber with high efficiency and excellent laser stability," Opt. Fiber Technol. **41**, 7–11 (2018).
95. D. C. Brown and H. J. Hoffman, "Thermal, stress, and thermo-optic effects in high average power double-clad silica fiber lasers," IEEE J. Quantum Electron. **37**(2), 207–217 (2001).
96. G. Canat, J.-C. Mollier, Y. Jaouën, and B. Dussardier, "Evidence of thermal effects in a high-power Er^3+–Yb^3+ fiber laser," Opt. Lett. **30**(22), 3030 (2005).
97. P. Becker, A. Olsson, and J. Simpson, *Erbium-Doped Fiber Amplifiers: Fundamentals and Technology*, 1st ed. (Academic Press, 1999).
98. K. Yelen, L. M. B. Hickey, and M. N. Zervas, "Experimentally verified modeling of erbium-ytterbium co-doped DFB fiber lasers," J. Light. Technol. **23**(3), 1380–1392 (2005).
99. N. V Kiritchenko, L. V Kotov, M. A. Melkumov, M. E. Likhachev, M. M. Bubnov, M. V Yashkov, A. Y. Laptev, and A. N. Guryanov, "Effect of ytterbium co-doping on erbium clustering in silica-doped glass," Laser Phys. **25**(2), 025102 (2015).
100. Y. Huo and P. K. Cheo, "Modeling of passively Q-switched Er3+/Yb3+-codoped clad-pumped fiber lasers," IEEE J. Sel. Top. Quantum Electron. **11**(3), 658–666 (2005).
101. J. Yang, Y. Tang, R. Zhang, and J. Xu, "Modeling and characteristics of gain-switched diode-pumped Er-Yb codoped fiber lasers," IEEE J. Quantum Electron. **48**(12), 1560–1567 (2012).
102. S. Pavlova, M. E. Yagci, S. K. Eken, E. Tunckol, and I. Pavlov, "High power microsecond fiber laser at 1.5 μm," Opt. Express **28**(12), 18368 (2020).
103. J. Nilsson, P. Scheer, and B. Jaskorzynska, "Modeling and Optimization of Short Yb3+-Sensitized Er3+-Doped Fiber Amplifiers," IEEE Photonics Technol. Lett. **6**(3), 383–385 (1994).
104. M. Karásek, "Optimum design of Er3+-Yb3+ codoped fibers for large-signal high-pump-power applications," IEEE J. Quantum Electron. **33**(10), 1699–1705 (1997).
105. G. C. Valley, "Modeling Cladding-Pumped Er/Yb Fiber Amplifiers," Opt. Fiber Technol. **7**(1), 21–44 (2001).
106. E. Yahel and A. A. Hardy, "Modeling and Optimization of Short Er3+-Yb3+ Codoped Fiber Lasers," IEEE J. Quantum Electron. **39**(11), 1444–1451 (2003).
107. Q. Han, J. Ning, and Z. Sheng, "Numerical investigation of the ASE and power scaling of cladding-pumped Er-Yb codoped fiber amplifiers," IEEE J. Quantum Electron. **46**(11), 1535–1541 (2010).
108. X. Zhao, Q. Han, D. Wang, H. Hu, K. Ren, J. Jiang, and T. Liu, "Optimal design of high-power cascade co-pumping Er/Yb-codoped fiber lasers," Opt. Lett. **44**(5), 1100 (2019).
109. J. K. Sahu, Y. Jeong, D. J. Richardson, and J. Nilsson, "A 103 W erbium-ytterbium co-doped large-core fiber laser," Opt. Commun. **227**(1–3), 159–163 (2003).
110. J. K. Sahu, Y. Jeong, D. J. Richardson, and J. Nilsson, "Highly efficient high-

power erbium-ytterbium co-doped large core fiber laser," in *Optics InfoBase Conference Papers* (Optical Society of America, 2005), p. MB33.
111. Y. Jeong, S. Yoo, C. A. Codemard, J. Nilsson, J. K. Sahu, D. N. Payne, R. Horley, P. W. Turner, L. Hickey, A. Harker, M. Lovelady, and A. Piper, "Erbium:ytterbium codoped large-core fiber laser with 297-W continuous-wave output power," IEEE J. Sel. Top. Quantum Electron. **13**(3), 573–578 (2007).
112. Y. Jeong, J. K. Sahu, D. B. S. Soh, C. A. Codemard, and J. Nilsson, "High-power tunable single-frequency single-mode erbium:ytterbium codoped large-core fiber master-oscillator power amplifier source," Opt. Lett. **30**(22), 2997 (2005).
113. R. Francini, F. Giovenale, U. M. Grassano, P. Laporta, and S. Taccheo, "Spectroscopy of Er and Er-Yb-doped phosphate glasses," Opt. Mater. (Amst). **13**(4), 417–425 (2000).
114. D. de Sousa, J. Sampaio, L. Nunes, M. Baesso, A. Bento, and L. Miranda, "Energy transfer and the 2.8−μm emission of Er3+ and Yb3+ -doped low silica content calcium aluminate glasses," Phys. Rev. B - Condens. Matter Mater. Phys. **62**(5), 3176–3180 (2000).
115. S. Hraiech, M. Ferid, Y. Guyot, and G. Boulon, "Structural and optical studies of Yb3+, Er3+ and Er3+/Yb3+ co-doped phosphate glasses," J. Rare Earths **31**(7), 685–693 (2013).
116. Q. Wang, J. Wen, Y. Luo, G.-D. Peng, F. Pang, Z. Chen, and T. Wang, "Enhancement of lifetime in Er-doped silica optical fiber by doping Yb ions via atomic layer deposition," Opt. Mater. Express **10**(2), 397 (2020).
117. G. Canat, J.-C. Mollier, J.-P. Bouzinac, G. M. Williams, B. Cole, L. Goldberg, Y. Jaouën, and G. Kulcsar, "Dynamics of high-power erbium–ytterbium fiber amplifiers," J. Opt. Soc. Am. B **22**(11), 2308 (2005).
118. A. W. Snyder and J. D. Love, *Optical Waveguide Theory*, 1st ed. (Chapman & Hall, 1983).
119. Q. Han, T. Liu, X. Lü, and K. Ren, "Numerical methods for high-power Er/Yb-codoped fiber amplifiers," Opt. Quantum Electron. **47**(7), 2199–2212 (2015).
120. M. K. Davis, M. J. F. Digonnet, and R. H. Pantell, "Thermal effects in doped fibers," J. Light. Technol. **16**(6), 1013–1023 (1998).
121. D. Y. Shen, J. K. Sahu, and W. A. Clarkson, "Highly efficient Er,Yb-doped fiber laser with 188W free-running and > 100W tunable output power," Opt. Express **13**(13), 4916 (2005).
122. D. Creeden, H. Pretorius, J. Limongelli, and S. D. Setzler, "Single frequency 1560nm Er:Yb fiber amplifier with 207W output power and 50.5% slope efficiency," in *Fiber Lasers XIII: Technology, Systems, and Applications*, J. Ballato, ed. (SPIE, 2016), **9728**(11), p. 97282L.
123. O. De Varona, W. Fittkau, P. Booker, T. Theeg, M. Steinke, D. Kracht, J. Neumann, and P. Wessels, "Single-frequency fiber amplifier at 15 μm with 100 W in the linearly-polarized TEM_00 mode for next-generation gravitational wave detectors," Opt. Express **25**(21), 24880 (2017).
124. J. R. Limongelli, S. D. Setzler, and D. Creeden, "Experimental and numerical analysis of high power Er:Yb co-doped fiber amplifiers," in *Proc. SPIE*, C. A.

Robin and I. Hartl, eds. (SPIE, 2017), **10083**, p. 100831O.
125. J. E. Townsend, W. L. Barnes, K. P. Jedrzejewski, and K. P. Grubb, "Yb doped silica optical fibre with ultrahigh transfer efficiency and gain," Electron. Lett. **27**(21), 1958–1959 (1991).
126. M. Laroche, S. Girard, J. K. Sahu, W. A. Clarkson, and J. Nilsson, "Accurate efficiency evaluation of energy-transfer processes in phosphosilicate Er^3+-Yb^3+-codoped fibers," J. Opt. Soc. Am. B **23**(2), 195 (2006).
127. M. A. Melkumov, A. Y. Laptev, M. V. Yashkov, N. N. Vechkanov, A. N. Guryanov, and I. A. Bufetov, "Effects of Yb 3+ and Er 3+ concentrations and doping procedure on excitation transfer efficiency in Er-Yb doped phosphosilicate fibers," Inorg. Mater. **46**(3), 299–303 (2010).
128. M. M. Khudyakov, A. S. Lobanov, D. S. Lipatov, A. N. Abramov, N. N. Vechkanov, A. N. Guryanov, M. A. Melkumov, K. K. Bobkov, S. S. Aleshkina, T. A. Kochergina, L. D. Iskhakova, F. O. Milovich, M. M. Bubnov, and M. E. Likhachev, "Single-mode large-mode-area Er–Yb fibers with core based on phosphorosilicate glass highly doped with fluorine," Laser Phys. Lett. **16**(2), 025105 (2019).
129. J. Nilsson, S. U. Alam, J. A. Alvarez-Chavez, P. W. Turner, W. A. Clarkson, and A. B. Grudinin, "High-power and tunable operation of erbium-ytterbium co-doped cladding-pumped fiber lasers," IEEE J. Quantum Electron. **39**(8), 987–994 (2003).
130. A. Yusim, J. Barsalou, D. Gapontsev, N. S. Platonov, O. Shkurikhin, V. P. Gapontsev, Y. A. Barannikov, and F. V. Shcherbina, "100 watt single-mode CW linearly polarized all-fiber format 1.56-μm laser with suppression of parasitic lasing effects," in *Fiber Lasers II: Technology, Systems, and Applications*, L. N. Durvasula, A. J. W. Brown, and J. Nilsson, eds. (SPIE, 2005), **5709**(22), p. 69.
131. Y. Jeong, J. Nilsson, J. K. Sahu, D. B. S. Soh, C. Alegria, P. Dupriez, C. A. Codemard, D. N. Payne, R. Horley, L. M. B. Hickey, L. Wanzcyk, C. E. Chryssou, J. A. Alvarez-Chavez, and P. W. Turner, "Single-frequency, single-mode, plane-polarized ytterbium-doped fiber master oscillator power amplifier source with 264 W of output power," Opt. Lett. **30**(5), 459 (2005).
132. M. A. Jebali, J.-N. Maran, and S. LaRochelle, "264 W output power at 1585 nm in Er–Yb codoped fiber laser using in-band pumping," Opt. Lett. **39**(13), 3974 (2014).
133. L. V. Kotov, M. E. Likhachev, M. M. Bubnov, O. I. Medvedkov, M. V. Yashkov, A. N. Guryanov, J. Lhermite, S. Février, and E. Cormier, "75 W 40% efficiency single-mode all-fiber erbium-doped laser cladding pumped at 976 nm," Opt. Lett. **38**(13), 2230 (2013).
134. L. V. Kotov, M. E. Likhachev, M. M. Bubnov, O. I. Medvedkov, M. V. Yashkov, A. N. Guryanov, S. Février, J. Lhermite, and E. Cormier, "Yb-free Er-doped all-fiber amplifier cladding-pumped at 976 nm with output power in excess of 100 W," in *Proc. SPIE*, S. Ramachandran, ed. (SPIE, 2014), **8961**(7), p. 89610X.
135. V. Kuhn, P. Weßels, J. Neumann, and D. Kracht, "Stabilization and power scaling of cladding pumped Er:Yb-codoped fiber amplifier via auxiliary signal at 1064 nm," Opt. Express **17**(20), 18304 (2009).

136. V. Kuhn, D. Kracht, J. Neumann, and P. Weßels, "Dependence of Er:Yb-codoped 1.5μm amplifier on wavelength-tuned auxiliary seed signal at 1μm wavelength," Opt. Lett. **35**(24), 4105 (2010).
137. G. Sobon, P. Kaczmarek, A. Antonczak, J. Sotor, and K. M. Abramski, "Controlling the 1 μm spontaneous emission in Er/Yb co-doped fiber amplifiers," Opt. Express **19**(20), 19104 (2011).
138. K. Tankala, B. Samson, A. Carter, J. Farroni, D. Machewirth, N. Jacobson, U. Manyam, A. Sanchez, M.-Y. Chen, A. Galvanauskas, W. Torruellas, and Y. Chen, "New developments in high power eye-safe LMA fibers," in *Proc. SPIE*, A. J. W. Brown, J. Nilsson, D. J. Harter, and A. Tünnermann, eds. (SPIE, 2006), **6102**(23), p. 610206.
139. M. M. Khudyakov, D. S. Lipatov, A. N. Gur'yanov, M. M. Bubnov, and M. E. Likhachev, "High-peak-power highly-efficient combined Er/Er-Yb fiber amplifier," in *Fiber Lasers XVI: Technology and Systems*, L. Dong and A. L. Carter, eds. (SPIE, 2019), **10897**(7), p. 67.
140. O. De Varona, W. Fittkau, P. Booker, T. Theeg, M. Steinke, D. Kracht, J. Neumann, and P. Wessels, "Single-frequency fiber amplifier at 1.5 μm with 100 W in the linearly-polarized TEM_00 mode for next-generation gravitational wave detectors," Opt. Express **25**(21), 24880 (2017).
141. M. M. Khudyakov, A. S. Lobanov, D. S. Lipatov, A. N. Abramov, N. N. Vechkanov, A. N. Guryanov, M. A. Melkumov, K. K. Bobkov, S. S. Aleshkina, T. A. Kochergina, L. D. Iskhakova, F. O. Milovich, M. M. Bubnov, and M. E. Likhachev, "Single-mode large-mode-area Er–Yb fibers with core based on phosphorosilicate glass highly doped with fluorine," Laser Phys. Lett. **16**(2), 025105 (2019).
142. G. G. Vienne, W. S. Brocklesby, R. S. Brown, Z. J. Chen, J. D. Minelly, J. E. Roman, and D. N. Payne, "Role of aluminum in ytterbium-erbium codoped phosphoaluminosilicate optical fibers," Opt. Fiber Technol. **2**(4), 387–393 (1996).
143. D. Ouyang, C. Guo, S. Ruan, P. Yan, H. Wei, and J. Luo, "Yb band parasitic lasing suppression in Er/Yb-co-doped pulsed fiber amplifier based on all-solid photonic bandgap fiber," Appl. Phys. B Lasers Opt. **114**(4), 585–590 (2014).
144. C. Robin, I. Dajani, and B. Pulford, "Modal instability-suppressing, single-frequency photonic crystal fiber amplifier with 811 W output power," Opt. Lett. **39**(3), 666 (2014).
145. N. A. Naderi, A. Flores, B. M. Anderson, and I. Dajani, "Beam combinable, kilowatt, all-fiber amplifier based on phase-modulated laser gain competition," Opt. Lett. **41**(17), 3964 (2016).
146. I. Dajani, C. Zeringue, C. Lu, C. Vergien, L. Henry, and C. Robin, "Stimulated Brillouin scattering suppression through laser gain competition: scalability to high power," Opt. Lett. **35**(18), 3114 (2010).
147. A. Flores, C. Robin, A. Lanari, and I. Dajani, "Pseudo-random binary sequence phase modulation for narrow linewidth, kilowatt, monolithic fiber amplifiers," Opt. Express **22**(15), 17735 (2014).
148. Y. Jeong, J. Nilsson, J. K. Sahu, D. N. Payne, R. Horley, L. M. B. Hickey, and P.

W. Turner, "Power scaling of single-frequency ytterbium-doped fiber master-oscillator power-amplifier sources up to 500 W," IEEE J. Sel. Top. Quantum Electron. **13**(3), 546–550 (2007).
149. A. Liu, "Suppressing stimulated Brillouin scattering in fiber amplifiers using nonuniform fiber and temperature gradient," Opt. Express **15**(3), 977 (2007).
150. I. Dajani, A. Flores, R. Holten, B. Anderson, B. Pulford, and T. Ehrenreich, "Multi-kilowatt power scaling and coherent beam combining of narrow-linewidth fiber lasers," in *Proc. SPIE*, J. Ballato, ed. (SPIE, 2016), **9728**(9), p. 972801.
151. P. Dragica, N. Yua, G. Pan, B. Meehan, M. Tuggle, M. Cavillon, T. Hawkins, and J. Ballato, "Power Scaling of Diffraction-Limited, Narrow-Linewidth Fiber Lasers to Beyond 10 kW," in (Institute of Electrical and Electronics Engineers (IEEE), 2020), pp. 1–4.
152. R. Y. Chiao, C. H. Townes, and B. P. Stoicheff, "Stimulated brillouin scattering and coherent generation of intense hypersonic waves," Phys. Rev. Lett. **12**(21), 592–595 (1964).
153. S. Gray, A. Liu, D. T. Walton, J. Wang, M.-J. Li, X. Chen, A. B. Ruffin, J. A. DeMeritt, and L. A. Zenteno, "502 Watt, single transverse mode, narrow linewidth, bidirectionally pumped Yb-doped fiber amplifier," Opt. Express **15**(25), 17044 (2007).
154. C. Robin and I. Dajani, "Acoustically segmented photonic crystal fiber for single-frequency high-power laser applications," Opt. Lett. **36**(14), 2641 (2011).
155. C. Mart, B. Ward, B. Pulford, I. Dajani, L. Dong, and K. Kieu, "Brillouin gain spectroscopy on LMA Yb-doped photonic bandgap fiber," in *Optics InfoBase Conference Papers* (OSA - The Optical Society, 2016), p. FW5B.4.
156. P. D. Dragic, J. Ballato, S. Morris, and T. Hawkins, "The Brillouin gain coefficient of Yb-doped aluminosilicate glass optical fibers," Opt. Mater. (Amst). **35**(9), 1627–1632 (2013).